DETECTING LOW FREQUENCY EARTHQUAKES WITHIN DEEP TECTONIC TREMOR

A DISSERTATION

SUBMITTED TO THE DEPARTMENT OF GEOPHYSICS

AND THE COMMITTEE ON GRADUATE STUDIES

OF STANFORD UNIVERSITY

IN PARTIAL FULFILLMENT OF THE REQUIREMENTS FOR THE DEGREE

DOCTOR OF PHILOSOPHY

Justin R. Brown

June 2012

This dissertation is online at: http://purl.stanford.edu/tt858fb2944

I certify that I have read this dissertation and that, in my opinion, it is fully adequate in scope and quality as a dissertation for the degree of Doctor of Philosophy.

Gregory Beroza, Primary Adviser

I certify that I have read this dissertation and that, in my opinion, it is fully adequate in scope and quality as a dissertation for the degree of Doctor of Philosophy.

Jesse Lawrence

I certify that I have read this dissertation and that, in my opinion, it is fully adequate in scope and quality as a dissertation for the degree of Doctor of Philosophy.

Paul Segall

I certify that I have read this dissertation and that, in my opinion, it is fully adequate in scope and quality as a dissertation for the degree of Doctor of Philosophy.

Norman Sleep

Approved for the Stanford University Committee on Graduate Studies.

Patricia J. Gumport, Vice Provost Graduate Education

This signature page was generated electronically upon submission of this dissertation in electronic format. An original signed hard copy of the signature page is on file in University Archives.

ABSTRACT

Prior to analyzing any earthquake, the event must be detected. Although fundamental, earthquake detection remains a challenging task- particularly for small-magnitude events where the amplitudes of the signal of interest approach the noise level of the recording instrument. In particular, high precision event detection is important with regard to analyzing tectonic tremor, formerly referred to as non-volcanic tremor. Tectonic tremor is a non-impulsive, low-amplitude, semi-continuous seismic signal whose time series is similar to volcanic tremor. Despite the time series similarity to volcanic tremor, tectonic tremor is often recorded at plate boundaries- mostly convergent boundaries at subduction zones- away from volcanic centers. Unlike large earthquakes where seismic signals are impulsive with high amplitudes and a finite duration, tectonic tremor is emergent, semi-continuous and low amplitude causing tremor locations to have large errors. In southwest Japan tectonic tremor has been shown to consist of several repeating low frequency earthquakes indicating shear failure on the subduction plate interface that occur during several days, however these events are difficult to detect due to their low amplitude approaching the noise level. In this thesis I demonstrate two methods to identify periods of waveform similarity during the tremor and show that these similar events are low frequency earthquake swarms located on the deep extent of four plate boundaries: southwest Japan, Cascadia, Costa Rica, and the Alaska-Aleutian subduction zones. Although each subduction zone has a different incoming plate rate, age and thermal profile, these factors do not exhibit a strong influence on tremor occurrence indicating tremor may occur in almost- if not all subduction zones.

ACKNOWLEDGEMENTS

There are numerous individuals who greatly contributed to the research endeavors in this thesis. I could not have completed this work without the support, encouragement and advising of several collaborators, friends and family members.

First and foremost, I would like to thank my advisor Gregory Beroza. Greg transformed me from being an undergraduate interested in science to becoming a scientist. Greg taught me how to ask questions for myself and subsequently seek the answers in an efficient, thorough and classy manner. Despite my tendency to stretch the many tasks he set for me to the last minute, Greg was always patient and more than willing to make sure all of the my work thorough, thought-provoking and complete.

Prior to matriculating at Stanford there were individuals who have been in my cheering corner to finish a PhD. Mrs. Barbara Dobson, my eighth grade earth sciences teacher, was the first person to encourage me to seek seismology as a career back when I was in junior high. Following her advice throughout high school I was able to land at the University of Wisconsin where I was an undergraduate research scholar under the advising of Professor Clifford Thurber. Cliff took a chance on me as a freshman and mentored me both academically and in research. While I was in his research group I was able to spend my first of two summers working for Dr. Stephanie Prejean of the Alaska Volcano Observatory. Stephanie, a PhD alumna of Stanford geophysics, was the first to point me in this direction for doctoral studies. She also taught me how to use a computer. She

taught me vi and how to relocate earthquakes. Little did I know at the time, Stephanie and I would be working together again when I started out as a graduate student. Not only has she been a great mentor, she is a great friend.

In addition to Stephanie, there are several U.S. Geological Survey scientists who helped me through my research including but not limited to Peter Haeussler, Joan Gomberg, Susan Hough, and Justin Rubinstein. I also had the pleasure of working with Japanese colleagues Satoshi Ide and Kazuaki Ohta in September 2008. They were instrumental in the work of chapter 3, as well as Honn Kao and Susan Schwartz.

My studies at Stanford exposed me to some of the most tremendous and intelligent peers anyone could ask for. It was a pleasure working in the earthquake seismology group with David Shelly, Seok Goo Song, Shuo Ma, German Prieto, Annemarie Baltay, Ana Aguiar, Randi Walters, Marine Denolle and Sarah Barrett in addition to members outside of the group including Emily Montgomery-Brown, Robert Clapp, Jeremy Brown, Owen Hurd, Noel Bartlow, Dan Sinnett, Stuart Schmitt, Danica Dralus, Vanessa Mitchell, and Jolene Robin-McCaskill.

My friends outside of geophysics were my rock throughout all six years of this process. Jennifer Upshaw, Cory Quinn, Michael Smith, Eric Hall, Kyle O'Malley, Praveen Shanbhag, Tri Chiem, Imeh Williams, and Joshua Rollins were my family away from family. They saw the good, bad and ugly but stuck it out regardless of which circumstance I was in.

Closest to my heart, and for whom this thesis is dedicated to are my Dad, Mom, and two older sisters Erica and Jessica. Despite missing holidays or being unreachable, you've always found a way to check in on me and make sure I am still on the correct path for my life, and I thank you for continuing to do so unconditionally.

Table of Contents

List of Tables

List of Figures

1. INTRODUCTION

Earthquake detection is fundamental to characterizing slip behavior on the faults where they occur. Since the discovery of deep non-volcanic tremor in subduction zones [*Obara*, 2002] seismologists have been motivated to improve event detection methods to characterize tremor. Unlike ordinary earthquakes, tremor lacks high amplitude impulsive arrivals used to pick phase arrivals to locate and characterize the source of the signal. However, *Shelly et al.,* [2007a] were able to identify swarms of repeating low frequency earthquakes (LFEs) that appear to compose the majority of tremor signals.

LFEs in tremor are indicative of shear failure on the deep extent of faults [*Ide et al.,* 2007]. LFEs belong to a class of slow earthquakes where stress drops are low and their moment scales linearly with duration unlike ordinary earthquakes where moment scales with the cube of the duration [*Ide et al.,* 2007]. In southwest Japan LFEs are located on the downdip extension of the subducting plate interface. The LFE locations are concentrated in a zone downdip of the seismogenic zone prone to rupturing large earthquakes and updip of the freely sliding plate interface. This suggests that LFEs occur due to a frictional transition of slip-weakening updip and slip strengthening-downdip.

Previous studies show that tracking the temporal and spatial patterns of LFEs can characterize tremor and slow slip in southwest Japan [*Shelly et al.,* 2007b] where

episodes can last anywhere from several hours to several days and the event swarms can migrate updip, downdip and along strike.

Detecting LFEs is not trivial. Using a set of previously cataloged template LFEs from the Japanese Meteorological Agency (JMA) *Shelly et al.* [2007a] were able to apply a matched filter method to indentify times where matches in the waveform reveal a repeating template. The requirement of this method to detect additional LFEs mandates previously catalogued templates. However, in other subduction zones where tremor occurs there are no LFE templates detected *a priori* preventing a similar analysis.

In the second chapter of this thesis I introduce an autocorrelation method to detect LFEs in tremor without the use of *a priori* template waveforms [*Brown et al.,* 2008]. This method exploits the repeating nature of LFEs by detecting pairs of the events recorded at a dense array of Hi-Net stations. Using this technique I show that non-volcanic tremor in western Shikoku is composed of several repeating LFEs . I detect almost all of the events previously cataloged by *Shelly et al.,* [2007a] in addition to several events previously undetected. The LFEs are localized at the deep extent of the seismogenic zone on the plate interface in southwest Japan.

In the third chapter I apply the running autocorrelation technique described in chapter 2 to three distinct circum-Pacific subduction zones. In this chapter I show that tremor in southwest Japan, Cascadia and Costa Rica is composed of LFEs that are located in the

downdip extent of the subducting plate interface despite these regions having different convergence rates, temperature profiles and incoming plate ages.

In chapter 4, I apply the running autocorrelation technique to tremor-like signals in the Alaska-Aleutian subduction zone. The Alaska-Aleutian subduction zone is an observationally challenging region due to limited seismic station coverage, interference of tremor signals with volcanic signals and noise. Of all subduction zones analyzed in this thesis the Alaska-Aleutian subduction zone is the most diverse along strike. Although this subduction zone has varying convergence rates, temperature, and incoming plate age along strike, I am able to show that tremor-like signals along the arc are composed of repeating LFEs that range in depths between 45 and 75 km depth (+/- 11km; *Brown et al.,* submitted). This range in depths is the widest and deepest of any observations of tremor known (at the date of this thesis submission) on the planet.

In the fifth chapter I demonstrate an alternate technique that utilizes the logarithmic power spectrum, known as the cepstrum, to detect any phase-shifted disturbance in continuous signals including LFEs within tremor. I show that the cepstrum can recover previously detected low frequency earthquakes in southwest Japan in addition to several other events despite the non-repeating nature of the signals. Because the cepstrum is calculated from the logarithmic spectral domain the computation time is drastically decreased to a matter of tens of seconds compared to tens of minutes using autocorrelation.

REFERENCES

Brown, J. R., G. C. Beroza, and D. R. Shelly (2008), An autocorrelationmethod to detect low frequency earthquakes within tremor, Geophys. Res.Lett., 35, L16305, doi:10.1029/2008GL034560.

Shelly, D. R., G. C. Beroza, and S. Ide (2007a), Non-Volcanic Tremor and Low Frequency Earthquake Swarms, *Nature* 446, 305-307, doi:10.1038/nature05666.

Obara, K., (2002), Nonvolcanic deep tremor association with subduction in southwest Japan, *Science,* 296, pp. 1679-1681.

Shelly, D. R., G. C. Beroza, and S. Ide (2007b), Complex evolution oftransient slip derived from precise tremor locations in western Shikoku,Japan, *Geochem. Geophys. Geosyst.*, 8, Q1 00 14, doi:10.1029/2007GC001640.

Shelly, D. R., G. C. Beroza, S. Ide, and S. Nakamula (2006), Lowfrequency earthquakes in Shikoku, Japan, and their relationship to episodic tremor and slip, Nature, 442, 188 – 191, doi:10.1038/nature04931.

2. AN AUTOCORRELATION METHOD TO DETECT LOW FREQUENCY EARTHQUAKES WITHIN TREMOR

ABSTRACT

Recent studies have shown that deep tremor in the Nankai Trough under western Shikoku consists of a swarm of low frequency earthquakes (LFEs) that occur as slow shear slip on the down-dip extension of the primary seismogenic zone of the plate interface. The similarity of tremor in other locations suggests a similar mechanism, but the absence of cataloged low frequency earthquakes prevents a similar analysis. In this chapter, I develop a method for identifying LFEs within tremor. The method employs a matched-filter algorithm, similar to the technique used to infer that tremor in parts of Shikoku is comprised of LFEs; however, in this case I do not assume the origin times or locations of any LFEs *a priori*. I search for LFEs using the running autocorrelation of tremor waveforms for 6 Hi-Net stations in the vicinity of the tremor source. Time lags showing strong similarity in the autocorrelation represent either repeats, or near-repeats, of LFEs within the tremor. I test the method on an hour of Hi-Net recordings of tremor and demonstrate that it extracts both known and previously unidentified LFEs. Once identified, I cross correlate waveforms to measure relative arrival times and locate the

LFEs. The results are able to explain most of the tremor as a swarm of LFEs and the locations of newly identified events appear to fill a gap in the spatial distribution of known LFEs. This method should allow seismologists to extend the analysis of *Shelly et al.* [2007a] to parts of the Nankai Trough in Shikoku that have sparse LFE coverage, and may also allow to extend the analysis to other regions that experience deep tremor where LFEs have not yet been identified.

This material appeared in Brown, J. R., G. C. Beroza, and D. R. Shelly (2008), An autocorrelation method to detect low frequency earthquakes within tremor, Geophys. Res.Lett., 35, L16305, doi:10.1029/2008GL034560.

INTRODUCTION

Since the discovery of deep, non-volcanic tremor [*Obara*, 2002] many studies have attempted to locate it and understand its origin; however, tremor has proven difficult to study due to the lack of impulsive wave arrivals, such as those used to locate and constrain the mechanism of ordinary earthquakes. The character of tremor is similar at widely spaced stations, however, and this similarity has been exploited to localize the tremor source. An approach first used by *Obara* [2002] measures the relative arrival times of smoothed waveform envelopes to locate tremor. Another approach migrates waveform amplitudes to all possible locations to find areas of constructive interference [*Kao and Shan,* 2004]. Both these methods yield tremor locations, but are susceptible to large uncertainties, particularly in depth. They are also likely to result in large location uncertainties at times when the tremor source is spatially extended.

A different approach to tremor location was introduced by *Shelly et al.* [2006] who located LFEs. LFEs are small, slow earthquakes [*Katsumata and Kamaya*, 2003; *Ide et al.,* 2007a,b] that occur primarily during periods of deep tremor. Because LFEs have discernible *S*-wave, and sometimes *P*-wave arrivals, they can be located by conventional methods. *Shelly et al.* [2006] found that LFEs locate on the down-dip extension of the seismogenic zone of the Nankai Trough. The mechanisms of LFEs were subsequently shown to be consistent with shear slip across the plate boundary [*Ide*, 2007a]. Previously identified LFEs represent only a small fraction of tremor, but *Shelly et al.* [2007a,b] demonstrated that much of the rest of tremor can be represented as a swarm of LFEs and in doing so they were able to localize that component of tremor under Shikoku to the plate interface.

There remains an important fraction of deep tremor that does not match previously identified LFEs. Although its spectral behavior matches that of LFEs [*Shelly et al.,* 2007a], its location and mechanism remains uncertain. Moreover, in other regions where tremor has been detected, no LFEs have been identified, and hence tremor must be located by other, potentially less accurate methods. In Cascadia, for example, current locations of tremor span a very wide range in depths [*Kao et al.,* 2005], which has led to fundamentally different conclusions about the origin of tremor there. Polarization analysis of seismic array data, however, suggests that tremor in Cascadia may also be generated by slow plate-boundary slip [*Wech and Creager*, 2007].

In this chapter I present a new method for detecting LFEs using the running autocorrelation of tremor seismograms, and apply it to an hour of tremor under Shikoku previously analyzed by *Shelly et al.* [2007a]. I detect most of the known LFEs, as well as

a large number of newly identified LFEs. The new detections fill temporal gaps in matches between tremor and LFEs. I measure the relative arrival times of the newly detected LFE waveforms, locate them, and find that they also may fill a spatial gap in previously identified LFEs. This suggests that periods of tremor in western Shikoku not previously matched with LFEs, are generated by the same mechanism, *viz.*, shear slip on the plate interface, and hence that the entirety of deep tremor in this region has a common origin.

AUTOCORRELATION FOR DETECTION

Results on deep tremor in western Shikoku reported by *Shelly et al.* [2007a,b] indicate that much of tremor consists of a swarm of LFEs that are highly clustered in both space and time. This observation means that the waveforms from temporally adjacent LFEs will be highly similar, which is the fundamental premise of our technique.

I analyzed velocity data from six high sensitivity (Hi-Net) stations: KWBH, OOZH, HIYH, TBEH, YNDH, TSYH. Hi-Net is composed of over high sensitivity seismic stations installed across the Japanese archipelago after the 1995 Hyogoken-nanbu Earthquake by the National Research Institute for Earth Science and Disaster Prevention (NIED) [Obara, 2003]. Hi-Net stations are distributed with an average spacing of 20–30 km, and consist of three-component short period velocity seismometers installed in boreholes at depths of 100 m or greater.

I bandpass filter the data from 1-8 Hz to emphasize the frequency range in which tremor and LFEs are most prominent. I use the autocorrelation of the data to search for waveforms that nearly repeat as observed across a seismic network. This approach is

closely related to that used to associate LFEs with tremor [*Shelly et al.,* 2007a]; however, in this case, the origin times and locations of potential LFEs are unknown, which means that it is necessary to search for similarity at all possible lags. I analyze an hour on 29 August, 2005 from 17:00-18:00. I chose this hour because it contains a mixture of tremor that was previously matched with LFEs and tremor that was not [*Shelly et al.,* 2007a], use the former to evaluate the effectiveness of this approach, and the latter to draw more general conclusions about the origin of tremor.

This method essentially uses the running-window autocorrelation to search for similarity at all stations and over all components. The tremor is segmented into 6-second windows that are lagged by 0.5 seconds (see Figure 1).

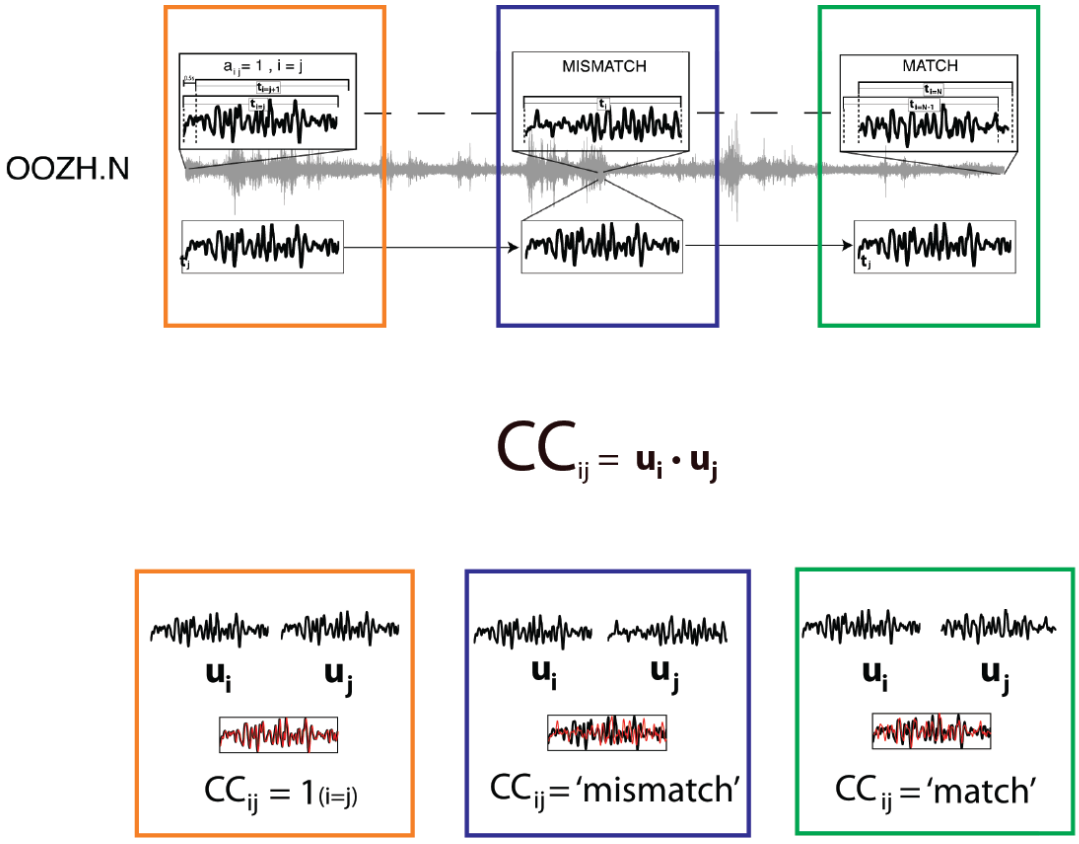

Figure 2.1. Schematic illustrating the autocorrelation technique. One hour of tremor is segmented into 6-second windows lagged by 0.5 seconds. This corresponds to N = 7,188

windows. The correlation coefficient, a_{ij}, is calculated for every window pair at a common station and component and summed over the entire network.

This is longer than the 4-second window length used by *Shelly et al.* [2007a] because the move-out of the seismic phases across the network is unknown *a priori*. I experimented with longer windows, but that resulted in fewer significant detections. Because the waveform similarity is of limited duration, as is the case for known LFEs, using a longer time window results in a lower signal-to-noise ratio. I also experimented with different lag spacing. When the spacing is too small the computation time increases; whereas, large lags yield few detections because the similarity is aliased. A lag of 0.5 seconds has the potential to miss some detections, but as will become clear below, it is sufficient to detect nearly all of the previously identified LFEs.

Consider a network of N station components (3-component Hi-Net stations, 6 stations corresponds to n = 18) on which we record ground motion at windows represented by the vector u at time t_i and t_j. The corresponding network array correlation coefficient (CC) sum, a_{ij} can be written as:

$$A_{ij} = \sum_{N} CC_{ij}^{N} = \left[u(t_i) \bullet u(t_j) \right]^{N} \qquad (1)$$

i.e., the sum of the normalized *CC* across the network. *N* in eqn 1 is not an exponent. Summing across the network allows the search for times when the entire network exhibits waveform similarity during tremor, and greatly enhances the ability to distinguish signal from noise. A detection is determined on the statistics of A_{ij} relative to that of all other lags and use the median absolute deviation (MAD) to set a detection threshold [*Shelly et al.,* 2007a]. The MAD ensures that the detection statistics are not adversely affected by

the fraction of the population with high values corresponding to positive detections. Time lags showing strong similarity in the autocorrelation represent either repeats, or near-repeats, of LFEs within the tremor. Window pairs that exceed a detection threshold of 5 times MAD were saved and defined as candidate events.

I subsequently apply waveform cross-correlation for all pairs of candidate events recorded at a common station. The window size of each detection is decreased to the middle 4-seconds of the original window and the taper was removed. At this stage, all similar windows are treated like "weak" detections found by *Shelly et al.,* [2007a]. Closely spaced earthquakes with similar source processes should yield similar waveforms at a common station due to the similar source mechanisms and nearly identical source-receiver paths. Next, I apply cross-correlation the new windows at a sampling frequency of 100 Hz within a 15-second segment (appending +/- 4.5 seconds to the initial window). For periods where the matched-filter running autocorrelation frequently revealed at least one detection every 15 seconds I apply waveform cross-correlation at 0.01s precision within 15-second windows to search for near-repeats of tremor sample by sample. I sum the waveform cross-correlation coefficients for all components across the network and save event pairs with CC sum exceeding 5.4, which corresponds to an average coefficient value of 0.3 per component, based on typical CC measurements for previously detected LFEs [*Shelly et al.,* 2007a].

EVENT VERIFICATION AND LOCATION

The waveforms are organized into 52 exclusive groups exhibiting a higher degree of similarity at all stations and components and stack them. Events showing

similarity to more than one group are organized into the group where the CC value was highest. I treat each of these stacks as a template event and repeat the autocorrelation using the stacked waveform, as recorded across the network, as matched filters [*Gibbons and Ringdal*, 2006; *Shearer*, 1994]. In this round of correlation, I decrease lag to 0.05 s intervals. Because there are only 52 templates to consider, the processing time is manageable. The lag size decrease also enables the search for a more precise window for which the correlation coefficient, a_{ij}, can be found. The detection threshold is increased to a very conservative value of 8*MAD to reduce the probability of false detections to extremely low levels [*Shelly et al.*, 2007a].

Once a set of of robust LFEs is assembled waveform cross correlation is applied to all events recorded at a common station and component in order to solve for the lags at each. Since the data is sampled at 100 Hz, this permits the alignment of seismograms with a resolution of 0.01 s. I treat the horizontal and vertical components separately and analyze 15-second search windows. Windows for horizontal components are created as before, but for the vertical component, I append 9 s of tremor preceding the 6-second autocorrelation window in order to measure the *P*-wave arrival (Figure 2a). I first cross-correlate events pairs recorded at a common horizontal component and sum the waveform cross-correlation values across the entire network of horizontal components. If the average coefficient value of exceeds 0.3, then we perform a cross-correlation of vertical component cross-correlation and save values that exceed 0.3 (Figure 2a).

Applying the detection algorithm to the 1-hour time interval resulted in 479 detections. To avoid possible repetition of overlapping events, we allow no more than 1 detection every twelve seconds, which reduces the catalog to 287 events. Included in

these 287 events are 174 of the 188 events previously detected by *Shelly et al.,* [2007a] during the same period. The fact that a few events go undetected may be attributable to the fact that we are not comparing these events to the stronger LFEs that were previously identified by the Japanese Meteorological Agency (JMA). Instead, I detect by comparing relatively weak LFEs, with lower *snr*, with each other. It is worth noting that this approach will also not work on events that do not have near repeats during the hour analyzed. Applying this approach to a longer time interval, or even multiple tremor episodes, would allow this effect to be reduced.

The waveforms for a representative LFE are shown in Figure 2b. The correlation coefficients are modest, but overwhelmingly positive and therefore unlikely to occur due to chance. The new detections fill temporal gaps (*Figure 4, top panel*) in matches between tremor and LFEs, strongly suggesting that this part of the tremor is composed of nearly repeating LFEs.

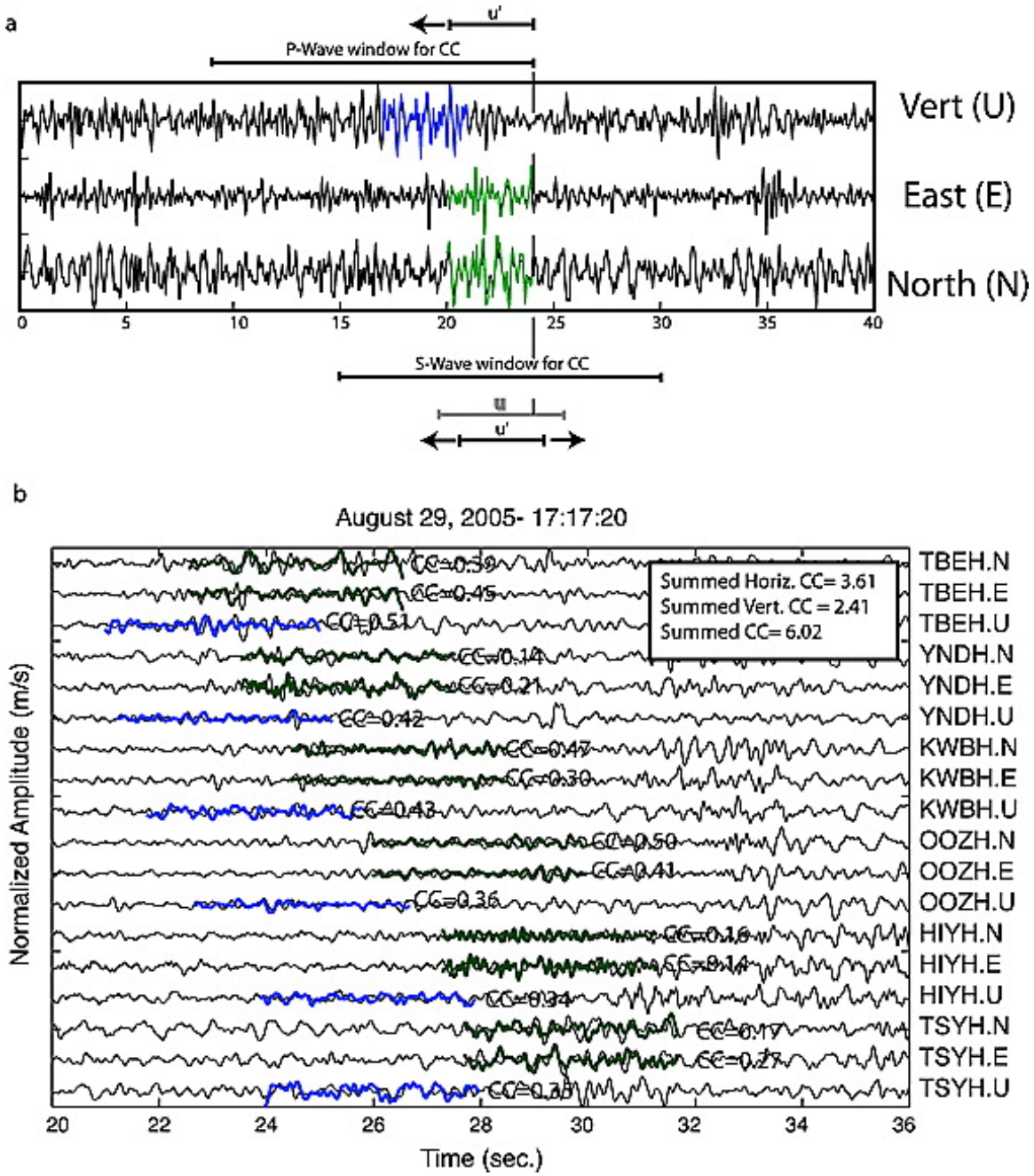

Figure 2.2. *P* and *S* wave search within tremor using cross correlation. Original 6-second windows, **u**, are narrowed to a new 4-second window **u'**. a.) Horizontal components search within a 15-second time segment in order to align around the *S*-wave window (green). Subsequently, the vertical component searches for the *P*-wave window (blue) in a 15-second time segment that precedes the final horizontal alignment. b.) Continuous tremor waveforms are shown in gray. LFE waveforms are shown in blue (P-wave,

vertical component) and green (S-wave, horizontal components). The normalized CC coefficient is shown for each. The CC coefficients for individual components are modest, but taken together they indicate a similarity that is very unlikely to be due to random chance.

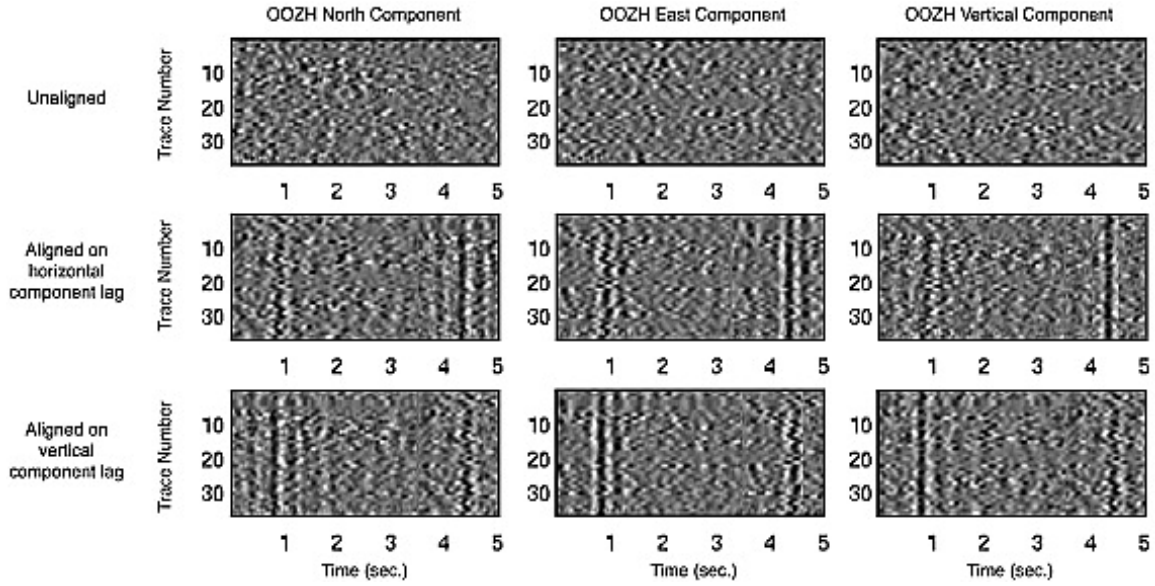

Figure 2.3. 38 LFEs recorded at Hi-Net station OOZH: before (top) and after (bottom two rows) cross-correlation alignment. The same seismograms are plotted below in grayscale (black = -1 and white = +1 amplitude) and are aligned corresponding to lags derived from horizontal and vertical component waveform cross-correlation (second and third rows, respectively) in order to demonstrate the detection of both P and S arrivals. 5-second waveforms are plotted to effectively demonstrate the alignment of P and S waves. Variations in *S-P* time, and hence location, lead to slightly variable *S* wave arrival times, which are apparent when the waveforms are aligned on the *P* wave.

Figure 3 illustrates an alignment of 38 events that yield significant correlations across the network as seen on the three components of station OOZH. The waveform similarity on all components indicates that near-repeats of the LFE are being detected and alignments are possible on all three components. I assume the alignment in the horizontal and vertical components correspond to *S*- and *P*-wave arrivals respectively, and extract *S-P* times for these events. For this hour of tremor, estimated *S-P* times at OOZH are 3.85

seconds (+/- 0.60 seconds), which indicates that the events are tightly clustered in space. *S-P* times for other stations vary from 3.5 to 4.5 seconds. I use *tomoDD* [*Zhang and Thurber,* 2003] to estimate event locations assuming a fixed velocity model from *Shelly et al.* [2006] using the cross-correlation derived relative arrival time measurements.

Figure 2.4 shows our locations for 287 LFEs, together with previously detected LFEs from *Shelly et al.* [2007a]. As mentioned previously, nearly all of the known LFEs are detected, as well as a large number of previously unrecognized LFEs. As *Shelly et al.* [2007a] documented, their method for associating tremor with LFEs will only work if the target LFE is located within a couple of km of one of the template events. This result suggests that periods of tremor that were not previously matched with known LFEs can be explained as a swarm of LFEs a different part of the plate interface as well. Hence, the LFE locations provide strong additional evidence that tremor in this region is generated by shear slip on the plate interface.

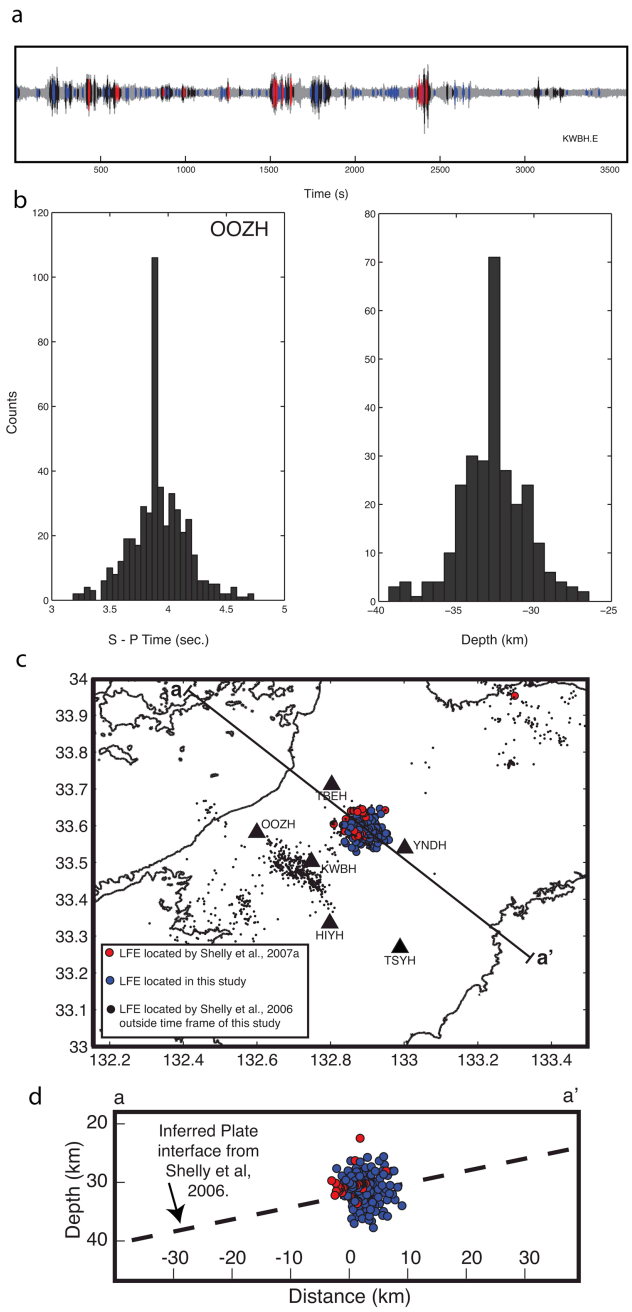

Figure 2.4 LFE detections and locations. a) Temporal detections of one hour of LFEs from tremor. Black ticks indicate LFEs detected by both the previous and current study. Blue ticks are the additional events, whereas red events are events are missed LFE detections in this study. b) Histograms for S-P times and depth distribution of locations. S-P times determined from waveform CC alignment around 3.85 sec. (±0.6 sec.) at station OOZH. Depths of LFE center around 33 km below sea level in the vicinity of the plate interface. (c) Map view and (d) crosssection view of LFEs. Blue circles indicate the 287 located in this study. Red circles indicate locations of previously identified LFEs [Shelly et al., 2007a]. Black dots are other LFEs. The dashed line denotes

inferred plate interface. It is worth noting that the color schemes for 2.4a and 2.4cd are different.

CONCLUSIONS

A new method for detecting low frequency earthquakes within tremor using a running window autocorrelation was developed. This method of extracting LFEs from tremor detects both previously identified LFEs, as well as a large number of previously unidentified LFEs, without the use of prior information. The work in this chapter supports the hypothesis that deep tremor in southwest Japan is a swarm of repeating LFEs that occur on the plate interface down-dip of the primary seismogenic zone between 30-35 km. The newly identified LFEs fill temporal gaps in detections from tremor and are spatially co-located with the previous LFEs during the same hour of tremor. Applying this approach to a complete tremor sequence should allow a generalization of this conclusion. It may also allow the analysis of tremor using LFEs in other regions where deep tremor is observed.

ACKNOWLEDGEMENTS

I thank S. Ide for helpful discussion and Haijiang Zhang for providing the *tomoDD* code. This work was supported by NSF Grant EAR-0710835. All data were obtained from the NIED Hi-net data server. This work utilized the Stanford Center for Computational Earth and Environmental Science.

REFERENCES

Gibbons, S. J., and F. Ringdal (2006), The detection of low magnitude seismic events using array-based waveform correlation, *Geophys. J. Int.*, 165, 149 – 166.

Ide, S., D. R. Shelly, and G. C. Beroza (2007a), The mechanism of deep low frequency earthquakes: further evidence that deep non-volcanic tremor is generated by shear slip on the plate interface, *Geophys. Res. Lett.*, 34, L03308, doi:10.1029/2006GL028890.

Ide, S., G. C. Beroza, D. R. Shelly, and T. Uchide (2007b) , A scaling law for slow earthquakes, *Nature*, 447, 76-79, doi:10.1038/nature05780.

Kao, H., and S.-J. Shan (2004), The source-scanning algorithm: mapping the distribution of seismic sources in time and space, *Geophys. J. Int.* 157, doi:10.1111/j.1365-246X.2004.02276.x.

Kao, H., S.-J. Shan, H. Dragert, G. Rogers, J. F. Cassidy, K. Ramachandran (2005), A wide depth distribution of seismic tremors along the northern Cascadia margin, *Nature,* 436, 841-844.

Katsumata, A., and N. Kamaya (2003), Low-frequency continuous tremor around the Moho discontinuity away from volcanoes in the southwest Japan, *Geophys. Res. Lett.*, 30(1), 1020, doi:10.1029/2002GL015981.

Obara, K. (2002), Nonvolcanic deep tremor associated with subduction in southwest Japan, *Science*, 296, 1679-1681.

Obara, K. (2002), Hi-net: High sensitivity seismograph network, Japan, *Lecture Notes in Earth Sciences,* 98, 79-88.

Shearer, P. (1994), Global seismic event detection using a matched filter on long-period seismograms, *J. Geophys. Res.,* 99, 13,713-13,725.

Shelly, D. R., G. C. Beroza, S. Ide, and S. Nakamula (2006), Low-frequency earthquakes in Shikoku, Japan, and their relationship to episodic tremor and slip, *Nature*, 442, 188-191.

Shelly, D. R., G. C. Beroza, and S. Ide (2007a), Non-Volcanic Tremor and Low Frequency Earthquake Swarms, *Nature* 446, 305-307, doi:10.1038/nature05666.

Shelly, D. R., G. C. Beroza, and S. Ide (2007b), Complex evolution of transient slip derived from precise tremor locations in western Shikoku, Japan, *Geochem. Geophys. Geosyst*., 8, Q10014, doi:10.1029/2007GC001640.

Wech, A.G., and K. C. Creager (2007), Cascadia tremor polarization evidence for plate interface slip, *Geophys. Res. Lett.,* 34, L22306-L22318, DOI 10.1029/2007GL031167, 2007.

Zhang, H., and C. H. Thurber (2003), Double-difference tomography: The method and its application to the Hayward fault, California, *Bull. Seismol. Soc. Am.* 93, 1875-1889.

3. DEEP LOW-FREQUENCY EARTHQUAKES IN TREMOR LOCALIZE TO THE PLATE INTERFACE IN MULTIPLE SUBDUCTION ZONES

ABSTRACT

Deep tremor under Shikoku, Japan, consists primarily, and perhaps entirely, of swarms of low-frequency earthquakes (LFEs) that occur as shear slip on the plate interface. Although tremor is observed at other plate boundaries, the lack of cataloged low-frequency earthquakes has precluded a similar conclusion about tremor in those locales. In this chapter I use a network autocorrelation approach to detect and locate LFEs within tremor recorded at three subduction zones characterized by different thermal structures and levels of interplate seismicity: southwest Japan, northern Cascadia and Costa Rica. In each case I find that LFEs are the primary constituent of tremor and that they locate on the deep continuation of the plate boundary. This suggests that tremor in these regions shares a common mechanism and that temperature is not the primary control on such activity.

The material in this chapter appeared in Brown, J. R., G. C. Beroza, S. Ide, K. Ohta, D. R. Shelly, S. Y. Schwartz, W. Rabbel, M. Thorwart, and H. Kao (2009), Deep low-frequency earthquakes in tremor localize to the plate interface in multiple subduction zones, *Geophys. Res. Lett.,* 36, L19306, doi:10.1029/2009GL04002.

INTRODUCTION

Deep, non-volcanic tremor was discovered in Japan [*Obara*, 2002] and found to occur during episodes of slow slip in Cascadia [*Rogers and Dragert*, 2003] and elsewhere [*Schwartz and Rokosky,* 2007]. LFEs are small earthquakes (less than magnitude ~2) deficient in amplitude at frequencies above ~10 Hz that occur during episodes of deep tremor in southwest Japan [*Katsumata and Kamaya,* 2003]. LFEs belong to a newly discovered class of slow earthquakes [*Ide et al.,* 2007b] located above an area of elevated V_P/V_S, down-dip from the locked portion of the plate boundary in SW Japan [*Shelly et al.,* 2006]. Tremor generation has been related to fluid release during oceanic slab dehydration [*Katsumata and Kamaya,* 2003]; however, empirical moment tensor analysis reveals that LFEs are generated by shear slip [*Ide et al.,* 2007a] on the deep extension of the plate boundary [*Shelly et al.,* 2007b]. The spectral characteristics of tremor and LFEs are essentially identical [*Shelly et al.,* 2007a] and comparison of tremor and LFE waveforms indicate that most tremor in southwest Japan is comprised of LFE swarms [*Shelly et al.,* 2007a, 2007b; *Brown et al.,* 2008].

The picture of tremor in other subduction zones is less clear. Studies of non-volcanic tremor in northern Cascadia using a source-scanning algorithm [*Kao and Shan,* 2004] find that the tremor source has a peak in activity near the plate interface, but that it occurs at depths from about 15-50 km. This suggests the possibility of a different relationship between tremor and slow slip events in Cascadia [*Kao et al.,* 2005]. On the other hand, particle motion analysis of tremor farther south in Cascadia [*Wech and Creager,* 2007] suggests slip in the direction of relative plate motion, and cross correlation of vertical and

horizontal ground motion indicates that tremor originates near the plate boundary [*La Rocca et al.,* 2009]. These discrepancies in the origin of the tremor source need to be resolved if tremor is to be fully understood in other tectonic settings and subduction zones that differ from SW Japan. The signature and frequency characteristics of deep tremor and its association with longer term slow slip events is similar wherever it is well observed, which motivates the application of techniques used to study tremor in Japan more widely.

METHOD

The data consists of three hours of tremor in three different subduction zones. For Japan I use 8 Hi-Net borehole velocity recordings of tremor in western Shikoku from 19:00-22:00 on April 18, 2006, sampled at 100 samples per second. In Cascadia I use tremor data from 00:00-03:00 on September 22, 2005, as recorded at seven 3-component stations on southern Vancouver Island, including both CNSN and POLARIS broadband networks, sampled at 100 samples per second. In Costa Rica I use data from 00:00-03:00 on May 17, 2007, as recorded on 4 broadband STS2 sensors and 4 short period sensors of at least 25 samples per second. Tremor is most clearly recorded in the 1-8 Hz frequency band, which is well within the recording capabilities of all these instruments.

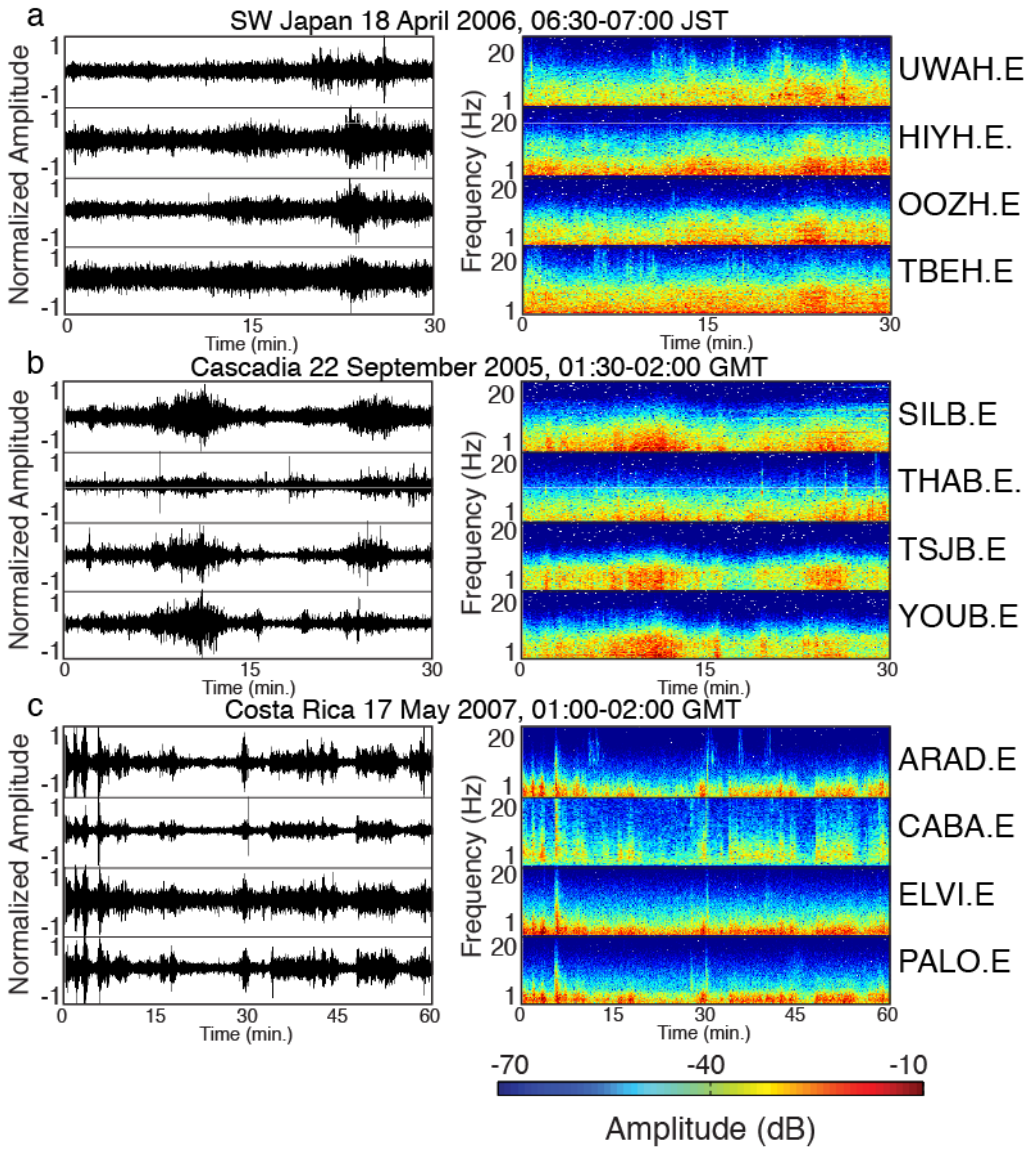

Figure 3.1 Non-volcanic tremor recordings and spectrograms a) SW Japan, b) Cascadia and c) Costa Rica. Tremor in all three subduction zones is characterized as a long-duration low-amplitude and low frequency (1-8 Hz) signal resembling volcanic tremor in some respects.

I apply a running network autocorrelation [*Brown et al.,* 2008] to detect LFEs within tremor for each of these subduction zones. This approach is used to detect waveforms that nearly repeat as observed across a seismic network in each region and is closely related to that used to associate LFEs with tremor [*Shelly et al.,* 2007a], however in this

case, the origin times and locations of potential LFEs are unknown. This requires a search for similarity at all possible lags. Consider a network of n station components (e.g. 3-component Hi-Net stations, 8 stations corresponds to $n = 24$) on which the record ground motion at windows are represented by the vector u at time t_i and t_j. The corresponding network correlation coefficient (CC) sum, a_{ij} can be written as:

$$A_{ij} = \sum_{N} CC_{ij}^{N} = \left[u(t_i) \bullet u(t_j) \right]^{N} \qquad (1)$$

i.e., the sum of the normalized CC across the network. Summing across the network allows a search for times when the entire network exhibits waveform similarity, and greatly enhances the ability to distinguish signal from noise. I detect on the statistics of a_{ij} relative to that of all other lags and use the median absolute deviation (MAD) to set a detection threshold [*Shelly et al.,* 2007a, *Brown et al.,* 2008]. The MAD ensures that detection statistics are not adversely affected by windows with high values (positive detections). Time lags exhibiting very strong similarity represent either repeats, or near-repeats, of LFEs within the tremor.

All window pairs that exceed the detection threshold of 6 times MAD are saved and verified as LFEs based on the comparison of stacks of aligned events by re-applying the autocorrelation with a detection threshold of 9 times MAD for Japan and Cascadia, and 10 times MAD for Costa Rica data. The detection criterion for Costa Rica is higher due to a lower sampling rate of data compared to SW Japan and Cascadia. I apply sample precision waveform cross-correlation to measure relative arrival times for all windows that pass the event detection statistic. Because both horizontal and vertical components of ground motion for the tremor were saved, I search for *S*-waves and *P*-waves on these

components respectively. The first search is for *S*-waves via cross-correlation where arrival is flagged and search behind the *S* arrival for a *P*-wave on the vertical component. Figures 3.2a-c and d-f show alignments on the *S*- and *P*-waves respectively. Both *P* and *S* wave pick errors are between 0.1 and 0.5 seconds in all three locations. Starting locations for the LFE hypocenters are estimated using the *S*-*P* times for all events.

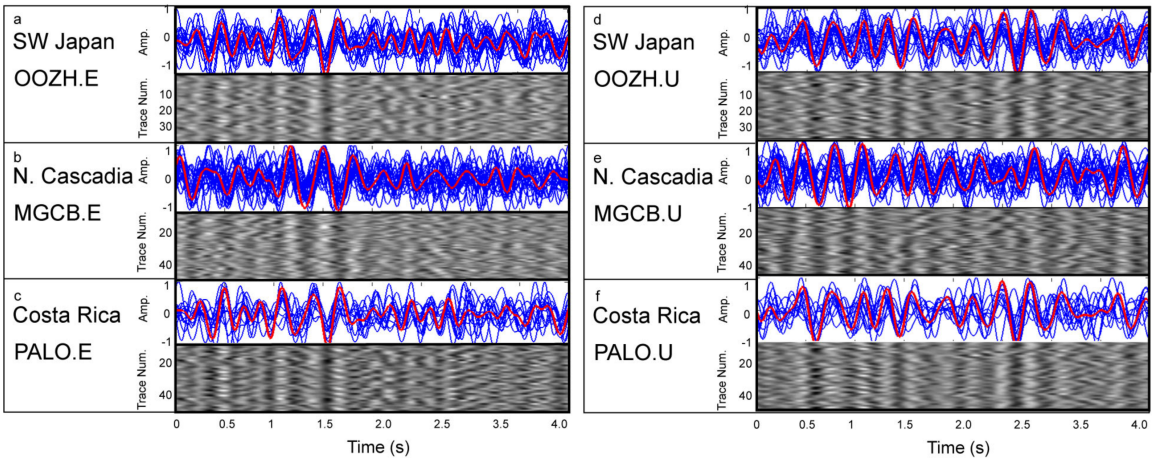

Figure 3.2 a-c. LFE detections within tremor from three subduction zones on horizontal components. Shown are stacks and alignments of similar LFEs recorded at a common station. Events are aligned on the (a–c) *S*-wave arrival after cross-correlation and (d–f) *P*-wave arrivals. (top) Individual events in blue and the normalized stack in red. (bottom) A grayscale plot of aligned seismograms. Positive values are white, and negative values are black.

I use a combination of *tomoDD* [*Zhang and Thurber,* 2003] and the summed network correlation coefficients [*Ohta and Ide,* 2008] to estimate accurate event locations assuming a fixed, 3-D velocity model from tomographic studies in each locale [*Shelly et al.,* 2006; *Ramachandran,* 2001; *DeShon et al.,* 2006]. Grid space sizes in both SW Japan and Cascadia were designed at 20 by 20 by 5 km grid spacing and 10 by 10 by 5 grid

spacing in Costa Rica. The aforementioned tomographic studies are appropriate to use for location due to the presence of recently modeled plate interfaces. The cross-correlation derived relative arrival time measurements are used as input data and it is required that all events used as data input in *tomoDD* belong to at least one coherent pair. The summed network correlation coefficient (NCC) is used as a basis for weighting event-pair differential times for all *P*- and *S*-wave recordings. This allows events with stronger network correlation coefficients, *viz*. those with stronger waveform similarity across the network, to have greater weight in the solution. Employing the summed NCC as data weight for the *tomoDD* location routine retains all LFE detections in each study region. Unlike the hypocenter distribution of *Brown et al.* [2008] this eliminates the potential negative impact on the estimated locations of including measurements with low correlation coefficients [*Ohta and Ide*, 2008].

RESULTS

There is an abundance of low-frequency earthquake activity during tremor in all three subduction zones comprising of 298 LFEs in SW Japan, 331 LFEs in northern Cascadia, and 232 LFEs in Costa Rica and find the occurrence of LFEs to be almost continuous. Figure 3.3a-c shows the locations of detected LFEs in the three regions. The high degree of similarity of LFEs in the regions corresponds to repeating locations of several events-particularly in SW Japan and Costa Rica. In each case the LFEs locate down-dip of the locked seismogenic zone of the plate boundary defined by: the down-dip extent of the last great earthquake (SW Japan) [*Yoshioka et al.,* 2008], geodetic observations (Cascadia) [*Hyndman and Wang,* 1995], and interplate seismicity (Costa Rica) [*DeShon et al.,*

2006]. I also detect six ordinary micro-earthquakes located on the plate interface, up-dip from the LFEs in a region of abundant interplate micro-earthquake activity [*DeShon et al.,* 2006] in Costa Rica, which suggests that the autocorrelation approach is useful for analyzing earthquake swarms as well. Based on the grid spacing and pick uncertainty, location error is no more than +/- 5 km in the vertical direction. It is worth noting that the plate interface modeled by *Ramachandran* (2001) is ~ 5 km deeper than the location of our LFEs. Recent studies of the plate interface in northern Cascadia reveal a slightly shallower plate interface [*Audet et al.,* 2009], consistent with the LFE locations. This result suggests that the plate interface is shallower and/or broader and more complex than previously envisioned.

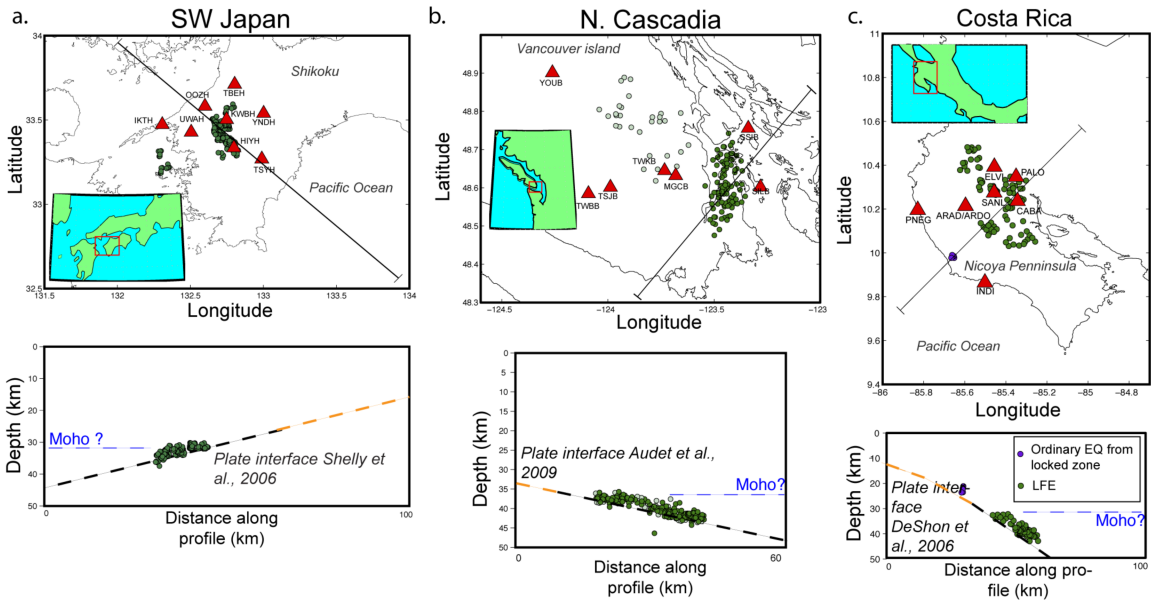

Figure 3.3 a-c. LFE locations in SW Japan, Cascadia, and Costa Rica. In SW Japan, the LFEs are located in western Shikoku between 30 and 35 km depth. In northern Cascadia the LFEs are located in southern Vancouver Island between 30 and 40 km depth on the

plate interface. Light green hypocenters represent LFEs away from the main cross section. In Costa Rica, the LFEs are beneath the Nicoya Penninsula between 30 and 40 km depth. The locked portions of these subduction zones and moho are inferred from previous tomography studies [*Shelly et al.*, 2006; *Audet et al.*, 2009, *DeShon et al.*, 2006] are shown in amber and blue, respectively. Black dashed lines correspond to the deep extent of the plate interface. Ordinary micro-earthquakes are shown in violet, and these events occur in the locked portion of the subduction zone. LFEs localize to the plate boundary in all three subduction zones.

The existence of LFEs during tremor in each of these subduction zones, and their locations, both support the hypothesis that non-volcanic tremor in subduction zones is generated by intermittent shear-slip in the vicinity of the plate interface. The three-hour sample is not long enough to explore many interesting questions, such as possible along-strike variations in tremor activity or other factors that might control tremor/LFE occurrence. Nonetheless, all of the LFEs we detect locate within 5 km of the plate interface.

Although the results reported in this chapter support the hypothesis that deep tremor is generated by shear slip, evidence exists that fluids play an enabling role in tremor as supported by tomographic and seismic reflection studies in both Cascadia [*Kao and Shan*, 2004; *Audet et al.,* 2009] and Japan [*Shelly et al.,* 2006] indicating high fluid pressure in the vicinity of LFEs. Although less definitive, seismic tomography studies in Costa Rica also suggest elevated V_P/V_S at the plate interface [*DeShon et al.,* 2006], co-located with the LFEs we detect in this study.

CONCLUSION

Given network coverage of the same density used for local earthquake monitoring, I can detect tremor and extract the LFEs that comprise it. This capability should help obtain a deeper understanding of what controls the distribution of tremor. There are variations in incoming plate age, convergence rate, and modeled temperatures on the plate interface in the LFE depth range for the locations studied. The Cascadia and SW Japan subduction zones are relatively hot with strongly locked shallow seismogenic zones displaying little or no inter-plate seismicity. LFEs in these locations occur between 30-45 km where modeled temperatures in the subducting oceanic crust reach 400-500^{o}C [*Yoshioka et al.,* 2008; *Wada et al.,* 2008]; conditions favorable for dehydration of hydrous minerals in oceanic basalt [*Hacker et al.,* 2003]. LFEs in the relatively cold and seismically active northern Costa Rica subduction zone occur at comparable depth but where temperatures in the down-going oceanic crust do not exceed 250^{o}C [*Hacker et al.,* 2003]. The cooler Costa Rica plate interface precludes the same dehydration reactions that likely occur in SW Japan and Cascadia; however, fluids may be liberated through dehydration of lower temperature hydrous phases [*Hacker et al.,* 2003]. Despite significant variations in both thermal structure and degree of seismic coupling, all three subduction zones record LFE swarms during tremor that localize to the deep extension of the plate interface (between 30 and 45 km depth). Other parameters may also play a role in controlling the distribution of LFEs, such as the thickness of the over-riding plate, pressure, or topographic load due to the overriding plate [*Brudzinski and Allen,* 2007].

Tremor is widely observed and offers new opportunities to understand fault behavior. Improved locations will help in monitoring possible time-dependent changes in tremor, and may provide important constraints on the role of the deep extension of faults in the earthquake process.

ACKNOWLEDGEMENTS

I thank Haijiang Zhang for providing the *tomoDD* code and Clifford Thurber provided helpful discussion. I also thank Heather DeShon for the velocity model in Costa Rica. This work was supported by NSF Grant EAR-0710835. All Japanese data were obtained from the NIED Hi-net data server. The Cascadia dataset consists of waveforms from the Canadian National Seismograph Network, the POLARIS consortium, and temporary arrays deployed by the Geological Survey of Canada. This work utilized the Stanford Center for Computational Earth and Environmental Science.

REFERENCES

Audet, P., M. G. Bostock, N. I. Christensen, and S.M. Peacock (2009), Seismic evidence for overpressured subducted oceanic crust and megathrust fault sealing. *Nature,* 457, 76-78.

Barckhausen, U., C. R. Ranero, R. von Huene, S. Cande, and H. A. Roeser (2001), Revised tectonic boundaries in the Cocos Plate off Costa Rica: implications for the segmentation of the convergent margin and for plate tectonic models. *J. Geophys. Res.,* 106, 19207-19220.

Brown, J. R., G. C. Beroza, and D. R. Shelly (2008), An autocorrelation method to detect low frequency earthquakes within tremor. *Geophys. Res. Lett*., 5, L16305, doi:10.1029/2008GL034560.

Brudzinski, M. R., and R. M. Allen (2007), Segmentation of episodic tremor and slip all along Cascadia. *Geology,* 35, 907-910.

DeMets, C., R. Gordon, D. Argus, and S. Stein (1994), Effect of recent revisions to the geomagnetic reversal timescale on estimates of current plate motions. *Geophys. Res. Lett.,* 21, 2191-2194.

DeShon, H. R., S. Y. Schwartz, A. V. Newman, V. González, M. Protti, M., L. M. Dorman, T. H. Dixon, D. E. Sampson, and E. R. Flueh (2006), Seismogenic zone structure beneath the Nicoya Peninsula, Costa Rica, from three-dimensional local earthquake *P*- and *S*-wave tomography. *Geophys. J. Intl.,* 164, 109-124.

Hacker, B. R., S. M. Peacock, G. A. Abers, and S. D. Holloway, (2003), Subduction factory - 2. Are intermediate-depth earthquakes in subducting slabs linked to metamorphic dehydration reactions? *J. Geophys. Res.,* 108, 2030, doi:10.1029/2001JB001129.

Hyndman, R. D., and K. Wang (1995), Constraints on the rupture zone of Cascadia great earthquakes from current deformation and the thermal regime. *J. Geophys. Res.,* 100, 22133-22154.

Ide, S., D. R. Shelly, and G. C. Beroza (2007a), The mechanism of deep low frequency earthquakes: further evidence that deep non-volcanic tremor is generated by shear slip on the plate interface. *Geophys. Res. Lett.*, 34, L03308, doi:10.1029/2006GL028890.

Ide, S., G. C. Beroza, D. R. Shelly, and T. Uchide, (2007b), A scaling law for slow earthquakes. *Nature*, 447, 76-79.

Kao, H., and S.-J. Shan (2004), The source-scanning algorithm: mapping the distribution of seismic sources in time and space. *Geophys. J. Int.,* 157, doi:10.1111/j.1365-246X.2004.02276.x.

Kao, H., S.-J. Shan, H. Dragert, G. Rogers, J. F. Cassidy, and K. Ramachandran (2005), A wide depth distribution of seismic tremors along the northern Cascadia margin. *Nature,* 436, 841-844.

Katsumata, A. and N. Kamaya (2003), Low-frequency continuous tremor around the Moho discontinuity away from volcanoes in the southwest Japan. *Geophys. Res. Lett.*, 30, 1020, doi:10.1029/2002GL015981.

La Rocca, M., K. C. Creager, D. Galluzzo, S. Malone, J. E. Vidale, J. R. Sweet, and A. G. Wech (2009), Cascadia Tremor Located Near Plate Interface Constrained by S Minus P Wave Times. *Science*, 323, 620 – 623.

Obara, K. (2002), Nonvolcanic deep tremor associated with subduction in southwest Japan. *Science*, 296, 1679-1681.

Ohta, K. and S. Ide (2008), An accurate hypocenter determination method using network correlation coefficients and its application to deep low frequency earthquakes. *Earth Planets Space*, 60, 877–882 (2008).

Okino, K., Y. Shimakawa, and S. Nagaoka (1994), Evolution of the Shikoku Basin. *JGG*, 46, 463-479.

Ramachandran, K. (2001), Velocity structure of S.W. British Columbia and N.W. Washington from 3-D non-linear seismic tomography. *PhD thesis, University of Victoria, Victoria, B.C. Canada*.

Rogers, G. and H. Dragert (2003), Episodic tremor and slip on the Cascadia subduction zone: The chatter of silent slip. *Science,* 300, 1942-1943.

Schwartz, S. Y. and J. M. Rokosky (2007), Slow slip events and seismic tremor at circum-Pacific subduction zones. *Rev. Geophys.*, 45, RG3004, doi:10.1029/2006RG000208.

Shelly, D. R., G. C. Beroza, S. Ide, and S. Nakamula (2006), Low-frequency earthquakes in Shikoku, Japan, and their relationship to episodic tremor and slip. *Nature*, 442, 188-191.

Shelly, D. R., G. C. Beroza, and S. Ide (2007a), Non-Volcanic Tremor and Low Frequency Earthquake Swarms. *Nature,* 446, 305-307.

Shelly, D. R., G. C. Beroza, and S. Ide (2007b), Complex evolution of transient slip derived from precise tremor locations in western Shikoku, Japan. *Geochem. Geophys. Geosyst*., 8, Q10014, doi:10.1029/2007GC001640.

Szeliga, W., T. Melbourne, M. Santillan, and M. Miller (2008), GPS constraints on 34 slow slip events within the Cascadia subduction zone, 1997-2005. *J. Geophys. Res.*, 113, B04404, doi:10.1029/2007JB004948.

Wada, I., K. Wang, J. He, and R. D. Hyndman (2008), Weakening of the subduction interface and its effects on surface heat flow, slab dehydration, and mantle wedge serpentinization. *J. Geophys. Res.,* 113, B04402, doi:10.1029/2007JB005190.

Wech, A. G., and K. C. Creager (2007), Cascadia tremor polarization evidence for plate interface slip. *Geophys. Res. Lett.,* 34, L22306, doi:10.1029/2007GL031167 (2007).

Yoshioka, S., M. Toda, and J. Nakajima (2008), Regionality of deep low-frequency

earthquakes associated with subduction of the Philippine Sea plate along the Nankai Trough, southwest Japan. *Earth and Planetary Sci. Lett.,* 272, 189–198.

Zhang, H., and C. H. Thurber (2003), Double-difference tomography: The method and its application to the Hayward fault, California. *Bull. Seismol. Soc. Am.* 93, 1875-1889.

4. DETECTING LOW FREQUENCY EARTHQUAKES WITHIN TECTONIC TREMOR IN THE ALASKA-ALEUTIAN SUBDUCTION ZONE

ABSTRACT

I characterize and locate tremor not associated with volcanoes along the Alaska-Aleutian subduction zone using continuous seismic data recorded by the Alaska Volcano Observatory and the Alaska Earthquake Information Center from 2005 to the present. Visual inspection of waveform spectra and time series reveals dozens of 10 to 20-minute bursts of tremor along the length of the Alaska-Aleutian subduction zone. I use autocorrelation to demonstrate that these tremor signals are composed of hundreds of repeating low-frequency earthquakes (LFEs). Double difference locations of the LFEs based on seismic recordings from multiple monitoring networks indicate that the tremor source is deep. The tremor activity we characterize is localized in four segments, from

east to west: Kodiak Island, Shumagin Gap, Unalaska, and Andreanof Islands. Although the geometry, age, thermal structure, frictional and other relevant properties of the Alaska-Aleutian subduction zone are poorly known, these characteristics are likely to differ systematically from east to west. The findings indicate non-volcanic tremor occurs in a wider range of subduction environments than previously recognized. Locations near Kodiak Island are the most reliable because station coverage is more complete. LFE hypocenters in this region are located on the plate interface near the down-dip limit of the 1964 M_w 9.2 Alaska earthquake rupture area. LFE hypocenters in the remaining areas along the arc are also located down-dip of the most recent M_w 8+ megathrust earthquakes, between 50-75 km depth and almost directly trenchward of the volcanic arc. Although these locations are less well constrained, the results support the hypothesis that tremor activity marks the down-dip rupture limit for great megathrust earthquakes in this subduction zone. Lastly, there is no correlation between the presence of tremor and particular aspects of over-riding or subducting plate geology or coupling. It appears that LFEs are a fundamental characteristic of the Alaska-Aleutian subduction zone.

The material in this chapter has been submitted to Journal of Geophysical Research

INTRODUCTION

The Alaska-Aleutian subduction zone forms the plate boundary between the Pacific and North American plates for 3800 km between eastern Russia and central Alaska [*Ruppert et al.,* 2007]. From east to west: the sense of plate motion ranges from trench normal to transform, the velocity of relative plate motion ranges from about 5.1 to 7.5 cm/yr [*DeMets et al.,* 1994], and the Pacific Plate ranges in age from ~ 35 to ~ 63 Ma (Figure 4.1).

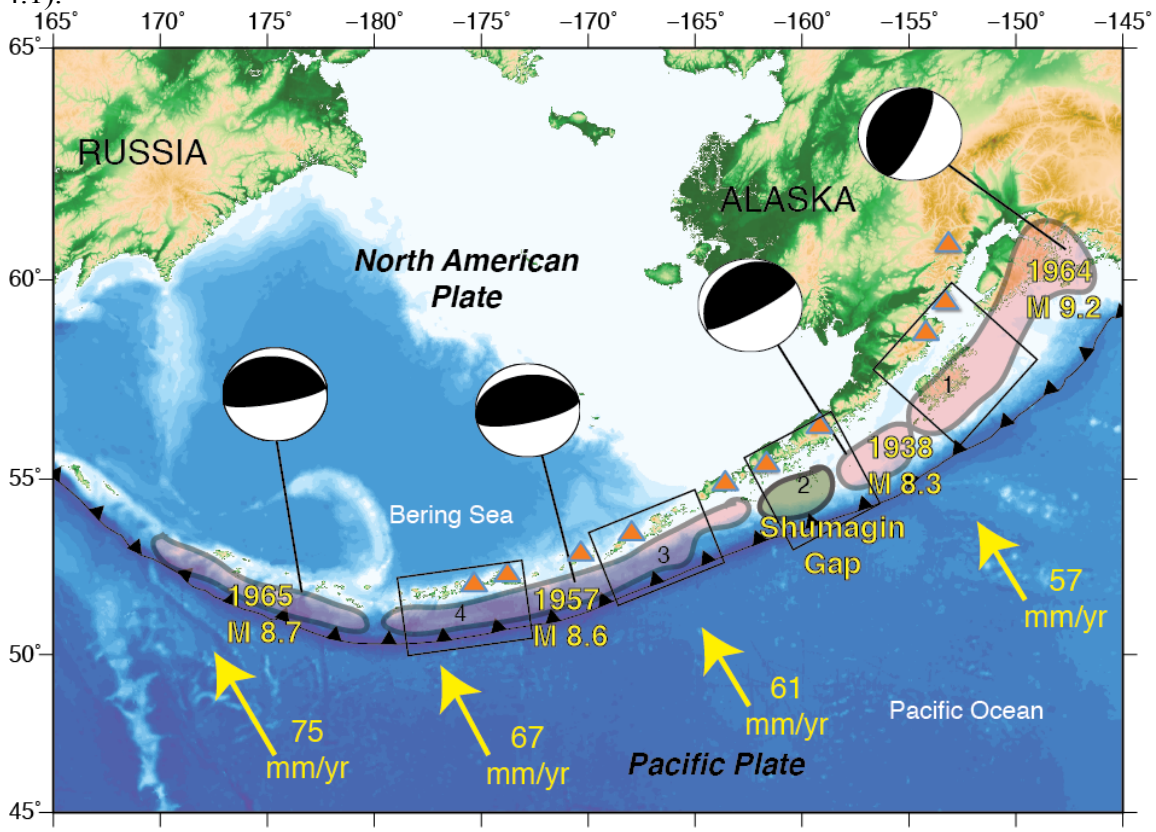

Figure 4.1. Regional bathymetric/topographic map of the Alaska-Aleutian Subduction Zone. Triangle-hinged line denotes subduction megathrust. Yellow arrows indicate the motion of the subducting Pacific Plate relative to the North American Plate. Rupture areas for the four largest megathrust events in the 20th century are shaded in pink and are shown with their respective focal mechanisms. Volcanoes with elevated activity during 2005-2010 are shown as orange triangles. Numbered boxes 1 through 4 correspond to the

Kodiak island, Shumagin Gap, Unalaska and Andreanof Islands regions where tremor is characterized in this study, respectively.

The Alaska-Aleutian subduction zone is both seismically and volcanically very active. This margin ruptured in four M_w 8+ earthquakes within the last 75 years: 1938 M_w 8.2 Shumagin Islands, 1957 M_w 8.6 Andreanof Islands, 1964 M_w 9.2 Good Friday, 1965 M_w 8.7 Rat Islands (Figure 4.1). While some portions are clearly locked between large earthquakes and accommodate the majority of deformation seismically, other areas, such as the Shumagin Gap, appear to lack large earthquakes and may deform aseismically [*Hauksson et al.,* 1984; *Freymueller et al.,* 2008]. Tremor and slow slip, commonly referred to as "episodic tremor and slip" (ETS), occur in other circum-Pacific subduction zones and in other parts of plate interfaces that are transitional between seismic and aseismic slip. *Ohta et al.* [2006] identified slow slip/creep events in the south-central Alaska portion of the subduction zone to the east of our study area, and *Peterson et al.* [2011] also identified tremor-like signals along the Alaska-Aleutian Subduction Zone.

Tremor is intrinsically difficult to study due to its low signal-to-noise ratio (*snr*). Studying non-volcanic tremor in the Alaska-Aleutian subduction zone is particularly challenging for three reasons: 1) Harsh weather conditions in this sparsely populated part of the world generate strong seismic noise. 2) Seismic and geodetic studies are restricted to land-based linear instrument deployments westward of Kodiak Island due to the

expense and logistics of amphibious geophysical studies. 3) The Alaska-Aleutian Arc seismic records include frequent signals from volcanoes, earthquakes, and possibly hydrothermal activity related to magmatic activity.

Deep, non-volcanic tremor was first discovered in southwest Japan [*Obara,* 2002 and in Cascadia it was found to occur during episodes of slow slip [*Rogers and Dragert,* 2003]. The understanding of tremor is evolving rapidly and accounts of the state of knowledge can be found in several review papers [*Schwartz and Rokosky,* 2007; *Gomberg,* 2010; *Rubinstein et al.,* 2010; *Beroza and Ide,* 2011]. In this chapter I focus on the analysis of LFEs as a way of understanding the Alaska-Aleutian subduction zone. In the previous chapter I demonstrated that low frequency earthquakes comprise tremor on the plate interface down-dip of the locked portion of three subduction zones. LFEs are small earthquakes (less than magnitude ~2) with amplitudes that decay at higher frequencies, particularly above ~10 Hz that occur during episodes of deep tremor in southwest Japan [*Katsumata and Kamaya,* 2003; *Shelly et al.,* 2006] and belong to a newly discovered class of slow earthquakes [*Ide et al.,* 2007]. Tremor generation may be related to fluid release during oceanic slab dehydration [*Katsumata and Kamaya,* 2003]; however, empirical moment tensor analysis reveals that LFEs are generated by shear slip [*Ide et al.,* 2007] on the deep extension of the plate boundary [*Shelly et al.,* 2007a]. The spectral characteristics of tremor and LFEs are essentially identical [*Shelly et al.,* 2006] and comparison of tremor and LFE waveforms indicate that tremor in southwest Japan is comprised of LFE swarms *Shelly et al.,* 2006; *Shelly et al.,* 2007b; *Brown et al.,* 2008].

Although tremor was detected along the Alaska-Aleutian Arc [*Peterson et al.,* 2011], not much is known about its location and possible relationship to slip in large earthquakes. For this chapter, I scan non-volcanic tremor-like signals previously cataloged by the Alaska Volcano Observatory (AVO) recorded throughout the Alaska-Aleutian subduction zone using running autocorrelation to detect LFEs within tremor [*Brown et al.,* 2008] and to distinguish deep tremor from other signals (long-period events, volcanic tremor, and noise). Once LFEs are detected, I relocate them using a combination of waveform-based differential arrival time measurements and the double-difference location technique [*Waldhauser and Ellsworth,* 2000]. Similar to results in the previous three chapters, I find that tremor occurs on the down-dip extension of the locked portion of the plate interface, and that it occurs in a wider range of subduction zone environments than had previously been recognized. An apparent depth dependence from east to west along the arc suggests that temperature may play a controlling role in tremor occurrence.

TECTONIC VS. VOLCANIC TREMOR

Volcanic tremor is a long duration low-amplitude signal that, in most cases, occurs within the upper 5 km of the crust within a volcanic edifice [*McNutt,* 1992]. Volcanic tremor can be attributed to a wide variety of processes including fluid migration, and degassing and is commonly associated with eruptive activity (eg. *Chouet et al.,* 1985; *Julian,* 1994; *Hellweg,* 2000; *Johnson and Lees,* 2000]. Discriminating between non-volcanic, or what I refer to as ‘tectonic tremor’ from here onwards and volcanic tremor in the Alaska-Aleutian subduction zone can be challenging due to similarities in their characteristics

and low *snr*. All of the seismic instrumentation in the Aleutians is deployed on volcanic islands, and many of the volcanoes are active.

It should be possible to discriminate between volcanic and tectonic tremor using their spectra. Tectonic tremor energy is confined to the 1-10 Hz band whereas volcanic tremor is often excited between 1-5 Hz and can extend to higher frequencies as well. In addition, tectonic tremor is inharmonic whereas volcanic tremor can be both harmonic and inharmonic. Because of the wide range of behavior for volcanic tremor, neither of these differences reliably discriminates one signal from the other. Depth and location, on the other hand, can be strongly diagnostic of volcanic vs. tectonic tremor. Typically volcanic tremor originates at shallow depths (< 5 km) [*McNutt,* 1992], whereas tectonic tremor in subduction zones locates at the deep extension of the locked portion of the megathrust [*Brown et al.,* 2009] at depths of ~40 km. In this portion of the thesis I use the locations of LFEs within tectonic tremor to show that the signal is tectonic in origin.

METHODS

The approach to characterizing tremor sources in the Alaska Aleutian subduction zone involves: 1) identifying tremor-like signals, 2) detecting and timing LFEs within these

signals, and 3) locating LFE sources. For the most part, the technique matches that of chapters 2 and 3.

Identification of Tremor-Like Signals

In order to study low-frequency earthquakes I first identify the tremor-like signals where LFEs may occur. Tectonic tremor detection in subduction zones has been successfully automated in some areas where station coverage allows it. *Kao and Shan* [2004] apply a source-scanning algorithm to detect and locate tremor bursts on Vancouver Island. *Wech and Creager* [2008] locate 50% overlapping 5-minute windows and apply bootstrap location error analysis to detect and locate tremor in northern Cascadia, mostly in Washington state. Unfortunately, the recording geometry in the Alaska-Aleutian margin is limited by geography compared to other subduction settings where tremor has been observed and prevents the successful application of these approaches. For that reason, I use visual inspection to identify possible tremor episodes in this more challenging environment.

The USGS Alaska Volcano Observatory (AVO) monitors seismic activity around volcanoes throughout the volcanic arc using a combination of short-period, high gain, and broadband sensors. An AVO seismologist inspects spectrograms of all operating channels every twelve hours and logs seismic activity that may be generated by diverse mechanisms, including: volcanic tremor, volcano-tectonic earthquakes, long-period earthquakes, deep magmatic-related activity, cultural noise, weather, and tectonic tremor (Figure 4.2). I searched the AVO log for any reference to tremor-like activity from 2005

to present, and visually inspected waveform spectra during these periods using Swarm and the online monitoring tool VALVE (Volcano Analysis and Visualization Environment) [*Cervelli et al.,* 2002].

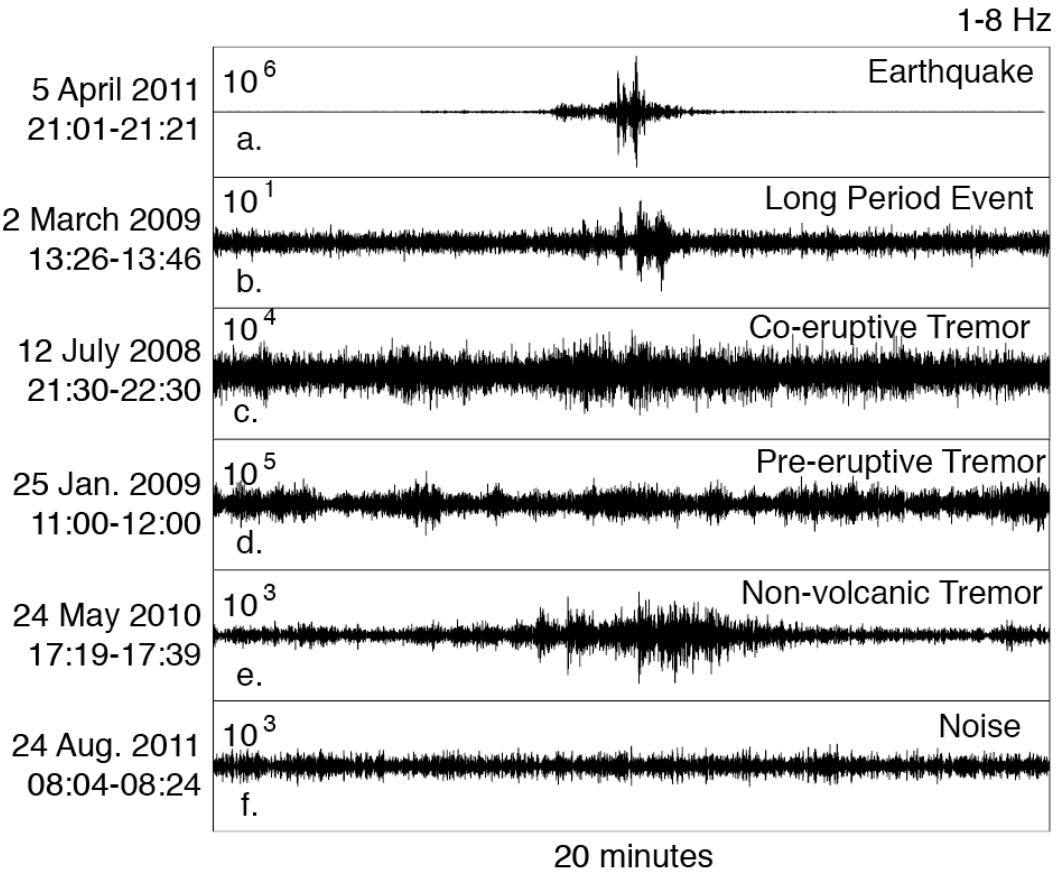

Figure 4.2. Examples of a) an earthquake, b) deep long period (DLP) from 18 km depth, c) co-eruptive tremor at Okmok Volcano, d) pre-eruptive tremor at Redoubt Volcano, e) non-volcanic tremor in the Eastern Aleutians, and f) noise in the Aleutians. Amplitudes are in nm/s.

A signal is considered tremor if it meets the following criterion from visual inspection of the waveforms and spectrograms. 1) The signal must be band-limited to 1-10 Hz to avoid analyzing high frequency volcanic tremor, weather and noise (Figure 4.3). 2) The waveforms should share a similar shape for at least 5 stations within a 50 km radius, but

not beyond. We use this criterion to ensure a local source and exclude teleseisms. 3) The duration of the signal must be at least 5 minutes (Figure 4.4). For subduction environments where deep tectonic tremor signals originating on the plate interface are known to occur, these criteria hold true [*Obara*, 2002; *Schwartz and Rokosky,* 2007; *Brown et al.,* 2009; Figure 3 and Figure 4]. Table 4.1 lists the tremor-like signals analyzed in this study. It is worth noting that, due to the inconsistent visual inspection, and the variability of noise levels, the tremor catalog is likely far from complete during 2005-2010. Rather this catalog represents the clearest recordings of tectonic tremor along the Alaska-Aleutian Arc during that period.

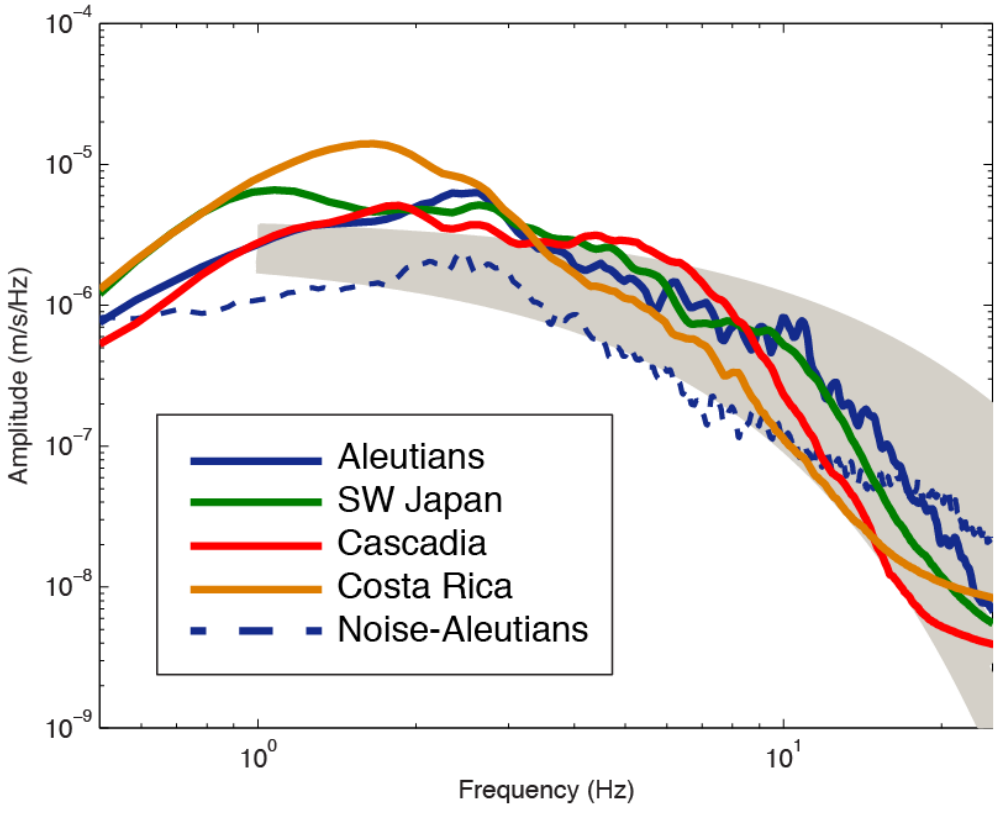

Figure 4.3. Velocity spectra of tectonic tremor from circum-pacific subduction zones. The stacked noise spectrum from Unalaska is the blue dashed curve. The shaded gray area are the attenuation curves using exp(-πft/Q) for t=19s and Q-200-400.

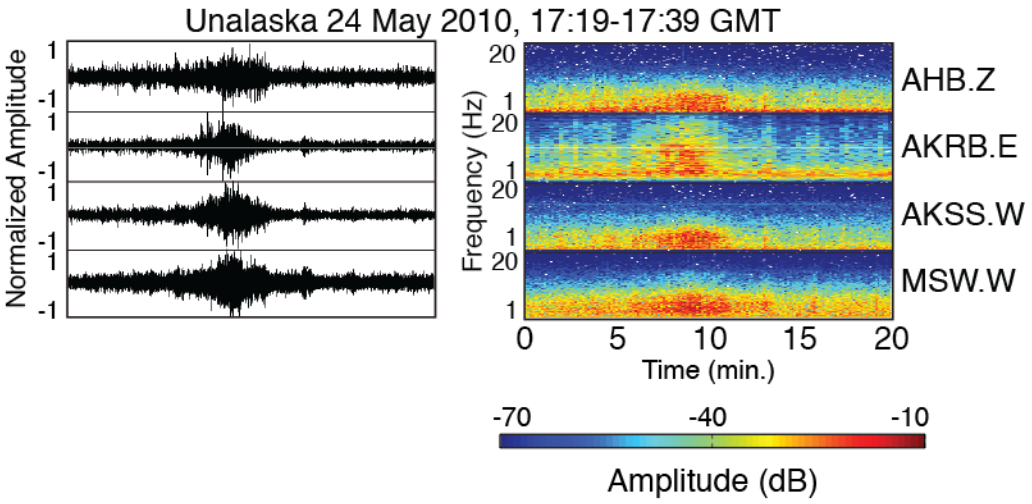

Figure 4.4. Tectonic tremor time series (left) and spectrograms (right) at four stations during the May 24, 2010 tremor episode in the Unalaska region. Time series are normalized. Spectrograms in all plots range from 1 to 20 Hz with spectral amplitudes in dB.

LOW FREQUENCY EARTHQUAKE DETECTIONS

Once the tremor was identified I searched for repeating LFEs within the signal using the running autocorrelation method as demonstrated in chapter 2 of this thesis. I analyzed continuous velocity seismograms recorded at a minimum of 5 stations for the time periods and locations listed in Table 1. Data were bandpass filtered from 1–8 Hz and autocorrelation was used to find waveforms that nearly repeat across the seismic network of interest. All available data is used that is sufficiently close to record a common signal. For example, seismologists are blind to tremor in the central portion of the 1957 rupture zone (between boxes 3 and 4 in Figure 4.1) due to a large hole in seismic networks. As a result, the coverage is uneven along the arc. Detections and locations are more reliable for areas closest to mainland Alaska where station coverage is densest.

A first pass at running-window autocorrelation was performed to search for similarity at all stations and over all components. Forty minutes of continuous data were segmented into 8-second windows lagged by 0.5 seconds. The first half of the signal presumably includes no tremor whereas the last half of the forty minutes includes the tremor-like signal identified in the AVO catalog (Figure 4.5). The 8-second windows are longer than the 6-second window length used previously by *Brown et al.* [2008], but I found it to be optimal for this study because moveout of the seismic phases were unknown across the network *a priori* which may lead to greater variation in LFE depths. Shorter time windows resulted in fewer significant detections. Longer time windows also resulted in fewer significant detections, because they include non-similar parts of the waveform, which results in a lower *snr*. We also experimented with different lags. The trade-off here is that computation time increases as the spacing

decreases, but large lags yield few detections because the similarity is aliase

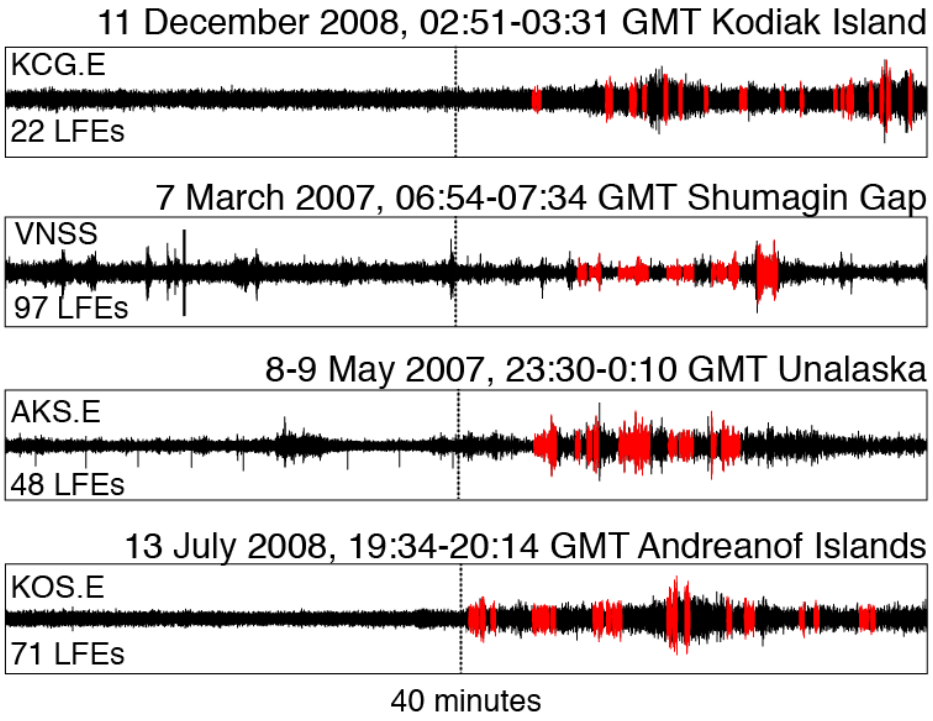

Figure 4.5. Detections (shown in red) of repeating LFEs within forty minutes of continuous data from a) Kodiak Island, b) Shumagin Gap, c,) Unalaska, and d) Andreanof Islands.

I consider a network of N channels recording ground motion in time windows represented by the vector u at time t_i as in previous chapters. The corresponding network array auto-correlation coefficient (CC) sum, A_{ij} is written as a correlation of the time-series with itself:

$$A_{ij} = \sum_{N} CC_{ij}^{N} = \left[u(t_i) \bullet u(t_j) \right]^{N} \qquad (1)$$

i.e., the sum of the normalized CC across the network. Summing across the network allows the search for times when the entire network exhibits waveform similarity during tremor, and greatly enhances the ability to distinguish signal from noise and other unwanted signals. I detect on the statistics of A_{ij} relative to that of all other lags and use the median absolute deviation (MAD) to set a detection threshold [*Shelly et al.,* 2007a]. The MAD ensures that the detection statistics are not adversely affected by the fraction of the population with high values corresponding to positive detections. Pairs of time lags showing strong similarity in the autocorrelation correspond either to repeats, or near-repeats, of any signal including LFEs within the tremor. Window pairs that exceed our detection threshold of 7 times the MAD are saved and regarded as candidate events. There is no evidence of LFEs from autocorrelation in the times of the data where the AVO finds no tremor-like signals (Figure 4.5). Table 4.1 catalogs the regions along the arc of where and when tremor occurs. Examples of detections of repeating LFEs within continuous data are shown in Figure 4.5 for all four regions.

Year	Month	Day	Hour:Min	Location
2007	January	31	13:14	Kodiak Island
2007	April	7	7:14	Shumagin Gap
2007	May	8	23:50	Unalaska
2007	July	24	3:32	Andreanof Islands
2008	May	27	4:30	Kodiak Island
2008	July	13	19:54	Andreanof Islands
2008	September	26	10:10	Unalaska
2008	November	7	5:58	Unalaska
2008	November	7	6:46	Unalaska
2008	November	7	10:02	Unalaska
2008	December	10	16:05	Kodiak Island
2008	December	11	3:17	Kodiak Island
2008	December	11	3:30	Kodiak Island
2008	December	11	11:19	Kodiak Island
2009	February	22	0:57	Unalaska
2010	March	24	21:32	Shumagin Gap
2010	May	24	17:08	Unalaska
2010	May	24	17:25	Unalaska

Table 4.1. Catalog of tremor bursts throughout the Alaska-Aleutian subduction zone.

Like ordinary earthquakes, LFEs from tremor in other circum-Pacific subduction zones cluster in both space and time. Closely spaced events with similar source processes should yield similar waveforms at a common station due to the similar source mechanisms and nearly identical source-receiver paths. After detecting the LFEs, I apply waveform cross-correlation for all pairs of candidate events recorded at a common station to find *P*- and *S*-wave arrivals. Next, we cross-correlate the windows at a sampling frequency of 50 Hz within a 24-second segment (appending ± 8 seconds to the initial window in an attempt to detect *P* waves). Due to the weak nature of tremor signals in general, *P*-waves prove to be difficult to detect; however, we are able to capture *S*-waves (Figure 4.6). I sum the waveform cross-correlation coefficients for all components across the network and save event pairs with *CC* sum exceeding $N * 0.3$, where N = total channels used. LFE waveform alignments from the cross-correlation

derived differential times are shown in Figure 4.7. An average coefficient value of 0.3 per component is consistent with typical CC measurements for previously detected LFEs [*Shelly et al*., 2007a; *Brown et al*., 2009].

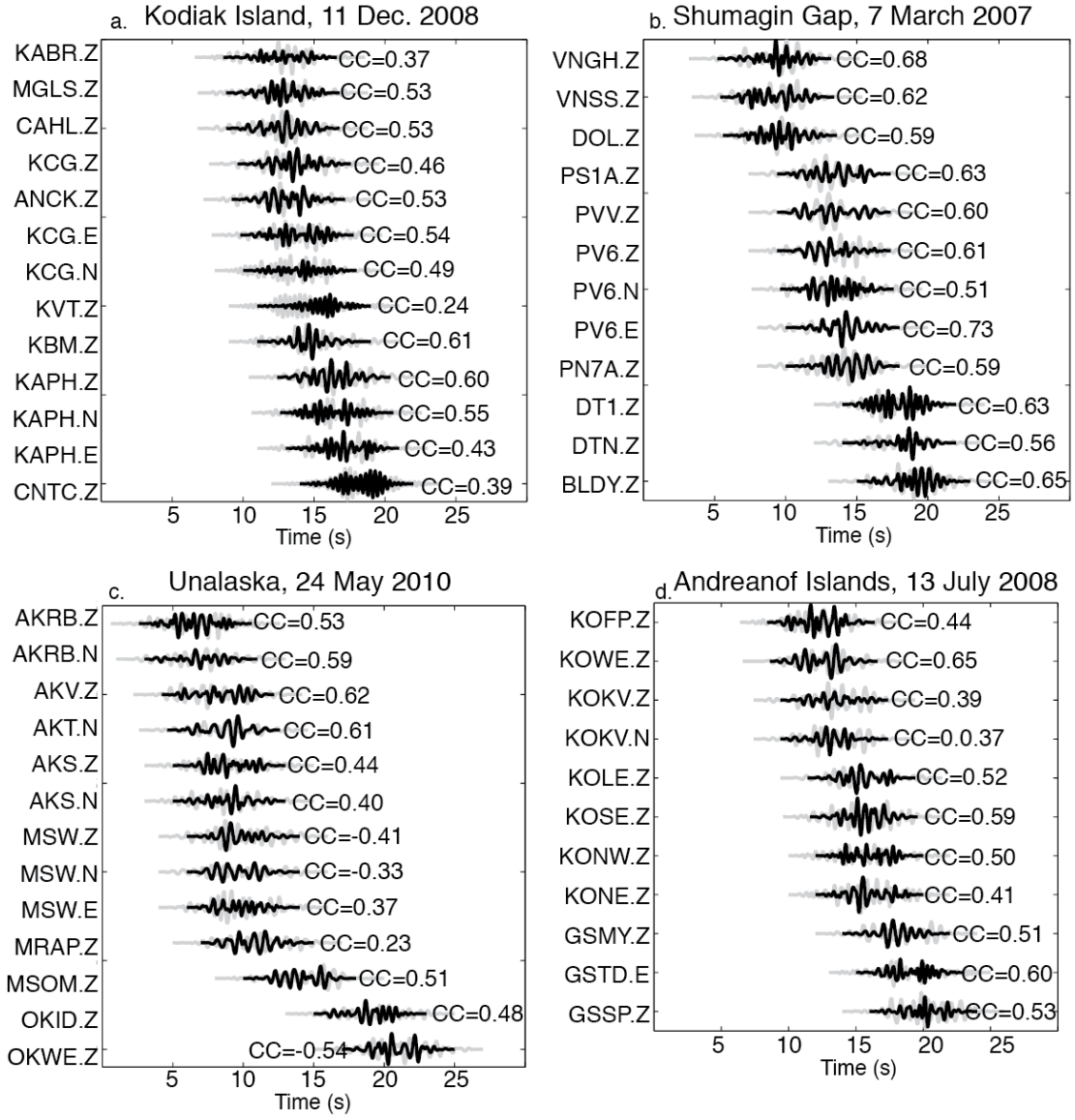

Figure 4.6. Waveform cross-correlation and moveout. 8-second stacked windows of LFEs at a common station at a) Kodiak Island, b) the Shumagin Gap, c) Unalaska, and d) Andreanof Islands. LFE waveforms in continuous data are shown in the background in gray. Correlation coefficients of the continuous data vs. the stack are shown to the right of the data.

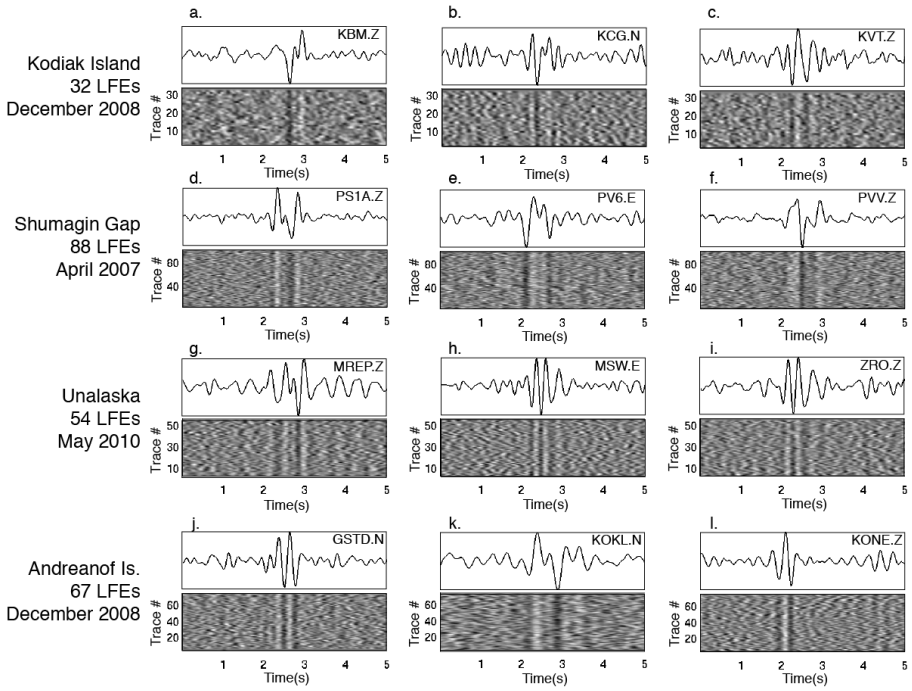

Figure 4.7. Waveform alignments and stacks. 5-second traces are plotted and aligned on the S-wave pick from cross-correlation and shown in grayscale (black = -1 and white = +1 amplitude) to demonstrate the detection of the S-phase arrival. Top traces show the corresponding stack.

LOW FREQUENCY EARTHQUAKE LOCATION

I use the program *hypoDD* [*Waldhauser and Ellsworth,* 2000] to estimate event locations assuming a fixed velocity model from the AEIC [*Hauksson,* 1985; *Ruppert et al.,* 2011] using relative *S* arrival time measurements. *S*-wave arrival time are automated by first choosing the peak amplitude of the absolute value of cross-correlation window pairs on all components. Next, I search for *P*-wave arrivals by cross-correlating 8-second window segments prior to the *S*-wave pick on all channels and choose the peak amplitude within the modified window with the requirement that a pick is more than 2 seconds behind the *S* arrival. This requirement ensures that any emergent *S* arrivals are not mispicked as *P* waves. Unfortunately, I am unable to

identify a set of repeating *P* waves that are coherent across an entire network. This poses a challenge for determining an initial starting location.

The *hypoDD* code can determine hypocenter locations from differenced arrival times measured by cross-correlation given a starting location for all events. Since the starting locations for LFEs are unknown, we assumed 45 different candidate starting locations (Table 4.2) assuming all events are initially located at an assumed centroid in a grid within the four regions we find tremor-like signals. This approach is reasonable given the relatively small dimension of each region along the Alaska-Aleutian Arc. The LSQR option of *hypoDD* was used to iteratively minimize the residuals between observed and calculated travel-time differences and assess the quality of each starting location with respect to final locations. Despite differing starting locations for each run in each region, *hypoDD* returned a common solution (with differences in depth of less than 5 km) and where the errors of the LFE hypocenters matched those of double-differenced local earthquake relocations [*Ruppert et al.,* 2011], so the results are not sensitive to the assumed starting location. This also verifies the differential times from cross-correlation are *S* waves, consistent with observation that the majority of the energy of LFEs from tremor are from *S*-waves [*Shelly, et al.,* 2006].

Table 4.2 Starting locations for LFEs. Region is italicized followed by depths. First column is longitude, second column is latitude.

Kodiak Island: 25, 40, 55, 70 and 85 km depth
-153.00 58.50
-152.50 58.00
-152.00 57.50
-154.00 58.25
-153.50 57.75
-153.00 57.25
-155.00 58.00
-154.50 57.50
-154.00 57.00

Shumagin Gap 20, 35, 50, 65 and 80 km depth
-159.00 56.00
-158.50 55.50
-158.00 55.00
-161.50 55.50
-161.00 55.00
-160.50 54.50
-164.00 55.00
-163.50 54.50
-163.00 64.00

Unalaska 20, 35, 50, 65 and 80 km depth
-168.00 53.50
-167.50 53.00
-167.00 52.50
-167.00 54.00
-166.50 53.50
-166.00 53.00
-166.00 54.50
-165.50 54.00
-165.00 53.50

Andreanof Islands 35, 50, 65 80 and 95 km depth
-174.00 52.00
-174.00 51.50
-174.00 51.00
-176.00 52.00
-176.00 51.50
-176.00 51.00
-178.00 52.00
-178.00 51.50
-178.00 51.00

There are several factors that contribute to uncertainty in the event locations. The first arises from *S*-wave arrival time measurements. The second source of error is from the uncertainty in the velocity structure. The errors reported for the hypocentral parameters are almost certainly underestimates [*Waldhauser and Ellsworth,* 2000]. Another source of uncertainty is the lack of quality *P*-wave arrivals. Given the limitations of the station geometry in this region we find our approach is adequate to identify and characterize deep LFEs within tectonic tremor.

LFE swarms within tremor are identified in four main regions between 2005 and 2010: Kodiak Island; the Alaska Peninsula near the Shumagin Gap; the East Aleutian Islands near Unalaska; and the Andreanof Islands near the towns of Adak and Atka.

Kodiak Island

I detect 156 LFEs within the six 20-minute tremor episodes listed in Table 4.1 in the vicinity of Kodiak Island using data from a combination of stations operated by the Alaska Earthquake Information Center (AEIC) operated by the University of Alaska at Fairbanks and the Katmai Volcanic Field operated by the AVO. To estimate LFE locations I used 72,628 *S*-wave cross-correlation derived differential times as input to the *hypoDD* algorithm with the AEIC velocity model used to locate earthquakes. The locations converge to approximately the same solutions indicating that our results are not sensitive to the initial locations.

LFEs epicenters in this area are concentrated on the north shore of Kodiak Island (Figure 8) at depths between 45 and 60 km. These events occur during January 2007, May 2008, and December 2008 (Table 4.3). In cross-section the locations form a cloud of seismicity that encompasses estimates of the subducting plate interface in this region from geodetic studies and elastic dislocation models [*Zweck et al.,* 2002]. The locations of these LFEs are concentrated at the best estimate of the down-dip edge of the 1964 M_w 9.2 earthquake. This is consistent with hypothesis that tremor and slow slip reflect persistent frictional differences along the dip direction of the plate interface. This region includes the shallowest LFEs we report in this study.

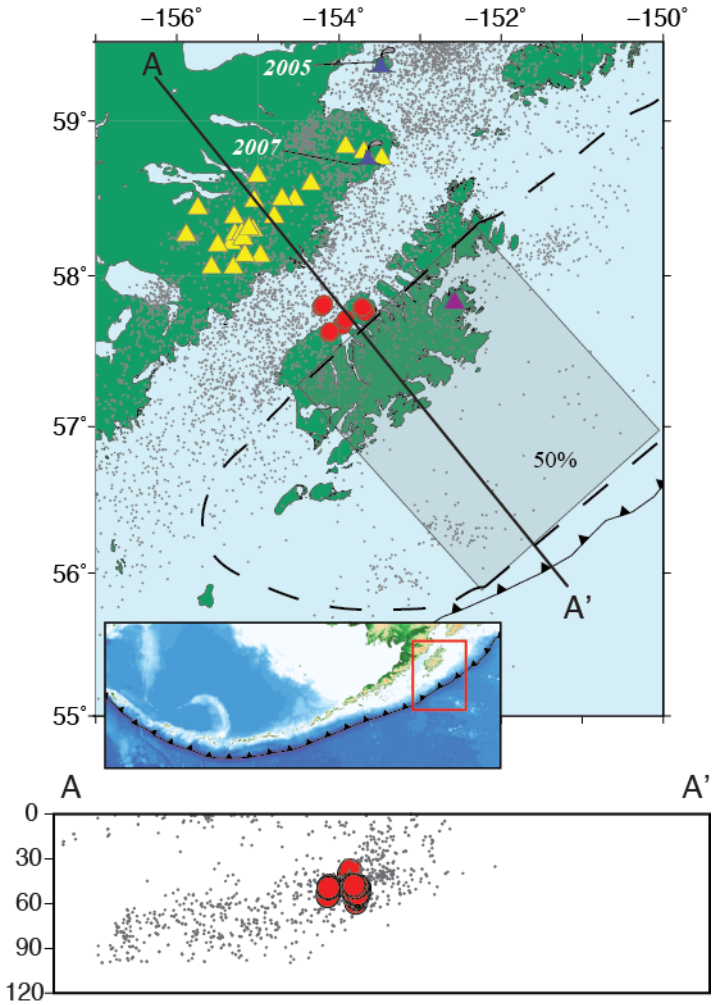

Figure 4.8. Map view and cross-sections of low-frequency earthquakes from tremor on Kodiak Island. LFEs are shown in red. Yellow triangles are stations operated by the AVO. The purple triangle is a station operated by the AEIC. Gray dots are earthquake hypocenters of M_w 4 and higher from 2005-2010. The black box denotes the Kodiak asperity which ruptured during the 1964 M_w 9.2 earthquake (Christensen and Beck, 1994) and its northwestern side marks down-dip rupture limit. The estimate of plate interface coupling up-dip of the LFEs is 50% (Zweck et al, 2002). Active volcanoes during the study are shown as violet volcano symbols.

Table 4.3

Year Month Day Hour Minute Second Latitude Longitude Depth

2007 1 31 13 15 17.83 57.867 -153.67 49.523
2007 1 31 13 15 29.44 57.872 -153.68 48.293
2007 1 31 13 15 40.11 57.872 -153.67 49.573
2007 1 31 13 15 54.82 57.864 -153.67 49.884
2007 1 31 13 16 54.16 57.863 -153.66 59.481

2007 1 31 13 17 24.57 57.865 -153.68 49.847
2007 1 31 13 17 33.57 57.868 -153.67 49.406
2007 1 31 13 17 44.58 57.865 -153.67 49.496
2007 1 31 13 17 53.87 57.865 -153.67 49.667
2007 1 31 13 18 4.94 57.864 -153.68 49.671
2007 1 31 13 18 27.36 57.86 -153.68 48.6
2007 1 31 13 18 39.42 57.872 -153.67 49.37
2007 1 31 13 18 51.75 57.866 -153.67 49.779
2007 1 31 13 19 0.86 57.868 -153.67 49.892
2007 1 31 13 19 14.17 57.873 -153.67 49.409
2007 1 31 13 19 25.06 57.859 -153.69 59.728
2007 1 31 13 19 56.67 57.862 -153.68 49.757
2007 1 31 13 20 16.72 57.867 -153.67 49.298
2007 1 31 13 20 26.61 57.864 -153.68 48.798
2007 1 31 13 20 36.18 57.861 -153.68 49.738
2007 1 31 13 21 4.26 57.863 -153.69 49.832
2007 1 31 13 21 13.35 57.863 -153.68 49.246
2007 1 31 13 21 38.2 57.861 -153.68 49.483
2007 1 31 13 22 18.94 57.867 -153.67 49.719
2007 1 31 13 22 43.5 57.867 -153.66 49.881
2007 1 31 13 23 14.04 57.87 -153.67 49.583
2007 1 31 13 23 24.88 57.874 -153.67 50.015
2007 1 31 13 23 38.71 57.863 -153.68 49.529
2008 5 27 4 30 31.11 57.9 -154.21 49.89
2008 5 27 4 32 17.2 57.9 -154.22 54.498
2008 5 27 4 32 29.88 57.9 -154.21 49.506
2008 5 27 4 32 46.8 57.899 -154.2 49.072
2008 5 27 4 33 41.67 57.905 -154.19 48.102
2008 5 27 4 34 0.43 57.908 -154.19 48.981
2008 5 27 4 34 12.53 57.909 -154.2 49.504
2008 5 27 4 34 37.04 57.9 -154.21 49.717
2008 5 27 4 34 49.95 57.907 -154.2 49.789
2008 5 27 4 35 11.15 57.901 -154.2 48.083
2008 5 27 4 35 20.61 57.901 -154.21 53.361
2008 5 27 4 35 30.44 57.908 -154.2 53.055
2008 5 27 4 35 55.55 57.906 -154.2 49.257
2008 5 27 4 36 10.16 57.903 -154.2 49.861
2008 5 27 4 36 29.83 57.894 -154.22 54.06
2008 5 27 4 36 40.17 57.9 -154.21 49.122
2008 5 27 4 37 0.9 57.897 -154.22 49.356
2008 5 27 4 37 12.34 57.913 -154.18 49.414
2008 5 27 4 37 24.69 57.91 -154.19 53.729
2008 5 27 4 37 34.21 57.914 -154.2 55.057
2008 5 27 4 37 48.35 57.911 -154.19 49.955
2008 5 27 4 38 2.78 57.905 -154.2 49.458
2008 5 27 4 38 13.76 57.906 -154.2 49.705
2008 5 27 4 38 25.29 57.903 -154.2 49.952
2008 5 27 4 38 37.12 57.902 -154.21 53.438
2008 5 27 4 38 52.45 57.895 -154.22 49.832
2008 5 27 4 39 7.07 57.9 -154.21 49.388
2008 5 27 4 39 28.63 57.906 -154.19 52.667
2008 5 27 4 39 48.01 57.907 -154.2 52.043
2008 5 27 4 40 3.69 57.894 -154.21 47.772

2008 5 27 4 40 22.17 57.904 -154.19 48.479
2008 5 27 4 40 53.8 57.904 -154.19 49.406
2008 5 27 4 41 4.7 57.902 -154.21 49.318
2008 5 27 4 41 28.41 57.894 -154.22 49.608
2008 5 27 4 42 10.42 57.91 -154.19 53.124
2008 5 27 4 42 31.13 57.904 -154.2 49.851
2008 5 27 4 42 46.13 57.916 -154.19 52.972
2008 5 27 4 43 11.52 57.909 -154.21 51.495
2008 5 27 4 43 26.86 57.91 -154.19 49.966
2008 5 27 4 43 38.73 57.909 -154.21 55.371
2008 5 27 4 43 56.31 57.9 -154.2 49.833
2008 5 27 4 45 5.04 57.91 -154.2 49.373
2008 5 27 4 45 14.85 57.917 -154.18 52.059
2008 5 27 4 45 28.25 57.905 -154.19 49.428
2008 12 10 16 6 56.49 57.885 -153.72 49.756
2008 12 10 16 8 22.8 57.893 -153.72 47.217
2008 12 10 16 8 54.46 57.892 -153.72 49.443
2008 12 10 16 9 24.64 57.9 -153.72 39.902
2008 12 10 16 9 39.48 57.894 -153.72 49.51
2008 12 10 16 10 11.75 57.896 -153.71 49.685
2008 12 10 16 10 29.33 57.893 -153.72 49.82
2008 12 10 16 10 41.58 57.897 -153.72 49.396
2008 12 10 16 10 52.49 57.886 -153.72 49.749
2008 12 10 16 11 20.71 57.885 -153.72 37.436
2008 12 10 16 11 43.1 57.89 -153.72 49.843
2008 12 10 16 12 6.83 57.892 -153.73 47.479
2008 12 10 16 12 17.25 57.894 -153.71 49.498
2008 12 10 16 13 50.73 57.891 -153.71 49.969
2008 12 11 3 17 34.51 57.782 -153.96 54.628
2008 12 11 3 17 48.65 57.781 -153.95 52.039
2008 12 11 3 19 45.95 57.781 -153.95 54.872
2008 12 11 3 19 55.8 57.777 -153.96 48.804
2008 12 11 3 20 15.59 57.778 -153.95 52.977
2008 12 11 3 20 24.89 57.776 -153.96 54.55
2008 12 11 3 20 53.32 57.781 -153.96 56.626
2008 12 11 3 21 15.86 57.777 -153.96 53.737
2008 12 11 3 21 57.88 57.772 -153.96 53.156
2008 12 11 3 22 32.06 57.778 -153.95 52.767
2008 12 11 3 23 33.81 57.778 -153.96 54.04
2008 12 11 3 23 44.72 57.777 -153.96 51.948
2008 12 11 3 24 51.73 57.776 -153.96 54.46
2008 12 11 3 25 9.64 57.779 -153.96 48.362
2008 12 11 3 26 6.23 57.775 -153.96 49.058
2008 12 11 3 26 26.55 57.775 -153.96 49.545
2008 12 11 3 26 43.59 57.778 -153.96 53.922
2008 12 11 3 26 52.79 57.78 -153.96 49.2
2008 12 11 3 27 9.32 57.774 -153.96 49.847
2008 12 11 3 27 40.37 57.773 -153.96 51.951
2008 12 11 3 27 59.54 57.783 -153.96 57.306
2008 12 11 3 28 23.01 57.777 -153.95 49.595
2008 12 11 3 33 7.86 57.815 -153.91 47.942
2008 12 11 3 33 37.37 57.808 -153.92 48.386
2008 12 11 3 33 48.74 57.814 -153.92 48.686

2008 12 11 3 34 0.67 57.814 -153.92 47.178
2008 12 11 3 34 55.06 57.817 -153.92 48.889
2008 12 11 3 35 6.86 57.805 -153.92 48.119
2008 12 11 3 35 29.24 57.814 -153.92 53.244
2008 12 11 3 35 49.94 57.808 -153.93 50.988
2008 12 11 3 36 26.4 57.811 -153.92 48.155
2008 12 11 3 36 48.97 57.809 -153.92 53.358
2008 12 11 3 36 58.5 57.811 -153.92 54.775
2008 12 11 3 37 15.91 57.811 -153.92 49.795
2008 12 11 3 37 33.99 57.811 -153.92 49.948
2008 12 11 3 38 21.51 57.814 -153.92 48.777
2008 12 11 3 38 43.64 57.811 -153.93 48.506
2008 12 11 3 39 49.17 57.815 -153.92 48.908
2008 12 11 3 40 7.01 57.811 -153.92 47.775
2008 12 11 3 40 39.05 57.813 -153.92 47.779
2008 12 11 19 42 25.02 57.732 -154.12 48.706
2008 12 11 19 42 38.49 57.723 -154.11 49.834
2008 12 11 19 42 57.87 57.731 -154.12 48.451
2008 12 11 19 43 33.05 57.72 -154.13 49.47
2008 12 11 19 44 28.9 57.734 -154.1 48.848
2008 12 11 19 44 40.72 57.723 -154.12 48.004
2008 12 11 19 45 6.52 57.734 -154.12 48.968
2008 12 11 19 45 18.35 57.73 -154.11 49.153
2008 12 11 19 46 35.46 57.736 -154.1 48.544
2008 12 11 19 46 49.71 57.733 -154.12 48.179
2008 12 11 19 47 14.31 57.727 -154.12 48.481
2008 12 11 19 47 27.35 57.724 -154.12 49.411
2008 12 11 19 48 12.75 57.736 -154.11 49.921
2008 12 11 19 48 24.07 57.726 -154.13 49.211
2008 12 11 19 49 1.84 57.738 -154.11 49.267
2008 12 11 19 49 18.8 57.727 -154.11 52.24
2008 12 11 19 49 36.16 57.727 -154.12 48.658
2008 12 11 19 50 14.06 57.73 -154.12 48.842
2008 12 11 19 50 55.84 57.729 -154.12 48.542
2008 12 11 19 51 45.93 57.722 -154.13 48.656
2008 12 11 19 52 32.2 57.731 -154.11 52.275
2008 12 11 19 53 27 57.727 -154.12 49.149
2008 12 11 19 53 46.57 57.734 -154.1 48.667
2008 12 11 19 54 49.9 57.737 -154.11 48.436
2008 12 11 19 55 19.97 57.734 -154.11 48.978
2008 12 11 19 56 4.78 57.728 -154.12 49.355
2008 12 11 19 56 13.8 57.722 -154.12 49.904
2008 12 11 19 57 27.34 57.736 -154.1 55.397
2008 12 11 19 58 9.59 57.722 -154.11 53.072
2008 12 11 19 58 39.66 57.734 -154.11 48.748

Shumagin Gap

I detect 151 LFEs during two bursts of tremor activity in vicinity of the Shumagin Islands (Table 4.1) using data operated by the AVO. Using the same techniques and assumptions

for Kodiak Island, we estimated locations using 141,090 *S*-wave cross-correlation derived differential times.

LFE epicenters in this area are concentrated on the south shore of the peninsula at depths between 50 and 60 km (Figure 4.9) and occur during April 2007 and March 2010 (Table 4.4). The locations with depth form two clouds of seismicity that encompass the best estimate of the subducting plate interface in this region. The two groups are also located in areas where the degree of coupling from east to west significantly decreases along strike. The east group of LFEs is concentrated at the best estimate of the west down-dip edge of the 1938 M_w 8.0 earthquake, though this location is highly uncertain. Up-dip of the LFEs the degree of coupling on the plate interface is around 30% [*Founier and Freymueller,* 2007] and is located east of the 1993 Ms 6.9 earthquake [*Abers, et al.,* 1995]. The west cloud is located in a patch of the Alaska-Aleutian Arc that has not ruptured in a M_w 7.0+ earthquake in the last 150 years referred to as the Shumagin Gap, where the degree of coupling is close to 0%. Geodetic measurements show the plate interface to be freely sliding [*Freymueller et al.,* 2008]. Although the possible role of tremor activity with respect to the seismic gap is uncertain, it motivates future investigations to understand the nature of deformation in this area.

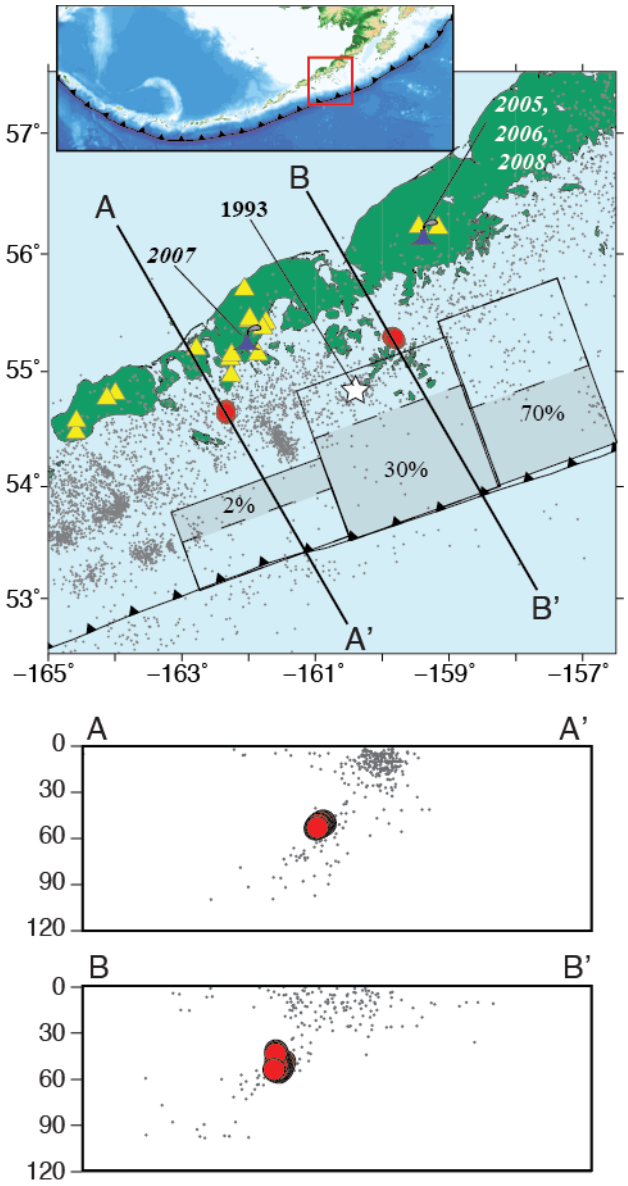

Figure 4.9. Map view and cross-sections of low-frequency earthquakes from tremor at the Shumagin Gap. Symbols are the same as in Figure 8. Variability in the degree of plate interface coupling is shown in the black boxes (Fournier and Freymueller, 2007).

Table 4.4

Year Month Day Hour Minute Second Latitude Longitude Depth

2007 4 7 18 14 19.69 55.496 -159.83 52.925
2007 4 7 18 14 28.67 55.499 -159.83 48.333
2007 4 7 18 14 46.01 55.489 -159.82 49.808
2007 4 7 18 14 58.97 55.479 -159.8 53.668
2007 4 7 18 15 7.91 55.465 -159.78 48.284

2007 4 7 18 15 17.79 55.487 -159.82 49.976
2007 4 7 18 15 29.79 55.489 -159.82 52.909
2007 4 7 18 15 42.6 55.492 -159.84 47.135
2007 4 7 18 15 51.83 55.492 -159.83 51.211
2007 4 7 18 16 2.82 55.48 -159.81 50.01
2007 4 7 18 16 13.96 55.478 -159.81 51.375
2007 4 7 18 16 24.27 55.479 -159.8 51.616
2007 4 7 18 16 34.07 55.476 -159.8 49.681
2007 4 7 18 16 50.02 55.493 -159.83 50.156
2007 4 7 18 17 1.42 55.483 -159.81 53.176
2007 4 7 18 17 10.68 55.491 -159.82 53.275
2007 4 7 18 17 23.43 55.487 -159.82 49.594
2007 4 7 18 17 32.6 55.477 -159.82 51.574
2007 4 7 18 17 48 55.487 -159.82 50.708
2007 4 7 18 17 59.11 55.48 -159.82 52.743
2007 4 7 18 18 10.25 55.495 -159.83 48.745
2007 4 7 18 18 20.27 55.496 -159.87 41.727
2007 4 7 18 18 31.06 55.465 -159.8 50.241
2007 4 7 18 18 43.09 55.495 -159.82 48.75
2007 4 7 18 18 54.08 55.503 -159.84 53.268
2007 4 7 18 19 2.92 55.492 -159.82 48.685
2007 4 7 18 19 17.97 55.506 -159.84 53.392
2007 4 7 18 19 35.67 55.489 -159.81 50
2007 4 7 18 19 44.83 55.483 -159.81 50.795
2007 4 7 18 19 54.48 55.483 -159.81 53.506
2007 4 7 18 20 5.43 55.484 -159.8 51.177
2007 4 7 18 20 17.98 55.487 -159.82 51.759
2007 4 7 18 20 29.52 55.492 -159.82 51.497
2007 4 7 18 20 39.65 55.495 -159.83 50.889
2007 4 7 18 20 51.82 55.499 -159.83 51.049
2007 4 7 18 21 4.84 55.492 -159.84 46.729
2007 4 7 18 21 14.05 55.488 -159.82 52.817
2007 4 7 18 21 23.52 55.488 -159.81 52.802
2007 4 7 18 21 32.72 55.485 -159.82 52.232
2007 4 7 18 21 41.79 55.477 -159.81 49.877
2007 4 7 18 21 51.23 55.496 -159.84 53.612
2007 4 7 18 22 0.5 55.489 -159.81 49.562
2007 4 7 18 22 11.86 55.491 -159.82 50.611
2007 4 7 18 22 24.9 55.51 -159.86 53.677
2007 4 7 18 22 33.6 55.503 -159.83 53.242
2007 4 7 18 22 43.23 55.48 -159.8 53.964
2007 4 7 18 22 56.34 55.498 -159.83 50.118
2007 4 7 18 23 10.17 55.502 -159.84 48.194
2007 4 7 18 23 19.35 55.491 -159.86 42.341
2007 4 7 18 23 36.88 55.48 -159.81 52.108
2007 4 7 18 23 46.44 55.476 -159.79 52.457
2007 4 7 18 24 0.32 55.49 -159.83 53.745
2007 4 7 18 24 9.24 55.488 -159.83 48.132
2007 4 7 18 24 20.8 55.487 -159.81 50.802
2007 4 7 18 24 31.18 55.492 -159.81 50.781
2007 4 7 18 24 42.56 55.48 -159.82 51.986
2007 4 7 18 24 55.12 55.479 -159.82 47.635
2007 4 7 18 25 6.65 55.487 -159.81 53.184

2007 4 7 18 25 15.64 55.491 -159.81 49.768
2007 4 7 18 25 26.65 55.488 -159.82 53.958
2007 4 7 18 25 35.64 55.491 -159.81 55.251
2007 4 7 18 25 45.3 55.489 -159.82 53.239
2007 4 7 18 25 54.45 55.483 -159.82 53.381
2007 4 7 18 26 4.64 55.488 -159.82 52.008
2007 4 7 18 26 14.07 55.495 -159.83 53.138
2007 4 7 18 26 23.25 55.498 -159.83 50.64
2007 4 7 18 26 38.27 55.48 -159.81 53.634
2007 4 7 18 26 51.2 55.486 -159.81 51.688
2007 4 7 18 27 0.4 55.48 -159.81 50.307
2007 4 7 18 27 12.18 55.473 -159.79 51.573
2007 4 7 18 27 23.01 55.488 -159.82 53.844
2007 4 7 18 27 35.4 55.488 -159.82 50.36
2007 4 7 18 27 44.96 55.508 -159.84 54.642
2007 4 7 18 27 57.92 55.492 -159.83 49.249
2007 4 7 18 28 12.99 55.501 -159.83 53.42
2007 4 7 18 28 23.39 55.48 -159.81 49.83
2007 4 7 18 28 39.83 55.489 -159.82 50.774
2007 4 7 18 28 50.4 55.479 -159.81 51.51
2007 4 7 18 29 5.61 55.493 -159.81 53.228
2007 4 7 18 29 16.19 55.48 -159.8 51.701
2007 4 7 18 29 26.02 55.493 -159.83 54.144
2007 4 7 18 29 49.23 55.488 -159.83 50.802
2007 4 7 18 30 2.11 55.484 -159.81 51.77
2007 4 7 18 30 10.92 55.48 -159.81 48.505
2007 4 7 18 30 31.83 55.492 -159.81 50.019
2007 4 7 18 30 43.65 55.489 -159.82 52.688
2007 4 7 18 30 58.41 55.477 -159.81 49.978
2007 4 7 18 31 17.68 55.497 -159.87 43.342
2007 4 7 18 31 30.48 55.483 -159.82 51.154
2007 4 7 18 31 39.83 55.48 -159.8 51.138
2007 4 7 18 31 58.07 55.496 -159.82 48.141
2007 4 7 18 32 19.65 55.493 -159.83 47.431
2007 4 7 18 32 33.48 55.49 -159.81 48.706
2007 4 7 18 32 43.71 55.492 -159.81 50.31
2007 4 7 18 33 4.15 55.493 -159.81 49.987
2007 4 7 18 33 19.19 55.481 -159.8 53.04
2007 4 7 18 33 28.66 55.49 -159.81 51.582
2010 3 25 29 32 40.19 54.852 -162.34 52.541
2010 3 25 29 32 49.59 54.852 -162.34 51.519
2010 3 25 29 33 15.15 54.869 -162.35 52.85
2010 3 25 29 33 48.63 54.858 -162.33 52.345
2010 3 25 29 34 4.33 54.874 -162.34 53.594
2010 3 25 29 34 14.89 54.851 -162.32 51.55
2010 3 25 29 34 33.36 54.849 -162.34 51.117
2010 3 25 29 34 44.72 54.855 -162.35 51.158
2010 3 25 29 35 14.62 54.854 -162.35 52.025
2010 3 25 29 35 28.63 54.879 -162.34 53.322
2010 3 25 29 35 41.3 54.849 -162.34 50.416
2010 3 25 29 35 56.11 54.846 -162.34 50.812
2010 3 25 29 36 5.46 54.851 -162.34 51.204
2010 3 25 29 36 16.88 54.848 -162.33 52.267

2010 3 25 29 36 31.77 54.858 -162.33 51.874
2010 3 25 29 36 41.77 54.837 -162.33 50.435
2010 3 25 29 37 10.28 54.859 -162.35 51.65
2010 3 25 29 37 24.14 54.827 -162.34 49.004
2010 3 25 29 37 33.64 54.843 -162.34 49.573
2010 3 25 29 37 56.48 54.837 -162.34 49.439
2010 3 25 29 38 11 54.853 -162.34 49.882
2010 3 25 29 38 29.28 54.852 -162.34 52.468
2010 3 25 29 39 5.75 54.827 -162.33 50.844
2010 3 25 29 39 32.51 54.841 -162.33 50.646
2010 3 25 29 39 42.47 54.862 -162.34 52.383
2010 3 25 29 39 51.72 54.862 -162.35 51.098
2010 3 25 29 40 5.81 54.854 -162.35 50.585
2010 3 25 29 40 19.22 54.862 -162.34 51.335
2010 3 25 29 40 42.05 54.846 -162.34 51.212
2010 3 25 29 40 57.32 54.844 -162.34 50.895
2010 3 25 29 41 14.11 54.877 -162.35 52.484
2010 3 25 29 41 40.38 54.844 -162.34 50.854
2010 3 25 29 41 55.41 54.83 -162.33 49.926
2010 3 25 29 42 5.06 54.862 -162.34 51.236
2010 3 25 29 42 22.97 54.848 -162.33 51.003
2010 3 25 29 42 53.1 54.859 -162.34 51.416
2010 3 25 29 43 17.8 54.834 -162.34 48.754
2010 3 25 29 43 50.74 54.85 -162.33 50.89
2010 3 25 29 44 17.68 54.856 -162.34 50.349
2010 3 25 29 44 45.51 54.865 -162.34 52.005
2010 3 25 29 45 6.15 54.85 -162.33 52.249
2010 3 25 29 45 22.53 54.864 -162.34 51.618
2010 3 25 29 45 48.55 54.862 -162.34 51.892
2010 3 25 29 46 1.24 54.855 -162.34 51.981
2010 3 25 29 46 12.25 54.825 -162.34 49.452
2010 3 25 29 46 35.39 54.871 -162.35 52.348
2010 3 25 29 46 56.29 54.882 -162.34 53.903
2010 3 25 29 47 7.57 54.835 -162.33 49.906
2010 3 25 29 48 3.87 54.873 -162.34 52.724
2010 3 25 29 48 18.59 54.868 -162.35 51.389
2010 3 25 29 48 32.42 54.824 -162.32 49.814
2010 3 25 29 49 42.11 54.83 -162.33 49.83
2010 3 25 29 49 52.3 54.835 -162.35 49.911
2010 3 25 29 50 1.8 54.851 -162.34 51.982

Unalaska

I detect 278 LFEs in vicinity of East Aleutians during eight 20-minute tremor episodes (Table 4.1) using data from a combination of stations on Umnak, Unalaska and Akutan Islands operated by AVO. These stations are primarily used to monitor volcanic activity at Okmok, Makushin and Akutan volcanoes. The volcanoes in this area of the arc have

recently been the most seismically active including one eruption at Okmok Caldera in 2008. I used 196,156 S-wave cross-correlation derived differential times to locate the LFEs.

LFE epicenters in this area are concentrated trench-ward of the arc at depths between 50 and 65 km. The tremor in this area occurs during May 2007, September 2008, November 2008, February 2009, and May 2010 (Table 4.5). The locations with depth form some of the sharpest lineations of seismicity compared to Kodiak Island and the Shumagin Gap and are concentrated at the best estimate of the downdip edge of the 1957 M_w 8.6 earthquake. Although the depths are greater, this is consistent with models of tremor and slow slip representing frictional differences along the dip direction of the plate interface. Tremor activity is the most frequent in this part of the arc.

.

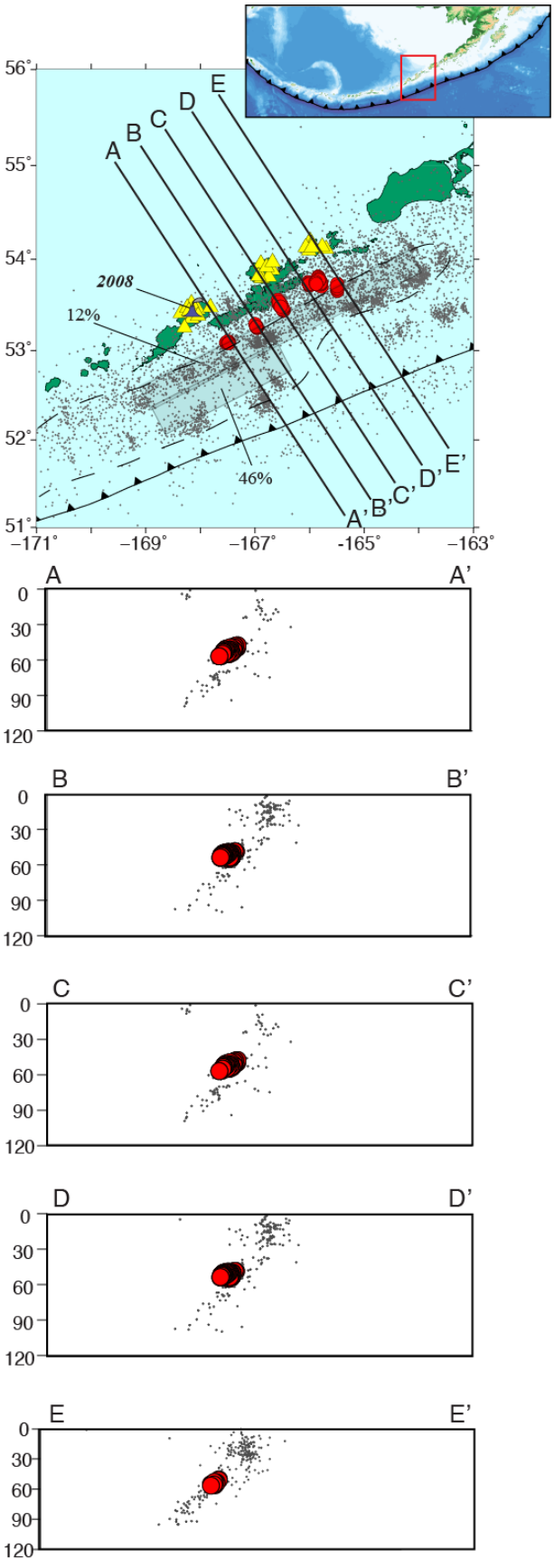
56°
55°
54°
53°
52°
51°
−171°
−169°
−167°
-165°
−163°
A
B
C
D
E
A'
B'
C'
D'
E'
2008
12%
46%
A
A'
B
B'
C
C'
D
D'
E
E'
0
30
60
90
120

Figure 4.10. Map view and cross-sections of low-frequency earthquakes from tremor near Unalaska. Symbols are the same as in Figure 8. The amber dashed line is an estimate of down-dip rupture limit for the 1957 M_w 8.6 earthquake. Variability in the degree of plate interface coupling is shown in the black boxes (Cross and Freymueller, 2008).

The degree of plate interface coupling trench-ward of the LFE hypocenters in this region is complex both in the along-strike and along-dip directions [*Cross and Freymueller,* 2008]. Plate interface coupling decreases from ~46% up-dip down to ~12% at the down-dip extent of the seismogenic zone in vicinity of the two westernmost streaks of LFEs (Figure 4.10). For the remaining three streaks, the degree of coupling at the down-dip extent remains ~12% whereas the up-dip extent decreases to 0% as it approaches the Shumagin Gap region further northeast along strike of the subduction zone [*Cross and Freymueller,* 2008]. Despite these changes along strike and dip, tremor appears to span a range of coupling behaviors in this region

Table 4.5

Year Month Day Hour Minute Second Latitude Longitude Depth

2007 5 9 5 50 6.78 53.855 -165.9 57.859
2007 5 9 5 50 12.29 53.831 -165.88 54.824
2007 5 9 5 50 18.22 53.84 -165.88 55.806
2007 5 9 5 50 27.83 53.833 -165.88 55.334
2007 5 9 5 50 34.36 53.834 -165.88 55.531
2007 5 9 5 51 8.44 53.83 -165.88 55.091
2007 5 9 5 51 13.98 53.825 -165.87 54.98
2007 5 9 5 51 23.90 53.832 -165.89 54.608
2007 5 9 5 51 31.45 53.832 -165.88 55.054
2007 5 9 5 52 1.45 53.841 -165.88 56.65
2007 5 9 5 52 7.35 53.841 -165.88 55.831
2007 5 9 5 52 13.17 53.845 -165.89 56.42
2007 5 9 5 52 18.91 53.838 -165.89 55.063
2007 5 9 5 52 24.80 53.836 -165.89 55.193
2007 5 9 5 52 30.27 53.842 -165.89 55.419
2007 5 9 5 52 35.98 53.854 -165.88 58.476
2007 5 9 5 53 5.69 53.843 -165.89 55.361
2007 5 9 5 53 12.39 53.83 -165.88 55.341
2008 9 27 6 44 10.3 53.29 -167.47 54.317
2008 9 27 6 44 20.15 53.284 -167.5 54.339

2008 9 27 6 44 29.72 53.279 -167.5 52.394
2008 9 27 6 44 48.37 53.287 -167.54 56.276
2008 9 27 6 45 42.39 53.293 -167.52 55.486
2008 9 27 6 46 6.45 53.289 -167.48 54.421
2008 9 27 6 49 59.79 53.278 -167.48 53.953
2008 9 27 6 50 15.3 53.287 -167.48 53.525
2008 9 27 6 50 28.55 53.298 -167.48 53.743
2008 9 27 6 50 39.52 53.306 -167.5 54.75
2008 9 27 6 50 54.66 53.288 -167.48 54.254
2008 9 27 6 52 43.16 53.284 -167.5 55.198
2008 9 27 6 55 31.64 53.282 -167.49 54.257
2008 9 27 6 55 41.34 53.285 -167.49 53.803
2008 9 27 6 55 50.31 53.281 -167.48 54.025
2008 11 7 20 58 45.67 53.833 -166.01 56.753
2008 11 7 20 59 5.37 53.826 -166.01 56.043
2008 11 7 20 59 27.84 53.833 -166 57.611
2008 11 7 20 59 37.24 53.836 -166.02 57.081
2008 11 7 21 0 3.19 53.836 -166.02 56.927
2008 11 7 21 0 17.8 53.829 -166.01 56.405
2008 11 7 21 0 30.2 53.825 -166.01 56.534
2008 11 7 21 0 49.2 53.825 -166 56.065
2008 11 7 21 1 21.23 53.834 -166.01 56.931
2008 11 7 21 1 32.8 53.838 -166.01 57.907
2008 11 7 21 2 48.07 53.815 -166 55.017
2008 11 7 21 3 22.74 53.824 -166 56.9
2008 11 7 21 3 43.16 53.827 -166 56.915
2008 11 7 21 4 39.24 53.841 -166.02 57.411
2008 11 7 21 5 20.4 53.838 -166.02 57.505
2008 11 7 21 5 31.82 53.828 -166.01 56.347
2008 11 7 21 5 58.61 53.827 -166.01 55.842
2008 11 7 21 6 8.93 53.833 -166.02 56.298
2008 11 7 21 6 23.96 53.814 -166 55.586
2008 11 7 21 6 35.87 53.838 -166.01 57.268
2008 11 7 21 6 53.18 53.824 -166 56.221
2008 11 7 21 7 2.9 53.855 -166.02 59.32
2008 11 7 21 7 59.57 53.84 -166.01 57.594
2008 11 7 21 8 11.29 53.839 -166.01 58.085
2008 11 7 21 8 41.95 53.83 -166.01 56.806
2008 11 7 21 9 6.16 53.818 -166.01 55.194
2008 11 7 21 9 21.53 53.847 -166.02 57.905
2008 11 7 21 9 32.63 53.828 -166.01 56.55
2008 11 7 21 10 9.84 53.826 -166.01 56.419
2008 11 7 21 10 21.02 53.834 -166.01 57.156
2008 11 7 21 10 38.98 53.83 -166 57.263
2008 11 7 21 10 57.47 53.835 -166.01 56.951
2008 11 7 21 11 32.14 53.833 -166.01 56.903
2008 11 7 21 11 49.31 53.83 -166.01 56.897
2008 11 7 21 50 16.29 53.84 -165.78 58.77
2008 11 7 21 50 47.2 53.857 -165.79 60.596
2008 11 7 21 51 14.43 53.826 -165.79 55.975
2008 11 7 21 51 47.04 53.844 -165.79 58.709
2008 11 7 21 51 59.36 53.848 -165.79 59.214
2008 11 7 21 52 8.47 53.818 -165.79 55.226

2008 11 7 21 52 18.81 53.839 -165.79 59.181
2008 11 7 21 52 31.06 53.834 -165.78 58.946
2008 11 7 21 52 52.56 53.821 -165.78 56.216
2008 11 7 21 53 21.69 53.834 -165.8 57.862
2008 11 7 21 53 33.77 53.84 -165.79 57.497
2008 11 7 21 53 44.2 53.833 -165.78 58.029
2008 11 7 21 53 53.43 53.835 -165.79 57.755
2008 11 7 21 54 11.57 53.805 -165.79 53.908
2008 11 7 21 54 26.79 53.802 -165.78 54.29
2008 11 7 21 54 44.1 53.84 -165.79 58.149
2008 11 7 21 54 53.36 53.834 -165.79 57.661
2008 11 7 21 55 28.45 53.839 -165.79 58.55
2008 11 7 21 55 45.14 53.835 -165.79 58.112
2008 11 7 21 56 20.25 53.83 -165.78 58.206
2008 11 7 21 57 2.71 53.823 -165.8 55.889
2008 11 7 21 57 22.07 53.835 -165.79 58.458
2008 11 7 21 57 34.9 53.833 -165.79 57.385
2008 11 7 21 57 45.37 53.825 -165.8 55.223
2008 11 7 21 57 54.48 53.832 -165.8 56.731
2008 11 7 21 58 5.53 53.836 -165.79 57.143
2008 11 7 21 58 19.4 53.847 -165.79 59.693
2008 11 7 21 58 28.33 53.831 -165.78 58.403
2008 11 7 21 58 40.86 53.836 -165.78 58.288
2008 11 7 21 59 11.07 53.839 -165.79 57.769
2008 11 7 21 59 43.48 53.848 -165.79 59.565
2008 11 7 22 0 1.51 53.837 -165.8 60.114
2008 11 8 1 3 29.3 53.881 -165.84 55.512
2008 11 8 1 3 58.17 53.868 -165.83 55.294
2008 11 8 1 4 14.28 53.877 -165.81 57.474
2008 11 8 1 5 12.96 53.902 -165.85 58.617
2008 11 8 1 5 26.85 53.891 -165.83 57.236
2008 11 8 1 5 37.76 53.883 -165.84 56.211
2008 11 8 1 6 5.45 53.866 -165.82 55.418
2008 11 8 1 6 23.8 53.906 -165.84 58.161
2008 11 8 1 7 7.82 53.915 -165.84 59.472
2008 11 8 1 7 53.1 53.89 -165.84 57.345
2008 11 8 1 8 23.15 53.878 -165.83 55.444
2008 11 8 1 9 31.34 53.882 -165.83 56.605
2008 11 8 1 9 41.81 53.888 -165.84 57.495
2008 11 8 1 10 32.63 53.879 -165.84 55.895
2008 11 8 1 11 22.99 53.903 -165.83 59.176
2008 11 8 1 11 34.16 53.907 -165.85 57.353
2008 11 8 1 11 48.4 53.871 -165.82 56.15
2008 11 8 1 12 23.49 53.901 -165.84 58.537
2008 11 8 1 13 29.04 53.886 -165.84 55.976
2008 11 8 1 14 44.4 53.903 -165.85 56.947
2008 11 8 1 15 15.45 53.886 -165.84 56.862
2008 11 8 1 15 38.81 53.891 -165.85 55.824
2008 11 8 1 16 15.36 53.889 -165.83 56.951
2008 11 8 1 16 36.07 53.904 -165.85 58.523
2008 11 8 1 17 44.41 53.874 -165.84 55.25
2008 11 8 1 17 53.19 53.891 -165.83 57.716
2008 11 8 1 18 8.56 53.878 -165.82 57.786

2008 11 8 1 18 28.91 53.88 -165.83 56.341
2008 11 8 1 18 55.03 53.873 -165.83 55.58
2008 11 8 2 2 20.43 53.467 -166.98 54.447
2008 11 8 2 2 40.06 53.468 -166.98 54.416
2008 11 8 2 2 48.92 53.448 -166.96 53.396
2008 11 8 2 3 50.06 53.458 -166.97 54.145
2008 11 8 2 3 59.2 53.464 -166.98 54.179
2008 11 8 2 6 22.01 53.477 -166.99 54.697
2008 11 8 2 6 34.85 53.47 -166.98 54.501
2008 11 8 2 6 59.73 53.455 -166.97 53.944
2008 11 8 2 7 10.83 53.457 -166.97 54.149
2008 11 8 2 7 27.7 53.452 -166.96 53.598
2008 11 8 2 8 22.12 53.458 -166.97 53.744
2008 11 8 2 9 31.15 53.466 -166.97 54.459
2008 11 8 2 11 52.78 53.461 -166.97 53.664
2008 11 8 2 14 20.39 53.476 -166.99 54.548
2008 11 8 2 14 48.54 53.465 -166.97 54.29
2008 11 8 2 15 15.81 53.496 -167 54.899
2008 11 8 2 15 35.14 53.467 -166.98 54.983
2008 11 8 2 16 5.74 53.464 -166.97 53.917
2009 2 22 22 57 17.77 53.729 -166.56 58.938
2009 2 22 22 57 27.21 53.674 -166.52 55.415
2009 2 22 22 57 37.36 53.704 -166.53 59.117
2009 2 22 22 57 47.78 53.701 -166.52 56.025
2009 2 22 22 57 57.2 53.724 -166.55 60.037
2009 2 22 22 58 8.17 53.7 -166.53 58.523
2009 2 22 22 58 33.56 53.674 -166.5 57.23
2009 2 22 22 58 47.88 53.699 -166.55 57.87
2009 2 22 22 59 2.58 53.709 -166.54 56.614
2009 2 22 22 59 12.29 53.652 -166.49 53.676
2009 2 22 22 59 24.71 53.682 -166.51 58.359
2009 2 22 22 59 36.14 53.682 -166.5 57.168
2009 2 22 22 59 48.16 53.723 -166.55 58.955
2009 2 22 22 59 58.84 53.724 -166.54 59.066
2009 2 22 23 0 9.01 53.705 -166.53 58.697
2009 2 22 23 0 17.72 53.644 -166.47 54.999
2009 2 22 23 0 33.48 53.712 -166.52 58.765
2009 2 22 23 0 43.09 53.707 -166.56 55.945
2009 2 22 23 0 53.48 53.684 -166.52 55.527
2009 2 22 23 1 2.9 53.722 -166.55 60.675
2009 2 22 23 1 25.54 53.728 -166.56 58.04
2009 2 22 23 1 36.28 53.71 -166.55 57.511
2009 2 22 23 1 45.81 53.714 -166.53 57.339
2009 2 22 23 1 55.14 53.665 -166.5 56.712
2009 2 22 23 2 6.18 53.673 -166.52 56.26
2009 2 22 23 2 22.32 53.681 -166.53 54.554
2009 2 22 23 2 34.28 53.677 -166.53 54.992
2009 2 22 23 2 51.95 53.655 -166.48 54.876
2009 2 22 23 3 3.22 53.676 -166.52 55.244
2009 2 22 23 3 14.96 53.709 -166.56 57.479
2009 2 22 23 3 26.94 53.698 -166.53 56.093
2009 2 22 23 3 43.59 53.744 -166.56 61
2009 2 22 23 3 54.61 53.713 -166.55 55.96

2009 2 22 23 4 7.14 53.728 -166.57 58.83
2009 2 22 23 4 15.12 53.66 -166.5 57.203
2009 2 22 23 4 27.56 53.649 -166.48 53.668
2009 2 22 23 4 38.17 53.697 -166.54 57.134
2009 2 22 23 4 56.76 53.658 -166.48 56.298
2009 2 22 23 5 7.28 53.735 -166.56 59.704
2009 2 22 23 5 24.22 53.698 -166.54 57.655
2009 2 22 23 5 35.81 53.681 -166.5 57.328
2009 2 22 23 5 45.6 53.698 -166.52 57.569
2009 2 22 23 5 58.04 53.679 -166.52 55.471

2009 2 22 23 6 34.11 53.727 -166.55 59.125
2009 2 22 23 6 51.09 53.692 -166.53 58.49
2009 2 22 23 7 5.38 53.716 -166.55 57.784
2009 2 22 23 7 15.45 53.636 -166.48 53.031
2009 2 22 23 7 33.78 53.725 -166.57 57.313
2009 2 22 23 7 43.22 53.691 -166.52 56.584
2009 2 22 23 7 59.01 53.729 -166.57 59.594
2009 2 22 23 8 9.41 53.72 -166.55 58.578
2009 2 22 23 8 18.8 53.654 -166.49 53.697
2009 2 22 23 8 32.95 53.699 -166.52 59.097
2009 2 22 23 8 45.12 53.696 -166.51 57.492
2009 2 22 23 8 57.55 53.711 -166.55 57.772
2009 2 22 23 9 10.23 53.666 -166.49 55.356
2009 2 22 23 9 22.66 53.724 -166.57 58.243
2009 2 22 23 9 40.49 53.738 -166.56 58.927
2009 2 22 23 9 49.54 53.761 -166.58 62.356
2009 2 22 23 10 4.45 53.725 -166.57 58.95
2009 2 22 23 10 23.84 53.655 -166.5 55.11
2009 2 22 23 10 42.04 53.704 -166.52 58.251
2009 2 22 23 10 54.22 53.691 -166.53 55.828
2009 2 22 23 11 8.05 53.684 -166.51 58.139
2009 2 22 23 11 26.26 53.679 -166.5 59.251
2009 2 22 23 11 36.33 53.705 -166.54 59.87
2009 2 22 23 11 50.36 53.719 -166.54 59.892
2009 2 22 23 11 59.78 53.7 -166.51 60.487
2009 2 22 23 12 12.4 53.663 -166.48 55.08
2009 2 22 23 12 25.1 53.691 -166.53 55.779
2009 2 22 23 12 42.54 53.682 -166.52 58.907
2009 2 22 23 12 52.71 53.704 -166.54 58.013
2009 2 22 23 13 4.27 53.68 -166.51 58.854
2009 2 22 23 13 25.6 53.7 -166.53 57.692
2009 2 22 23 13 42.63 53.739 -166.56 60.226
2009 2 22 23 14 30.33 53.657 -166.5 54.691
2009 2 22 23 14 43.31 53.651 -166.5 53.622
2009 2 22 23 14 55.75 53.688 -166.53 57.43
2009 2 22 23 15 12.29 53.685 -166.53 56.345
2010 5 24 17 19 43.23 53.976 -165.5 61.516
2010 5 24 17 19 53.54 53.986 -165.51 62.28
2010 5 24 17 20 4.8 53.958 -165.53 60.059
2010 5 24 17 20 16.96 53.987 -165.53 61.674
2010 5 24 17 20 37.17 53.933 -165.51 59.247
2010 5 24 17 21 1.59 53.958 -165.52 59.111

2010 5 24 17 21 19.11 53.903 -165.49 55.54
2010 5 24 17 22 23.32 53.928 -165.51 57.286
2010 5 24 17 22 37.44 53.961 -165.49 61.293
2010 5 24 17 22 54.9 53.906 -165.54 54.994
2010 5 24 17 23 11.02 53.923 -165.52 56.995
2010 5 24 17 23 55.3 53.905 -165.53 54.636
2010 5 24 17 24 6.37 53.914 -165.51 57.125
2010 5 24 17 24 18.63 53.907 -165.49 56.482
2010 5 24 17 24 37.18 53.943 -165.53 58.069
2010 5 24 17 25 21.83 53.964 -165.52 60.467
2010 5 24 17 25 40.39 54.035 -165.52 63.672
2010 5 24 17 26 16.76 53.905 -165.51 55.404
2010 5 24 17 26 35.6 53.97 -165.52 60.965
2010 5 24 17 26 48.81 53.969 -165.53 59.061
2010 5 24 17 27 1.56 53.92 -165.51 56.97
2010 5 24 17 27 27.81 53.922 -165.51 57.867
2010 5 24 17 27 42 53.928 -165.5 59.559
2010 5 24 17 27 52.79 53.985 -165.49 60.604
2010 5 24 17 28 5.51 54.01 -165.51 63.367
2010 5 24 17 28 14.48 54.008 -165.51 64.372
2010 5 24 17 28 55.39 53.921 -165.51 57.749
2010 5 24 17 29 39.41 53.944 -165.52 57.5
2010 5 24 17 30 11.3 53.945 -165.49 61.664
2010 5 24 17 30 55.02 53.938 -165.53 58.82
2010 5 24 17 31 10.16 54.018 -165.53 63.23
2010 5 24 17 31 21.72 53.969 -165.54 60.36
2010 5 24 17 31 34.55 53.938 -165.51 58.782
2010 5 24 17 31 56.18 53.965 -165.5 61.664
2010 5 24 17 32 20.48 53.972 -165.53 60.21
2010 5 24 17 32 35.19 53.985 -165.52 61.669
2010 5 24 17 32 44.08 53.982 -165.5 61.507
2010 5 24 17 32 54.2 54.004 -165.51 64.479
2010 5 24 17 33 6.68 53.913 -165.53 57.739
2010 5 24 17 33 18.43 53.95 -165.5 58.315
2010 5 24 17 33 28.12 53.975 -165.52 61.066
2010 5 24 17 33 37.47 53.943 -165.5 59.379
2010 5 24 17 33 48.06 53.986 -165.5 61.763
2010 5 24 17 33 59.96 53.92 -165.51 57.428
2010 5 24 17 34 13.58 53.942 -165.5 59.052
2010 5 24 17 34 33.07 53.93 -165.49 58.743
2010 5 24 17 34 43.24 53.92 -165.53 59.198
2010 5 24 17 35 15.61 53.937 -165.5 59.756
2010 5 24 17 35 28.78 53.955 -165.5 60.989

Andreanof Islands

I detect 175 LFEs during two tremor episodes in the Central Aleutians (Table 4.1) using seismic stations operated by AVO. These stations are primarily used to monitor volcanic activity at Gareloi, Tanaga, Kanaga, and Great Sitkin volcanoes (Figure 4.11). This area

of the arc is the most remote of the U.S. Aleutian Islands considered in our study. I used 246,714 S-wave cross-correlation derived differential times to locate the LFEs.

LFEs in this region are concentrated in two regions trench-ward of the arc. The westernmost concentration of LFEs throughout the subduction zone is on Adak Island (Figure 4.11) during July 2007 (Table 4.6). The LFEs cluster with background seismicity between 60 and 75 km depth, down-dip of the rupture extent of the 1957 M_w 8.6 earthquake. The second area of LFE are located on Atka Island ~120 km east of Adak and occurred during July 2008 (Table S5). LFEs are also clustered with background seismicity between 55 and 70 km depth down-dip of the 1957 rupture. The locations indicate this portion of the Aleutians is host to the deepest known global observations of tremor.

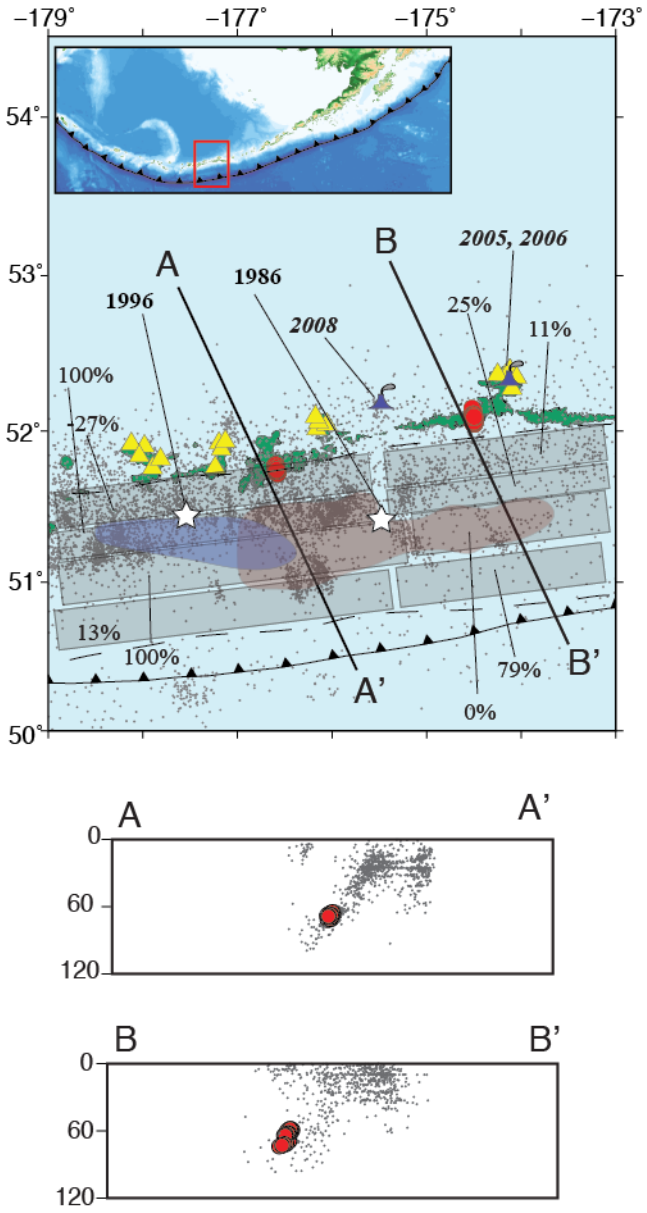

Figure 4.11. Map view and cross-sections of low-frequency earthquakes from tremor in the Andreanof Islands. Symbols are the same as in Figure 4.8. Variability in the degree of plate interface coupling is shown in the black boxes (Cross and Freymueller, 2008). Active volcanoes during the study are shown as violet volcano symbols. The dark blue and red shaded regions correspond to the 1986 M 8.0 and 1996 7.9 earthquake rupture patches respectively with the white stars referring to their centroid.

Like Unalaska, the degree of plate interface coupling in the Andreanof Islands region is complex along strike and dip in addition to experiencing oblique subduction (Figure 4.1). The western cluster of LFE activity is down-dip from a region where the degree of

coupling ranges from 13% near the trench, to fully coupled between ~20 and ~50 km depth. The LFEs are located down-dip of both the 1986 M 8.0 and 1996 M 7.9 rupture patches and roughly halfway between the centroid of each event (Figure 4.11). The degree of coupling near the eastern cluster is reversed compared to the western cluster. The degree of coupling for the up-dip limit closest to the trench is ~79% locked whereas the degree of coupling decreases to 0-25% at intermediate depths [*Cross and Freymueller,* 2008]. As in Unalaska, tremor activity continues to occur despite the variability of the degree of coupling along both strike and dip directions of the plate interface.

Table 4.6

Year Month Day Hour Minute Second Latitude Longitude Depth

2007 7 25 23 32 14.8 51.758 -176.59 63.634
2007 7 25 23 32 24.01 51.751 -176.58 62.862
2007 7 25 23 32 33.23 51.765 -176.59 63.778
2007 7 25 23 32 42.16 51.745 -176.59 62.939
2007 7 25 23 32 55.85 51.762 -176.59 64.702
2007 7 25 23 33 8.82 51.761 -176.59 62.765
2007 7 25 23 33 19.95 51.735 -176.58 62.157
2007 7 25 23 33 30.31 51.746 -176.59 61.277
2007 7 25 23 33 40.09 51.761 -176.59 63.278
2007 7 25 23 33 52.6 51.766 -176.58 64.578
2007 7 25 23 34 1.66 51.742 -176.59 64.956
2007 7 25 23 34 10.82 51.752 -176.59 63.283
2007 7 25 23 34 22.34 51.757 -176.59 63.152
2007 7 25 23 34 31.57 51.736 -176.59 60.723
2007 7 25 23 34 45.32 51.751 -176.6 61.683
2007 7 25 23 34 54.6 51.746 -176.59 62.091
2007 7 25 23 35 5.71 51.754 -176.59 66.812
2007 7 25 23 35 17.35 51.754 -176.59 63.381
2007 7 25 23 35 26.55 51.759 -176.59 62.663
2007 7 25 23 35 36.88 51.738 -176.58 62.63
2007 7 25 23 35 46.95 51.749 -176.58 63.152
2007 7 25 23 35 56.66 51.742 -176.59 61.676
2007 7 25 23 36 5.76 51.743 -176.59 64.852
2007 7 25 23 36 17.99 51.738 -176.59 62.429
2007 7 25 23 36 27.84 51.774 -176.6 63.332
2007 7 25 23 36 36.56 51.745 -176.59 62.284

2007 7 25 23 36 46.65 51.762 -176.6 62.975
2007 7 25 23 36 57.55 51.74 -176.58 62.259
2007 7 25 23 37 7.22 51.765 -176.59 63.066
2007 7 25 23 37 16.06 51.753 -176.59 63.593
2007 7 25 23 37 25.37 51.752 -176.59 62.181
2007 7 25 23 37 34.71 51.778 -176.6 63.875
2007 7 25 23 37 43.73 51.776 -176.6 64.502
2007 7 25 23 37 55.82 51.748 -176.59 61.454
2007 7 25 23 38 4.99 51.742 -176.59 64.955
2007 7 25 23 38 14.23 51.76 -176.59 63.081
2007 7 25 23 38 23.66 51.742 -176.59 61.871
2007 7 25 23 38 32.87 51.758 -176.59 63.576
2007 7 25 23 38 41.93 51.73 -176.59 61.262
2007 7 25 23 38 51.42 51.727 -176.58 61.58
2007 7 25 23 39 1.09 51.752 -176.59 66.308
2007 7 25 23 39 11.74 51.75 -176.59 62.709
2007 7 25 23 39 22.04 51.766 -176.59 63.886
2007 7 25 23 39 34.6 51.766 -176.59 64.35
2007 7 25 23 39 44.43 51.762 -176.59 64.259
2007 7 25 23 39 53.48 51.756 -176.59 63.813
2007 7 25 23 40 2.59 51.775 -176.59 67.882
2007 7 25 23 40 11.82 51.761 -176.59 63.528
2007 7 25 23 40 22.35 51.748 -176.59 63.077
2007 7 25 23 40 32.62 51.736 -176.59 61.064
2007 7 25 23 40 41.82 51.747 -176.59 62.682
2007 7 25 23 40 50.91 51.754 -176.59 63.601
2007 7 25 23 40 59.99 51.744 -176.59 66.558
2007 7 25 23 41 9.52 51.765 -176.6 62.907
2007 7 25 23 41 19.13 51.738 -176.59 62.601
2007 7 25 23 41 28.77 51.75 -176.59 61.733
2007 7 25 23 41 41.74 51.724 -176.58 61.767
2007 7 25 23 41 51.53 51.769 -176.6 62.776
2007 7 25 23 42 1.55 51.758 -176.59 67.028
2007 7 25 23 42 12.66 51.727 -176.59 60.994
2007 7 25 23 42 22.74 51.757 -176.59 62.838
2007 7 25 23 42 31.63 51.728 -176.58 60.786
2007 7 25 23 42 41.16 51.741 -176.58 62.289
2007 7 25 23 42 52.62 51.741 -176.59 61.538
2007 7 25 23 43 2.6 51.77 -176.59 66.891
2007 7 25 23 43 12.27 51.761 -176.59 62.842
2007 7 25 23 43 22.11 51.739 -176.59 62.483
2007 7 25 23 43 30.98 51.72 -176.58 61.676
2007 7 25 23 43 41.03 51.745 -176.59 62.09
2007 7 25 23 43 50.73 51.768 -176.6 64.099
2007 7 25 23 44 0.82 51.747 -176.59 65.701
2007 7 25 23 44 10.04 51.749 -176.59 63.033
2007 7 25 23 44 21.04 51.735 -176.59 60.865
2007 7 25 23 44 31.24 51.768 -176.6 62.942
2007 7 25 23 44 40.37 51.752 -176.59 62.367
2007 7 25 23 44 49.69 51.769 -176.59 64.379
2007 7 25 23 44 58.99 51.773 -176.59 64.356
2007 7 25 23 45 10.25 51.751 -176.59 61.942
2007 7 25 23 45 23.68 51.75 -176.59 62.393

2007 7 25 23 45 37.66 51.755 -176.59 64.304
2007 7 25 23 45 54.13 51.75 -176.59 63.277
2007 7 25 23 46 4.92 51.738 -176.59 65.483
2007 7 25 23 46 16.34 51.765 -176.6 63.382
2007 7 25 23 46 28.83 51.741 -176.59 62.116
2007 7 25 23 46 40.47 51.743 -176.58 63.434
2007 7 25 23 46 49.59 51.749 -176.58 64.365
2007 7 25 23 47 0.18 51.745 -176.59 65.617
2007 7 25 23 47 12.45 51.746 -176.59 61.718
2007 7 25 23 47 25.54 51.759 -176.59 63.304
2007 7 25 23 47 40.35 51.744 -176.59 61.895
2007 7 25 23 47 51.58 51.736 -176.58 62.32
2007 7 25 23 48 6.7 51.757 -176.59 62.71
2007 7 25 23 48 16.7 51.768 -176.6 63.693
2007 7 25 23 48 34.46 51.775 -176.59 63.553
2007 7 25 23 48 46.8 51.752 -176.59 63.125
2007 7 25 23 49 1.42 51.747 -176.59 65.836
2007 7 25 23 49 58.85 51.755 -176.59 63.464
2007 7 25 23 50 9.44 51.758 -176.59 62.466
2007 7 25 23 50 19.78 51.753 -176.59 62.704
2007 7 25 23 50 28.75 51.743 -176.59 62.521
2007 7 25 23 50 42.67 51.759 -176.59 64.079
2007 7 25 23 50 55.75 51.747 -176.58 63.163
2007 7 25 23 51 4.96 51.741 -176.59 64.03
2007 7 25 23 51 15.54 51.744 -176.58 63.016
2008 7 13 19 54 9.99 52.069 -174.5 62.507
2008 7 13 19 54 21.72 52.083 -174.53 60.948
2008 7 13 19 54 35.54 52.067 -174.5 62.637
2008 7 13 19 54 57.55 52.109 -174.52 70.972
2008 7 13 19 55 8.08 52.062 -174.49 61.904
2008 7 13 19 55 20.55 52.074 -174.49 65.153
2008 7 13 19 55 33.24 52.092 -174.51 63.221
2008 7 13 19 55 47.73 52.081 -174.5 63.625
2008 7 13 19 56 0.05 52.126 -174.51 73.408
2008 7 13 19 56 10.64 52.085 -174.51 62.7
2008 7 13 19 56 28.47 52.102 -174.5 65.747
2008 7 13 19 56 42.1 52.083 -174.5 64.227
2008 7 13 19 56 52.04 52.087 -174.5 63.126
2008 7 13 19 57 19.61 52.071 -174.5 63.356
2008 7 13 19 57 31.79 52.065 -174.5 62.038
2008 7 13 19 57 59.37 52.109 -174.51 72.62
2008 7 13 19 58 10.02 52.062 -174.49 62.634
2008 7 13 19 58 48.12 52.052 -174.49 61.352
2008 7 13 19 58 59.42 52.132 -174.5 74.217
2008 7 13 19 59 27.85 52.073 -174.5 62.257
2008 7 13 19 59 59.18 52.108 -174.51 72.309
2008 7 13 20 0 17.86 52.059 -174.52 58.898
2008 7 13 20 0 26.87 52.054 -174.5 60.039
2008 7 13 20 0 41.43 52.077 -174.51 61.282
2008 7 13 20 0 51.16 52.09 -174.5 64.237
2008 7 13 20 1 0.75 52.068 -174.5 69.82
2008 7 13 20 1 10.24 52.069 -174.5 61.559
2008 7 13 20 1 26.09 52.069 -174.52 59.584

2008 7 13 20 1 38.39 52.063 -174.5 62.084
2008 7 13 20 1 48.86 52.08 -174.5 62.966
2008 7 13 20 2 5.96 52.089 -174.49 65.517
2008 7 13 20 2 22.64 52.072 -174.5 62.863
2008 7 13 20 2 42.21 52.044 -174.49 59.93
2008 7 13 20 2 52.99 52.086 -174.5 64.009
2008 7 13 20 3 6.82 52.068 -174.5 62.06
2008 7 13 20 3 18.96 52.05 -174.5 59.86
2008 7 13 20 3 31.74 52.065 -174.5 61.566
2008 7 13 20 3 44.94 52.095 -174.51 63.698
2008 7 13 20 4 13.99 52.057 -174.51 59.742
2008 7 13 20 4 25.91 52.051 -174.51 58.948
2008 7 13 20 4 35.17 52.068 -174.51 60.841
2008 7 13 20 4 48.11 52.111 -174.51 64.8
2008 7 13 20 5 59.25 52.079 -174.5 63.154
2008 7 13 20 5 10.93 52.086 -174.5 63.194
2008 7 13 20 5 27.58 52.09 -174.5 65.103
2008 7 13 20 5 36.33 52.056 -174.51 59.275
2008 7 13 20 5 45.73 52.087 -174.5 71.369
2008 7 13 20 6 0.71 52.068 -174.49 62.605
2008 7 13 20 6 25.11 52.09 -174.51 62.741
2008 7 13 20 6 34.03 52.099 -174.5 64.994
2008 7 13 20 6 45.47 52.067 -174.49 63.001
2008 7 13 20 6 59.46 52.147 -174.52 74.508
2008 7 13 20 7 16.66 52.064 -174.5 61.189
2008 7 13 20 7 29.7 52.071 -174.5 62.633
2008 7 13 20 7 40.8 52.059 -174.52 59.068
2008 7 13 20 8 0.26 52.093 -174.5 72.48
2008 7 13 20 8 25.22 52.077 -174.51 62.893
2008 7 13 20 8 34.75 52.108 -174.51 65.154
2008 7 13 20 8 45.49 52.075 -174.49 63.007
2008 7 13 20 8 59.35 52.102 -174.51 72.304
2008 7 13 20 9 14.68 52.093 -174.51 64.149
2008 7 13 20 9 25.48 52.101 -174.5 64.71
2008 7 13 20 9 34.67 52.098 -174.51 64.587
2008 7 13 20 10 2.42 52.067 -174.5 69.323
2008 7 13 20 10 30.34 52.06 -174.5 60.894
2008 7 13 20 10 40.71 52.079 -174.5 63.268
2008 7 13 20 10 58.51 52.101 -174.5 71.587
2008 7 13 20 11 10.1 52.082 -174.5 62.655
2008 7 13 20 11 24.39 52.06 -174.5 61.153
2008 7 13 20 11 48.29 52.086 -174.5 63.589
2008 7 13 20 11 58.63 52.092 -174.5 71.852

To gain a better understanding of location errors we relocated the LFEs while resampling the station geometry in the Andreanof Islands region for the westernmost cloud of LFEs detected in July 2007 (Figure 4.11). Figure (4.12) shows the spread in hypocenter locations in map view and cross-section that results. I use the centroid of the cloud as the

starting epicenter and vary the starting depths at 55, 70 and 85 km. The variation in location of two LFEs is shown in Figure 4.12 a,b and c,d respectively. The location of the centroid of LFE hypocenters is -176.61 degrees longitude (+/-, 3.5 km) 51.75 degrees latitude (+/- 1.6 km) and 66.9 +/- 11.1 km. The average 95% confidence intervals for subsets of LFEs are +/-2.2 km, +/-2.4 km and +/- 12.1 km in the longitude, latitude and depth directions respectively.

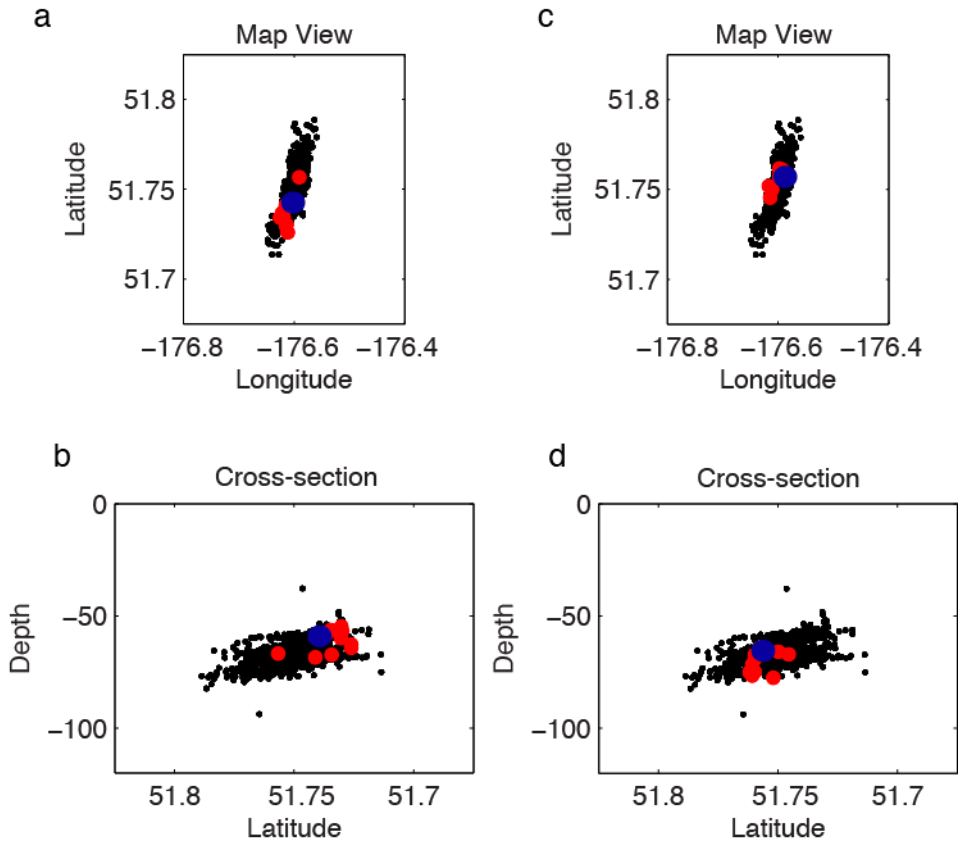

Figure 4.12. LFE locations from four different station geometries and three different starting locations for a total of twelve relizations. a) Map view. Blue event occurred on July 25, 2007. The red events are the locations of the reference LFE for all twelve realizations. b) Same as a), but in cross section. c) Same as a) for another reference event. d). Same as b) for a different reference event.

DISCUSSION

Using the running autocorrelation of continuous waveform records from the AVO and AEIC I demonstrate that tremor-like signals in various locations along the Alaska-Aleutian Arc are composed of repeating low frequency earthquakes. Although the locations of the events contain up to +/-20 km uncertainty in depth, the centroid of the depth distribution is within 5 km of the subducting plate interface.

Tremor occurs along all parts of the Alaska-Aleutian subduction zone. It occurs along the continental part, and it occurs along the oceanic part. It occurs where there is a broad forearc high at the east end, and it occurs where there is no forearc high at the west end. It occurs where there is relatively orthogonal subduction at the east end, and it occurs where there is highly oblique subduction at the western end. Moreover, it occurs beneath Kodiak Island, where there is more than 1 km of late Quaternary and Holocene sediment of the Surveyor Fan entering the trench [*Stevenson and Embley,* 1987; *von Huene et al.,* in press], and it occurs beneath the Andreanof Islands where there is as little as 200 m of sediment entering the trench. Lastly, the Kodiak-Bowie seamount chain was subducted beneath Kodiak Island [e.g. *von Huene et al.,* 2012], and these subducted seamounts likely are in the region of the Kodiak tremor observations. No such subducted plate topography lies in the other regions where tremor was located. Thus, there are no particular characteristics of the downgoing plate or overlyingsediment that appear correlated with the presence or absence of tremor.

In addition, there is no correlation between the presence or absence of LFEs with the degree of coupling updip along the megathrust. Plate interface coupling updip of regions of observed LFEs ranges between 2% and 100% (see Figures 4.8-4.11), therefore, the behavior of the megathrust is no predictor for the presence or absence of LFEs. This implies that the LFEs and the downdip extent of megathrust earthquakes could be influenced by other factors such as pressure and temperature conditions.

Epicenters of the LFEs are located near the down-dip extent of slip, to the extent known, for previous M_w 8.0+ earthquakes along the arc. This is consistent with the hypothesis that it marks a persistent difference in frictional characteristics of the subducting plate interface. The LFE locations in the Shumagin Gap could mark the down-dip extent of a future large megathrtust event in that area, though understanding strain accumulation and seismic potential at the Shumagin Gap will require further study. Our LFE locations from tremor could be used to help reduce non-uniqueness in modeling the geodetic observations in this area.

The age of the incoming plate interface increases across the study area from east to west, as does the incoming plate rate. The depths of the LFE activity also deepen from 45 km in the east to as deep as ~75 km in the Andreanof Islands (Figure 13). I suspect this is due to temperature-depth variation along the arc that control the depths to which hydrous minerals release fluids [*Katsumata and Kamaya,* 2003] to enable tremor activity. This will occur at greater depths when the incoming plate is older, faster and colder.

Observations of tremor in Japan strongly suggest that, where tremor occurs, it outlines the depth extent of extensive slip in large megathrust earthquakes [*Ide et al.,* 2007]. If this holds true for Cascadia, it places rupture in large earthquakes considerably closer to the major metropolitan areas of Portland and Seattle than has been assumed previously [*Chapman and Melbourne,* 2009]. The results for LFE locations near Kodiak Island suggest that tremor occurs near the down-dip extent of the 1964 Alaska earthquake, which suggests that the relationship holds there as well. Farther to the west, along the Aleutian Arc, our LFE locations are more uncertain, and it's possible that there is a gap between LFEs and large earthquake rupture zones, but that gap is small, with a depth difference of perhaps 15-20 km. More detailed studies of tremor in this area, perhaps aided by OBS deployments, and of tremor in areas that have well-constrained slip distributions for large earthquake rupture, should provide a clearer picture of the relationship between tremor activity, and slip in large earthquakes.

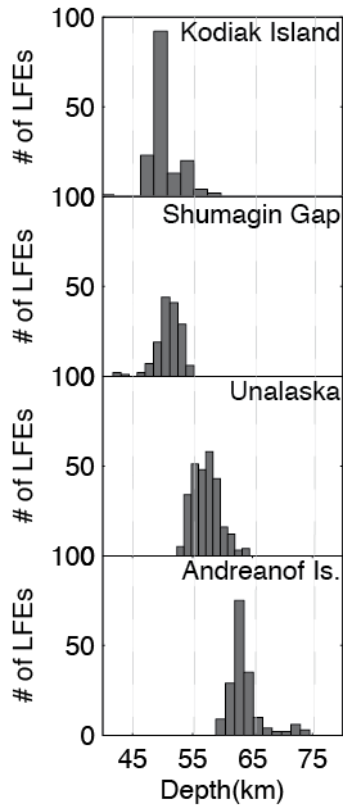

Figure 4.13. Depth distribution of tremor throughout the Alaska-Aleutian subduction zone. Depth distributions increase systematically from east to west.

ACKNOWLEDGEMENTS

I thank Robert Clapp, Natalia Ruppert, Doug Christensen and Chloe Peterson for helpful discussion. Steven McNutt, Scott Stihler, Jim Dixon and many duty seismologists at the AVO provided a thorough daily catalog of tremor-like signals. J.R.B. was supported by USGS Earthquake Hazards Program and Alaska Science Center. This work was supported by NSF grant EAR-07 10835. This work utilized the Stanford Center for Computational Earth and Environmental Sciences.

REFERENCES

Abers, G, J Beavan, S. Horton, S. Jaumeand and E. Triep (1995), Large accelerations and tectonic setting of the May 1993 Shumagin Islands earthquake sequence, *Bull. Seismol. Soc. Am., 85*, 1730-1738.

Beroza, G. C and S. Ide (2011), Slow earthquakes and nonvolcanic tremor, *Annual Rev. Planet. Earth Sci.,* 39, pp. 271-296.

Brown, J. R., G. C. Beroza, and D. R. Shelly (2008), An autocorrelation method to detect low frequency earthquakes within tremor, Geophys. Res.Lett., 35, L16305, doi:10.1029/2008GL034560.

Brown, J. R., G. C. Beroza, S. Ide, K. Ohta, D. R. Shelly, S. Y. Schwartz, W. Rabbel, M. Thorwart, and H. Kao (2009), Deep low-frequency earthquakes in tremor localize to the plate interface in multiple subduction zones, *Geophys. Res. Lett.,* 36, L19306, doi:10.1029/2009GL04002.

Cervelli, D. P., P. Cervelli, A. Miklius, R. Krug, M. Lisowski (2002). VALVE: Volcano Analysis and Visualization Environment, American Geophysical Union, Fall Meeting 2002, abstract #U52A-07.

Chouet, B., 1985. Excitation of a buried magmatic pipe: a seismic source model for volcanic tremor. *J. Geophys.Res.* 90, 1881–1893.

Christensen, D. H., S. L. Beck, (1994). The rupture process and implications of the great 1964 Prince William Sound earthquake,*Pure and Applied Geophys*.,
DOI: 10.1007/BF00875967

Cross, R. S. and J. T. Freymueller (2008), Evidence for implications of a Bering plate based on geodetic measurements from the Aleutians and western Alaska, *J. Geophys. Res.,* 113, B07405, doi:10.1029/2007JB005136.

Fournier, T. J. and J. T. Freymueller (2007), Transition from locked to creeping subduction in the Shumagin region, Alaska, *Geophys. Res. Lett., 34,* L06303, doi:10.1029/2006GL029073.

Freymueller, J.T., H Woodard, S.Cohen, R. Cross, J. Elliott, C. Larsen, S. Hreinsdottir, C. Zweck (2008), Active deformation processes in Alaska, based on 15 years of GPS measurements, in Active Tectonics and Seismic Potential of Alaska, AGU Geophysical Monograph, 179, J.T. Freymueller, P.J. Haeussler, R. Wesson and G. Ekstrom, eds., pp. 1-42, AGU, Washington, D.C.

Gomberg, J. S. (2010), Introduction of a special section on Phenomenology, Underlying Processes, and Hazard Implications of Aseismic Slip and nonvolcanic tremor, *J. Geophys. Res.,* 115, B00A00, doi:10.1029/2010JB008052.

Hauksson, E., J. Armbruster, and S. Dobbs, (1984), Seismicity pattersn (1963-1983) as stress indicators in the Shumagin seismic gap, Alaska. *Bull. Seismic Soc Amer.*, 74, pp 2541-2558.

Hauksson, E., (1985), Structure of the Benioff zone beneath the Shumagin Islands, Alaska: relocation of local earthquakes using three-dimensional ray tracing. *J. Geophys. Res.,* (90), pp 635-649.

Hellweg, M., 2000. Physical models for the source of Lascar's harmonic tremor. *J. Volc. and Geothermal Res.*101, 183–198

Ide, S., D. R. Shelly, and G. C. Beroza (2007), The mechanism of deep low frequency earthquakes: further evidence that deep non-volcanic tremor is generated by shear slip on the plate interface, *Geophys. Res. Lett.,* 34, L03308, doi:10.1029/2006GL028890.

Johnson, J.B., Lees, J.M., 2000. Plugs and chugs–seismic and acoustic observations of degassing explosions at Karymsky, Russia and Sangay, Ecuador. *J. Volc. Geothermal Res.* 101, 67–82.

Julian, B.R., 1994. Volcanic tremor: nonlinear excitation by fluid flow. *J. Geophys. Res.* 99, 11859–11877.

Kao, H., and S.-J. Shan (2004), The source-scanning algorithm: Mappingthe distribution of seismic sources in time and space, Geophys. J. Int.,157, doi:10.1111/j.1365-246X.2004.02276.x

Katsumata, A., and N. Kamaya (2003), Low-frequency continuous tremor around the Moho discontinuity away from volcanoes in the southwest Japan, *Geophys. Res. Lett.,* 30(1), 1020, doi:10.1029/2002GL015981.

McNutt, S. R. (1992), Volcanic tremor, *Encyclopedia of earth system science,* vol 4, Academic Press, San Diego, pp. 417-425.

Obara, K., (2002), Nonvolcanic deep tremor association with subduction in southwest Japan, *Science,* 296, pp. 1679-1681.

Ohta, Y, J. T. Freymueller, S. Hreinsdottir, and H. Suito (2006), A large slow slip event and the depth of seismogenic zone in the south central Alaska subduction zone, *Earth and Planet. Sci. Lett.,* 247, pp 108-116.

Peterson, C. L., S. R. McNutt, D. H. Christensen, (2011), Nonvolcanic tremor in the Aleutian Arc, *Bull. Seismo. Soc. Amer.,* 101, pp. 3081-3087.

Rogers, G. and H. Dragert (2003), Episodic tremor and slip in Cascadia subduction zone: The chatter of silent slip, *Science,* 300, pp. 1942-1943.

Rubinstein J. L., D. R. Shelly, and W. L. Ellsworth (2010), Non-volcanic tremor: A window into the roots of fault zones, in: New Frontiers of Solid Earth Sciences, doi:10/1007/987-90-481-2737-5_8

Ruppert, N. A., J. M. Lees, N. P. Kozyreva, (2007), Seismicity, earthquakes and rupture along the Alaska-Aleutian and Kamchatka-Kurile subduction zones: a review, *Volcanism and Subduction,* Geophys. Monograph 172.

Schwartz, S. Y. and J. M. Rokosky (2007), Slow slip events and seismic tremor and circum-Pacific subduction zones, *Rev. Geophys.,* 45, pp. 1-32.

Shelly, D. R., G. C. Beroza, and S. Ide (2007a), Non-Volcanic Tremor and Low Frequency Earthquake Swarms, *Nature* 446, 305-307, doi:10.1038/nature05666

Shelly, D. R., G. C. Beroza, and S. Ide (2007b), Complex evolution oftransient slip derived from precise tremor locations in western Shikoku,Japan, *Geochem. Geophys. Geosyst.*, 8, Q1 00 14, doi:10.1029/2007GC001640.

Shelly, D. R., G. C. Beroza, S. Ide, and S. Nakamula (2006), Lowfrequency earthquakes in Shikoku, Japan, and their relationship to episodic tremor and slip, Nature, 442, 188 – 191, doi:10.1038/nature04931.

Stevenson, A.J., and Embley, R., 1987, Deep Sea Fan Bodies, Terrigeneous Turbidite Sedimentation, and Petroleum Geology, Gulf of Alaska, *in* Scholl, D.W., Grantz, A., and Vedder, J.G., eds., Geology and resource. Potential of the continental margin of western N.America and adjacent ocean basins - Beaufort Sea to Baja California: American AssociationPetroleum *Geology*, p. 503-522.

Von Huene, R., Miller, J.J., and Weinrebe, W., in press, Subducting plate geology in three great earthquake ruptures of the western Alaska margin, Kodiak to Umnak: *Geosphere*.

Waldhauser, F., and W. L. Ellsworth (2000), A double-difference earthquake location algorithm: Method and application to the northern Hayward fault, California, Bull. Seismol. Soc. Am., 6, 1353 – 136.

Wech, A. G., and K. C. Creager (2008), Automated detection and locationof Cascadia tremor, Geophys. Res. Lett., 35, L20302, doi:10.1029/2008GL03545

Zweck, C, J. T. Freymueller and S. C. Cohen (2002), Three-dimensional elastic dislocation modeling of the postseismic response to the 1964 Alaska earthquake, *J. Geophys. Res., vol. 107*, (B4), 2064, doi:10.1029/2001JB000409. /2001JB000409.

5. A RAPID METHOD TO DETECT LOW FREQUENCY EARTHQUAKES WITHIN TREMOR USING THE COMPLEX CEPSTRUM

ABSTRACT

In this chapter I present a fast method to detect low frequency earthquakes within tremor using the complex cepstrum of continuous seismic records. Cepstrum analysis has been used in a variety of seismic event detection and classification in order to identify repeating source characteristics and temporal disturbances in the seismic record. In this part of the thesis I utilize the cepstrum, *viz*. the Fourier Transform of the logarithmic power spectrum, to detect low frequency earthquakes (LFEs) within continuous tremor recordings and show that it can be used to detect previously identified LFEs in addition to several undetected LFEs. Using a series of synthetic tests allows a direct calculation of the false alarm rate for detection, the minimum inter-event spacing to detect, and signal-to-noise ratio for which cepstral detection of LFEs within tremor are optimal. Also, the logarithmic power spectrum enables a fast calculation of a cepstral signal that identifies periods where phases of the signal are similar. This approach also demonstrates that LFE detections in southwest Japan can be obtained from the cepstrum at unprecedented speed.

The material in this chapter is in preparation for the Journal of Geophysical Research

INTRODUCTION

Deep tectonic tremor is a long-duration low-amplitude signal resembling volcanic tremor that was first discovered in southwest Japan by *Obara* [2002] and subsequently identified in tectonic settings elsewhere. The lack of impulsive phase arrivals common to ordinary earthquakes poses a challenge to accurately characterize tremor waveforms. Tectonic tremor is often, but not always, associated with geodetically observed slow slip events that can occur over the course of days to several weeks [*Rogers and Dragert,* 2003]. It is important to characterize tremor if slow slip and tremor are the mutual representation of fault slip behavior on major faults. Since the temporal resolution of tremor recordings is higher than that of geodetic instruments (eg., tilt, GPS), analyzing as much of the tremor waveform as possible may hold clues to understanding the slow slip process on major faults at high precision.

One approach, which utilizes tremor waveform amplitudes to characterize the signal, was first introduced by *Obara* [2002]. He was able to use cross-correlation to obtain relative arrival times of tremor envelopes and subsequently use the spatial distribution of arrival times to estimate tremor hypocenters with a temporal resolution of one solution per minute. Another approach to characterize the tremor source involves the extraction of repeating low frequency earthquakes (LFEs) imbedded within the signal in southwest Japan since the amplitude spectra of tremor and LFEs are very similar (Figure 5.1). *Shelly et al.* [2006] were able to locate previous and newly catalogued LFEs using a combination of waveform cross-correlation and tomographic double-difference methods [*Zhang and Thurber,* 2003]. They were able to extend their analysis by using templates as matched filters [*Gibbons and Ringdal,* 2006] to detect additional LFEs at high precision

[*Shelly et al.,* 2007a,b] supporting their hypothesis that tremor is composed of several repeating LFEs. Though powerful, this method requires a reference set of templates for matched filtering. In an approach presented by *Brown et al.* [2008] they were able to identify "template" events by applying running autocorrelation to continuous waveforms of tremor to extract pairs of events without the use of previously cataloged templates and were able to show that tremor consists of LFEs in other subduction zones [*Brown et al.,* 2009].

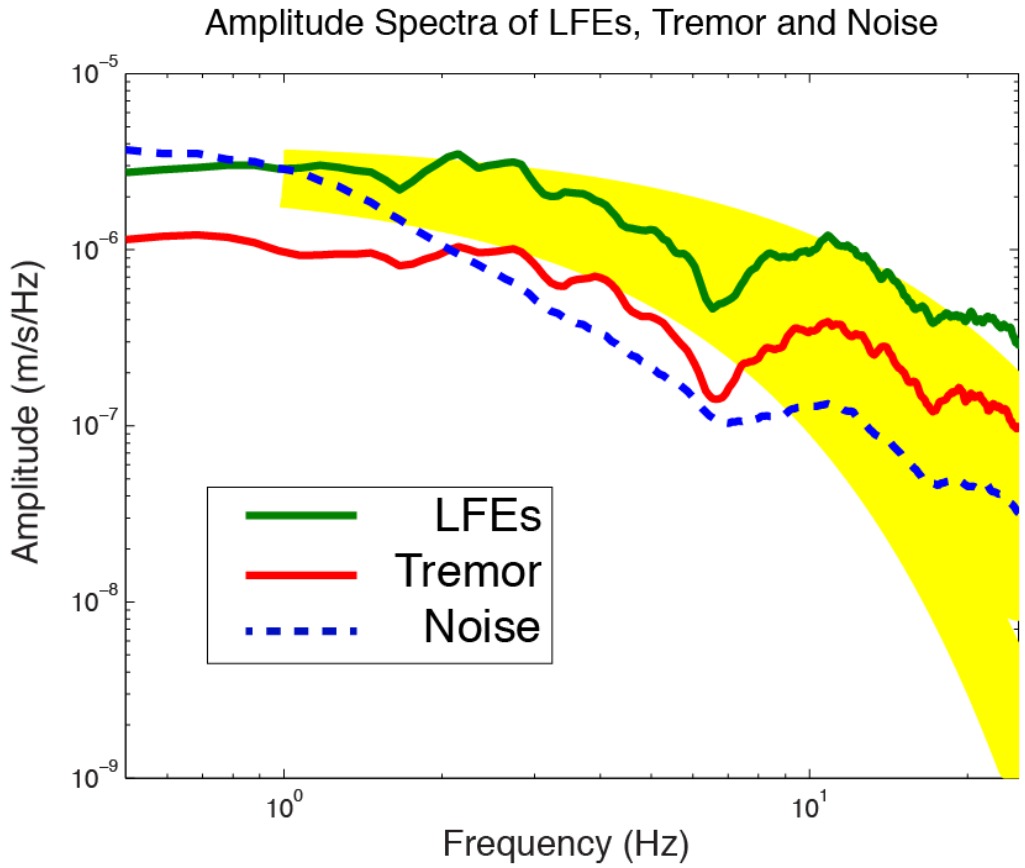

Figure 5.1. Velocity spectra of tectonic tremor (red) and LFEs from southwest Japan (green). The stacked noise spectrum is determined from 5 hours of continuous data shown as the blue dashed curve. The shaded gold area are the attenuation curves using exp(-πft/Q) for t=19s and Q-200-400.

Despite the aforementioned studies revealing tremor/LFE solutions, there is a tradeoff between computation time and event hypocenter precision. For example, solutions using smoothed waveform envelopes are modest in computation time but lead to larger uncertainties in location since waveform information is lost in the smoothing process. Conversely, running autocorrelation to detect LFEs- which retains waveform information such as spectra, is computationally intensive. However, the event location uncertainties are within 5 km. Since tremor episodes can last anywhere from hours to several weeks, rapid processing of the data with high accuracy lacking any reference events remains a challenge.

In this chapter an alternate method is presented to identify LFEs within tremor by using the complex cepstrum of continuous seismic recordings. First, I review what the cepstrum is and how it is useful for seismology. Next, I test how complex cepstrum analysis successfully identifies repeated LFEs in a synthetic test. Last, I apply the method to a week-long tremor episode in southwest Japan and compare detections and computational time to previous studies.

THE CEPSTRUM

The cepstrum was first introduced by *Bogert et al.* [1963] to characterize seismic "echoes" to help distinguish the seismic signature of bombs from that of earthquakes. The definition of the cepstrum, *C(t),* is the Fourier Transform of the logarithm of the spectrum of a time series (eqn. 1) and contains both real and complex parts.

$$C(t) = \int_{-\infty}^{\infty} \log|F(\omega)|e^{-i\omega t} d\omega \qquad (1)$$

where $F(\omega)$ is the Fourier Transform of the original time series $f(t)$ (eqn 2).

$$F(\omega) = \int_{-\infty}^{\infty} f(t) e^{-i\omega t} dt \qquad (2)$$

It is worth noting the outer transform in eqn. (1) does not use the inverse Fourier Transform. The independent variable of the cepstrum is the quefrency. The quefrency is measured in seconds although it is not the same measure of time as the original time-domain signal, rather it is the independent variable for the spectrum-of-the-spectrum of a time series. The complex cepstrum, introduced by *Oppenheim* [1965], permits the reconstruction of an original time-domain signal while maintaining information about the magnitude and phase of the spectrum of the original signal, whereas the real cepstrum only maintains information about the magnitude of the spectrum.

An advantage of using the cepstrum is that it explores the rate of change in the different spectrum bands of a signal as is the case with discriminating the seismic echoes resulting from an earthquake and of explosions [*Reymond et al*, 2003], nuclear bombs [*Davies and Smith,* 1968; *Wei and Li,* 2003], and quarry blasts [*Hedlin et al.,* 1990].

Other uses of the cepstrum are used in speech, signal returns and hearing aids, all of which belong to a class of signal processing referred to as homomorphic filtering. The advantage of homomorphic signal filtering is the use of the logarithmic spectrum on signals comprised of multiplicative components that are additive in spectral domain. As in the case of hearing aids, the cepstrum can isolate, or amplify, frequencies of interest in the log-spectral domain and conversely dampen unwanted signals.

A major difference between the real and complex cepstrum is that the phases of the signal are unwrapped in the complex cepstrum prior to taking the final Fourier Transform. This step is critical when considering the cepstral shape of long-duration mixed phase signals such as LFE swarms in tectonic tremor. The Fourier Transform is a

complex valued function and bound to integer multiples of 2π. And manifests in a discontinuous series unless the phases are unwrapped resulting in a continuous series.

APPLICATION OF THE COMPLEX CEPSTRUM TO IDENTIFY REPEATING EVENTS IN A TIME SERIES

The Complex Cepstrum of Noise

To explore the feasibility of cepstral analysis for LFE detection, we ran series of tests to understand 1) the noise cepstrum, 2) the signal-to-noise ratio (*snr*) dependence, and 3) type I (false alarm) vs. type II (failure to detect) error rates.

The noise cepstrum is analyzed by generating a twenty-minute signal composed of white noise with a sampling rate of 0.01s (Figure 5.2a). Two important features occur in the quefrency domain when the complex cepstrum is calculated. First, there are very strong peaks in the signal at both very low and very high quefrency (Figure 5.2b) due to signal edge effects. Second, the edge effects rapidly decay into the rest of the quefrency signal (Figure 5.2 c, d), which is unaffected and contains a uniform distribution of cepstral values. To avoid signal edge effects the synthetic signal length was increased by 3 times the original length and zero-padded. The complex cepstrum was recalculated and only the middle third of the signal where edge effects are absent is plotted (Figure 5.2e).

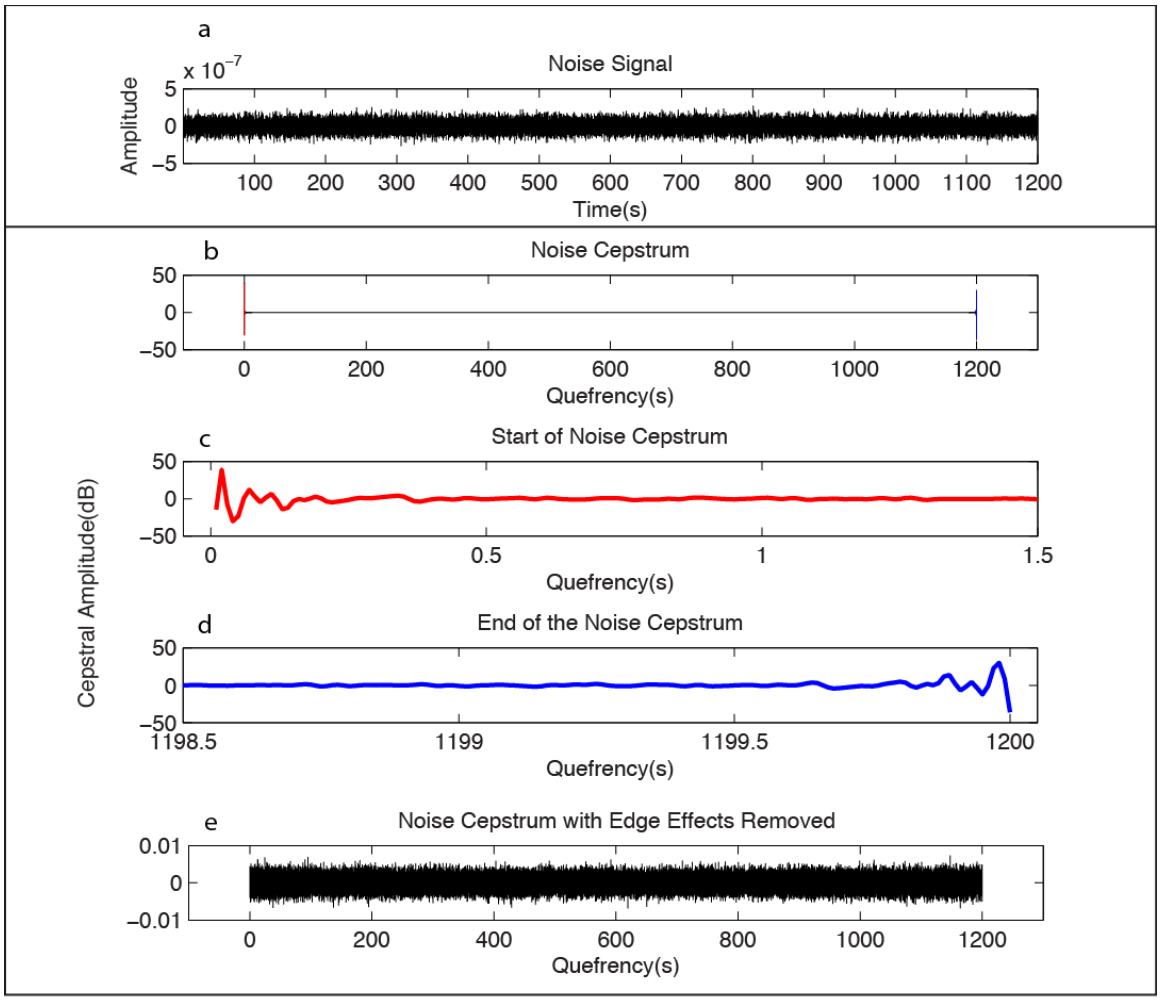

Figure 5.2. Characteristics of the complex cepstrum of noise. Noise waveform is shown in a). b) The raw complex cepstrum. High-amplitude cepstrum signal due to edge effects in the first and last 1.5 seconds of quefrency with rapid decay is plotted in c and d respectively. e) The cepstrum with edge effects removed.

A known LFE that occurred on 18 April 2006 at 01:39:57.6 JST (Figure 5.3a) in southwest Japan and embedding it twice within one hour of a synthetically generated noise signal (Figure 5.3a). Since tremor/LFE swarms radiate energy dominant in the 1-8 Hz band (Figure 5.1), the synthetic signal is bandpass filtered accordingly (Figure 5.3b) and the complex cepstrum is calculated (Figure 5.3c). The cepstral peaks at a quefrency

of ~140000 s and ~190000 s are recovered in Figure 5.3c and they correspond to their occurrence in the time series (Figure 5.3a) as if the two are "echoes" of each other.

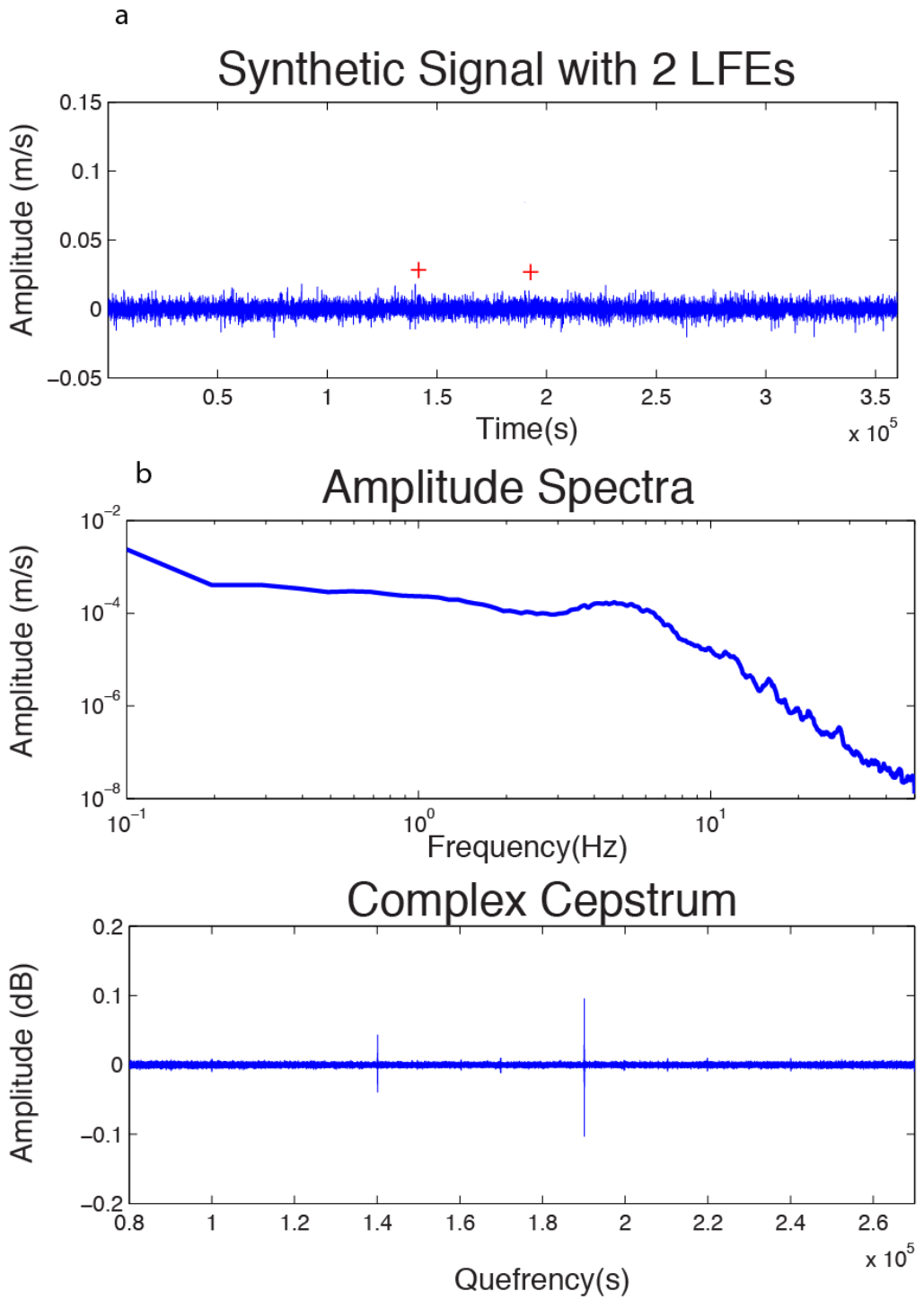

Figure 5.3. a) Synthetic Noise Signal with two LFEs embedded (red crosses) in a time series, b) the Amplitude spectra and c) complex cepstrum.

Similar to weak detections in band-limited data using matched filters and/or autocorrelation where signal amplitudes and correlation coefficients can be low, cepstral peaks also exhibit side lobes that can extend as much as +/- 8 seconds [*Brown et al.,* 2008].

Statistical Analyses of the Complex Cepstrum

Periods corresponding to repeating events embedded within a composite signal are identified from the median absolute deviation (MAD) of cepstral values. In this case, statistical outliers in the cepstrum correspond to a positive detection. This approach follows that of detecting outliers in correlation functions to detect repeating LFEs in tremor from matched filters and running autocorrelation [*Shelly et al.,* 2007a; *Brown et al.,* 2008]. Large cepstral values indicate periods where multiple phases of the signal are coherent indicating a self-similar resonance in the time series like an echo. Like previous studies, there is a trade-off between setting the detection threshold too high, resulting in reliable detections while potentially missing others, and setting a low threshold resulting in many detections sacrificing reliability.

To gain insight into this trade-off, a tremor-like signal is generated by attempting to recover a swarm of LFEs (using the same reference event in Figure 5.3) to assess the robustness of using the MAD, determine a constant R*MAD, which characterizes how much the cepstral peak deviates from the ensemble of all cepstral values, and the amplitude sensitivity at which detection is feasible.

LFEs swarm within tremor, however, the inter-event time is difficult to track due to waveform interference recorded at a common station. Since cepstral side lobes of LFEs

within tremor can be as high as 8 seconds in either direction, I embedded the reference LFE once every 20 seconds for fifteen minutes of data (Figure 5.4a) and calculate the complex cepstrum (Figure 5.4b). The distribution of cepstral values is shown in Figure 5.4c.

The synthetic detectability test to find the ideal *R**MAD for the given inter-event spacing comparable to the noise band 17 times with R values ranging from 3 to 7 at intervals of 0.25. The percent recovered and number of false alarms is shown in Figure 5.5a and b, respectively.

One would expect to detect events when the threshold of the cepstrum values corresponds to R = 4.00. At this level, we fail to detect only 5 out of 45 events and falsely detect 5 events (Figure 5.5b). When the detection threshold is lowered many of the missing events are recovered, however false detections are introduced, and vice versa. Figure 5.5c shows the threshold for detection vs. *snr.* When the amplitude of cepstral values of the LFEs blend into the noise distribution and become indistinguishable from other values it leads to a high false detection rate (Figure 5.5d).

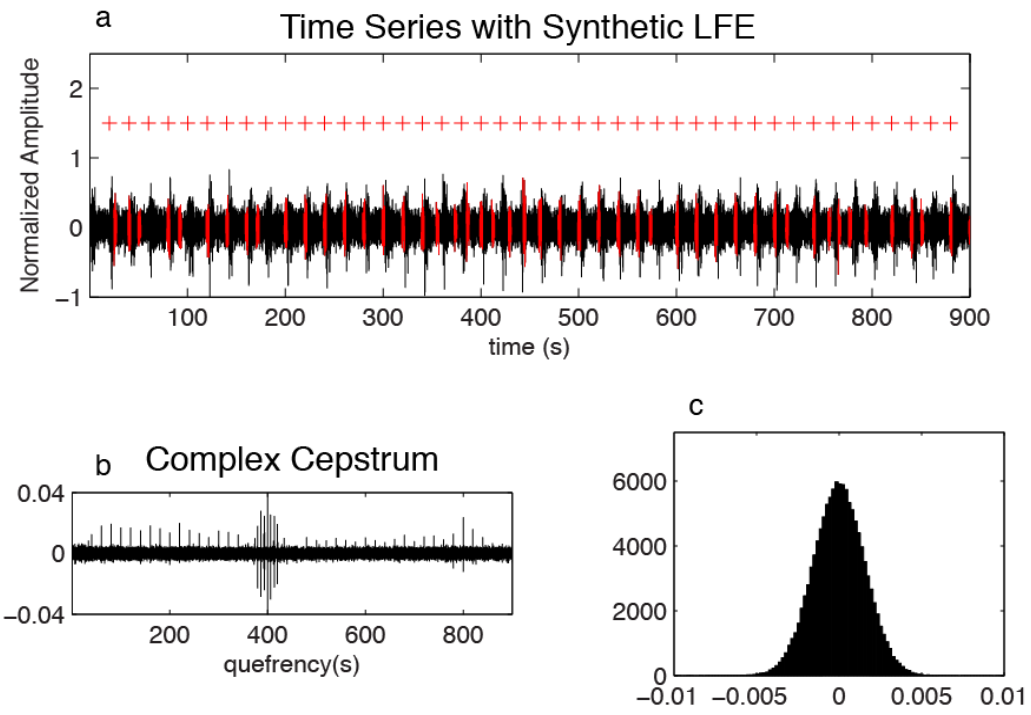

Figure 5.4. Time series with synthetic LFE swarm. b shows the cepstrum of the synthetic time series in a. c shows the distribution of cepstral values.

From the above analysis, we conclude that using cepstral analysis we can detect repeating LFEs with an inter-event spacing as little as 20s, but no less. Also, the amplitude sensitivity at which LFEs can be recovered hovers around the noise level of the signal (a *snr* of approximately 1), at a detection threshold of 4.25*MAD. This leads to a false detection rate- at most of 5 events per hour and a failure to detect rate maximum of 20 events per hour.

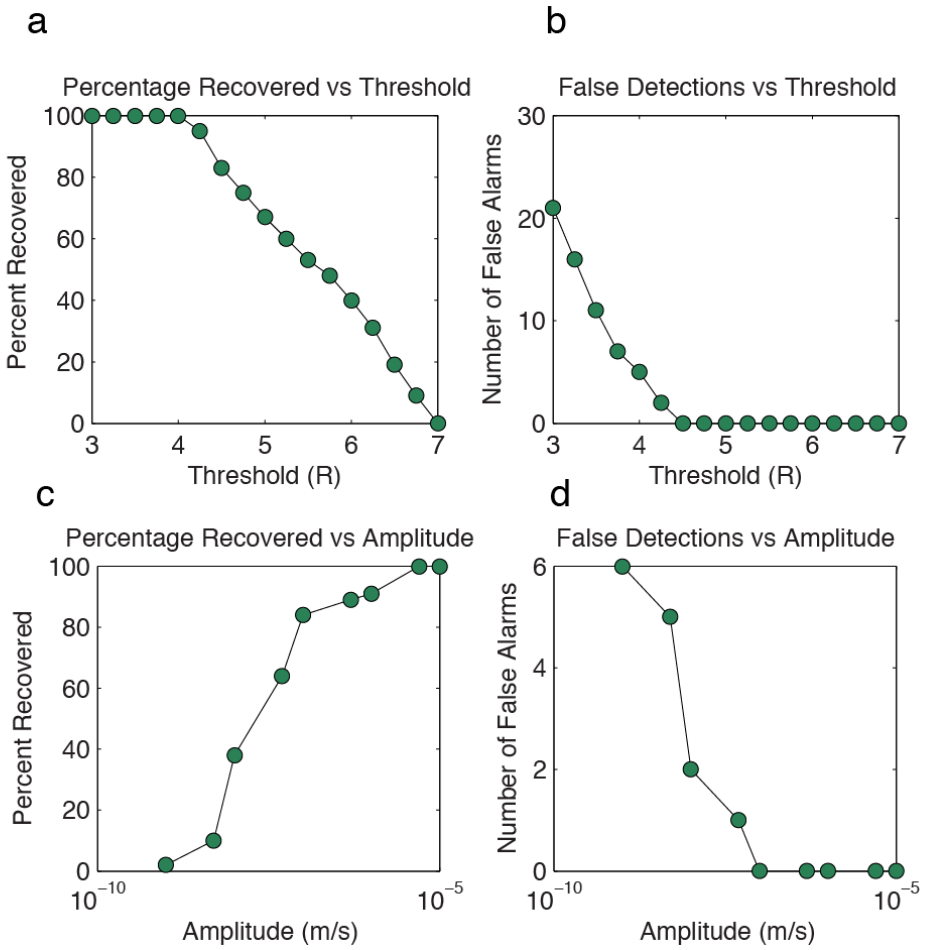

Figure 5.5. Repeated complex cepstrum calculation on synthetic seismograms. a) The recovery rate of embedded LFEs vs. threshold value, R, times the MAD. b) The number of false detection as a function of R. c) The recovery rate of embedded LFEs vs. amplitude levels. d) The number of false detections as a function amplitude rate.

APPLICATION TO DEEP TECTONIC TREMOR IN SOUTHWEST JAPAN

The possibility of detecting LFEs using the complex cepstrum is tested by applying the method to a one week-long tectonic tremor episode in April 2006. This episode was previously analyzed by *Shelly et al.* [2007b] where they were able to show that the tremor consists of several repeating LFEs in western Shikoku using a matched filter method [*Gibbons and Ringdal,* 2006; *Shelly et al.,* 2007a].

We down-sampled eight 3-component Hi-Net velocity recordings in western Shikoku from 0.01s to 0.05s and bandpass filter the data from 1-8 Hz, which is the frequency range where tremor and LFE activity is the strongest. LFEs are searched for by calculating the complex cepstrum of tremor signals one hour at a time for all channels.

In order to conserve the strongest detections we slightly elevated the detection threshold to 4.25*MAD, only allow 1 detection per 20 seconds, and require at least 5 stations to have cepstral peaks within a 20-second window. Doing so we were able to find 4261 LFEs throughout the week (Figure 5.6-19). The computation time to find this many events was 14 minutes for the entire week. This is an order of magnitude more events than previous studies and two orders of magnitude faster than running autocorrelation. The vast majority of previously detected events are detected using the cepstrum in addition to several more in both the high- and low-amplitude tremor. An example of a cepstral detection is shown in Figure 5.20.

I identify the times of the detection and apply waveform cross-correlation at sample precision for all 404 detections. Figure 5.21 shows waveform stacks and alignments for 404 of the strongest matches throughout the week.

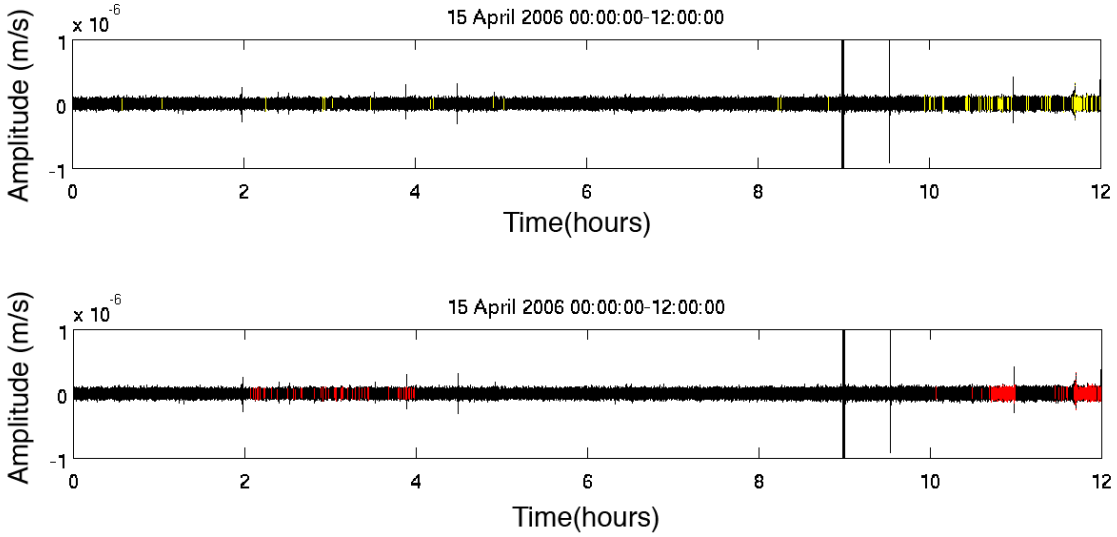

Figure 5.6. 12 hours of LFE detections from the cepstrum within continuous waveform data compared to previous studies. a. Results from template matching (Shelly et al., 2007b). b) ceptrum detections. We find similar events and additional events using the cepstrum method.

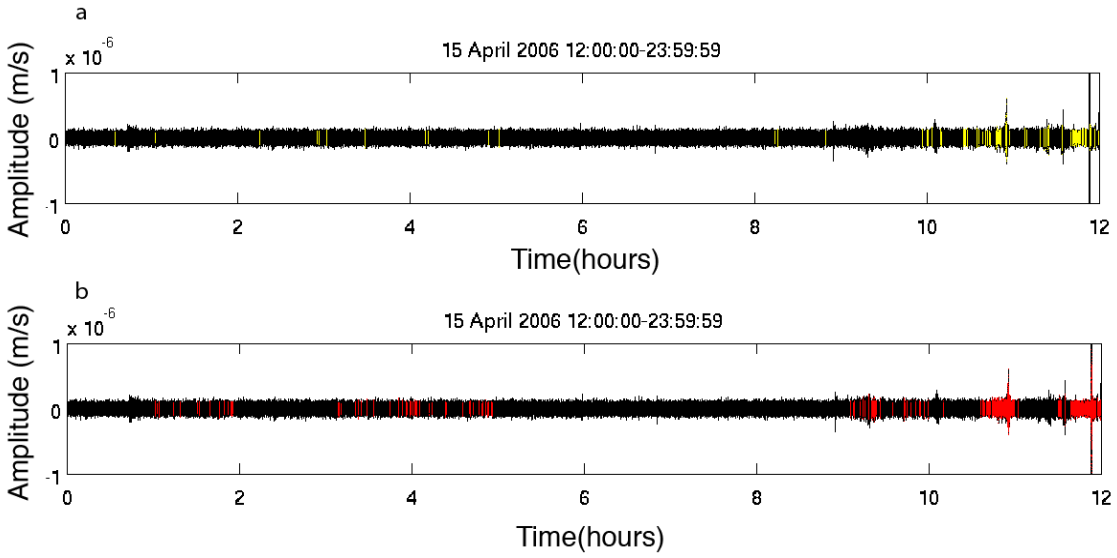

Figure 5.7 same as 5.6

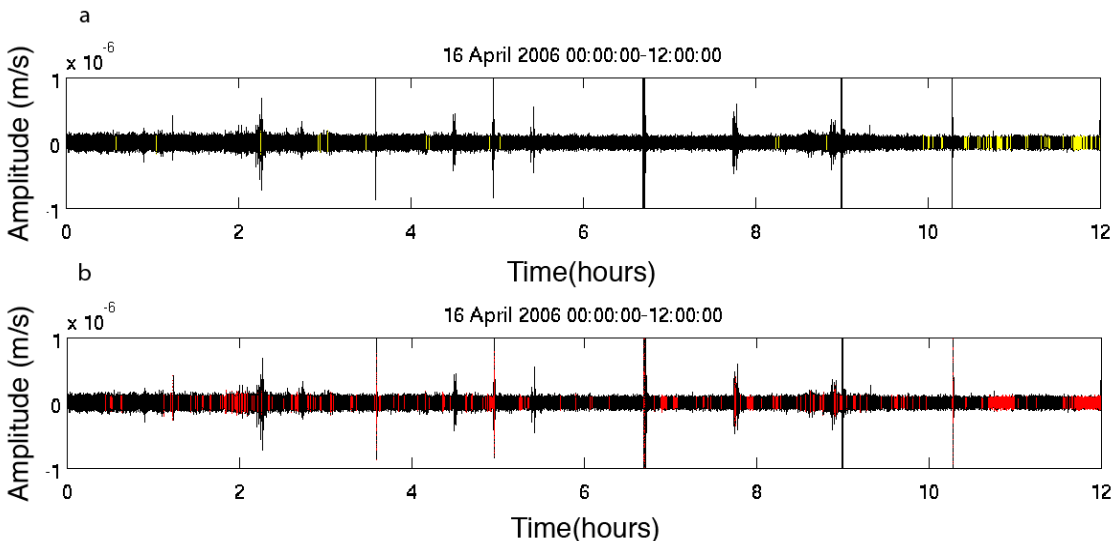

Figure 5.8 same as 5.6

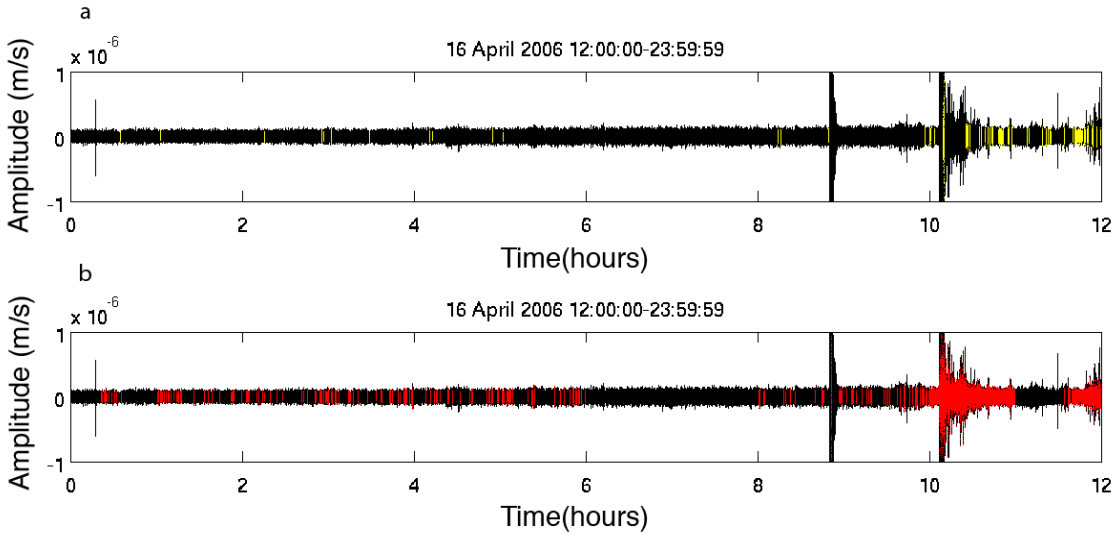

Figure 5.9 same as 5.6

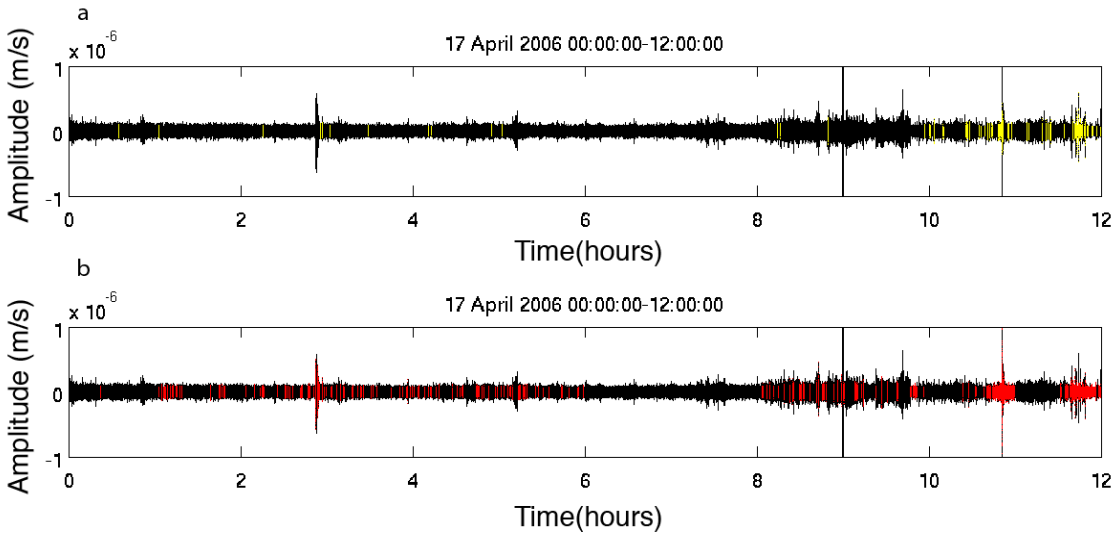

Figure 5.10 same as 5.6

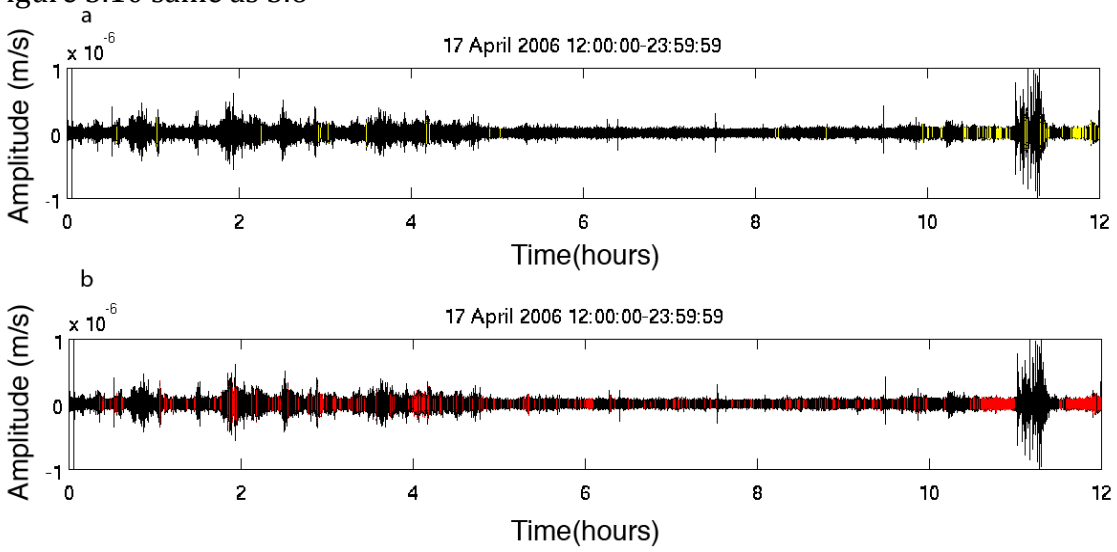

Figure 5.11 same as 5.6

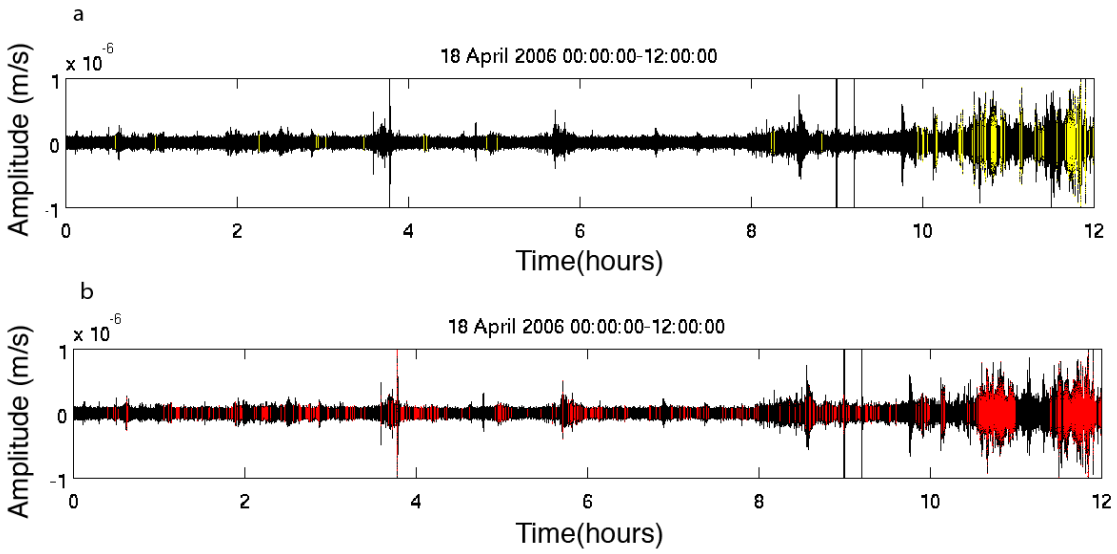

Figure 5.12 same as 5.6

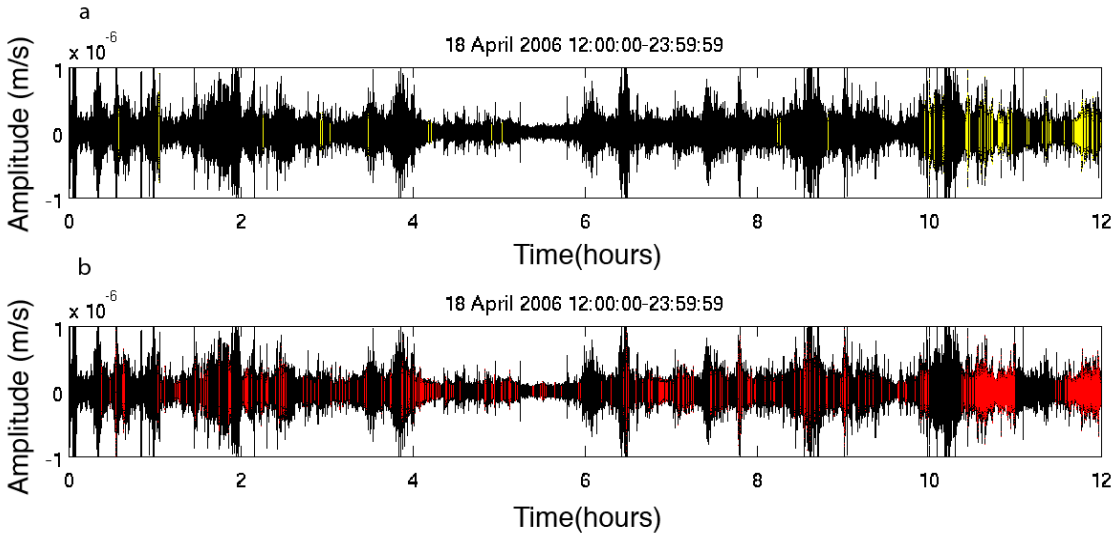

Figure 5.13 same as 5.6

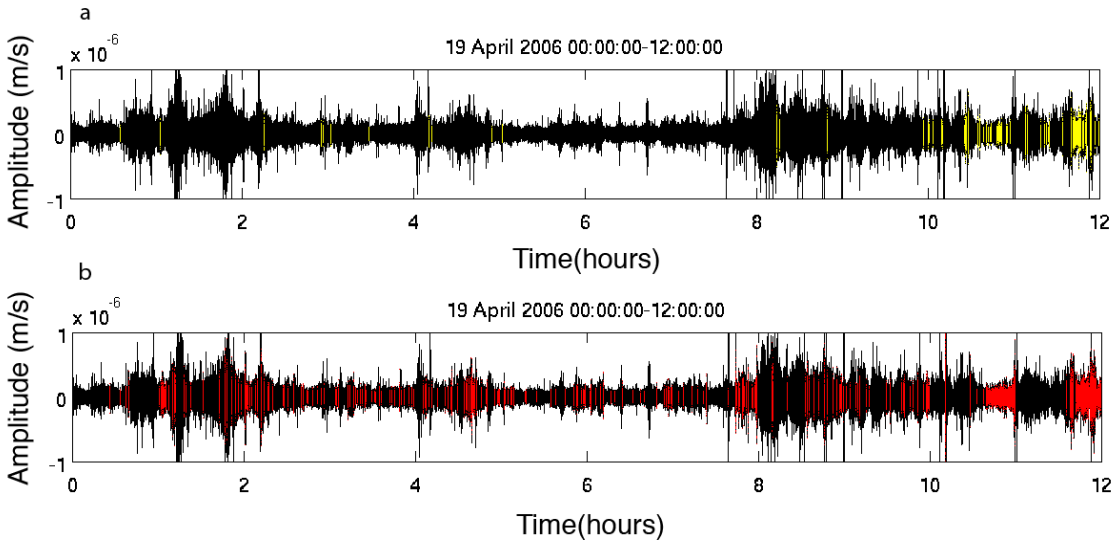

Figure 5.14 same as 5.6

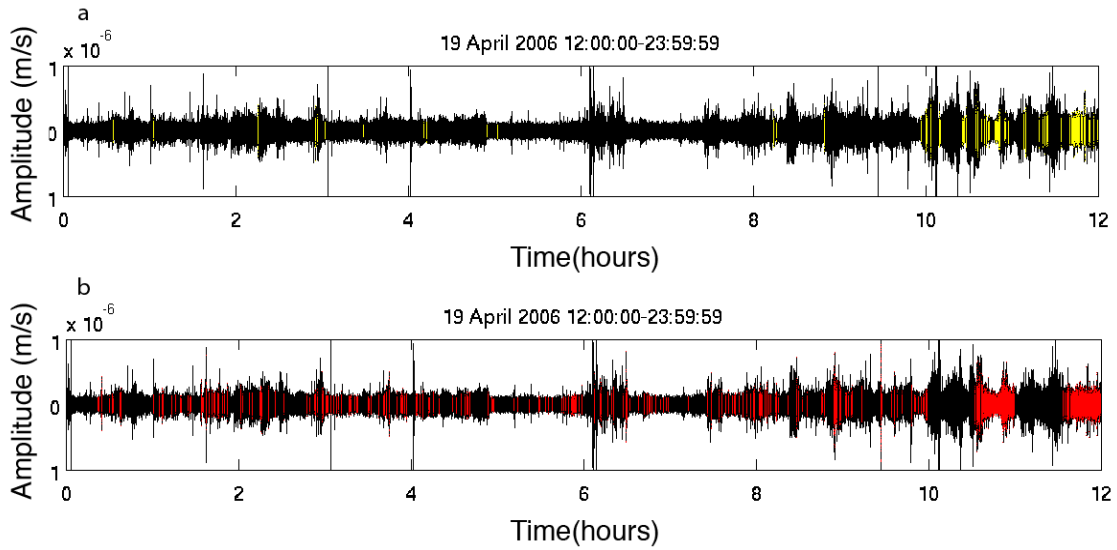

Figure 5.15 same as 5.6

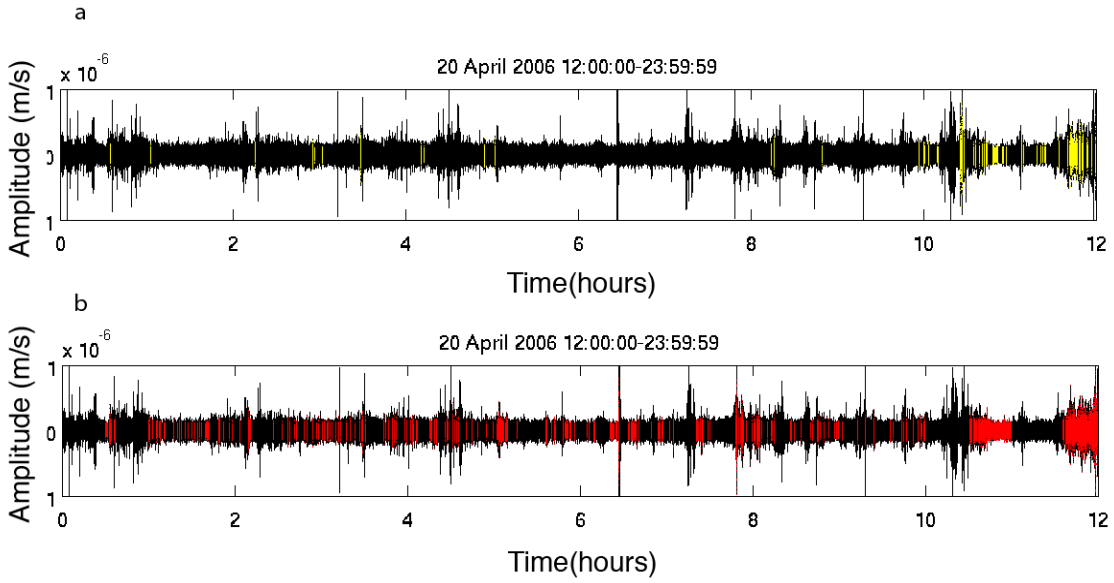

Figure 5.17 same as 5.6

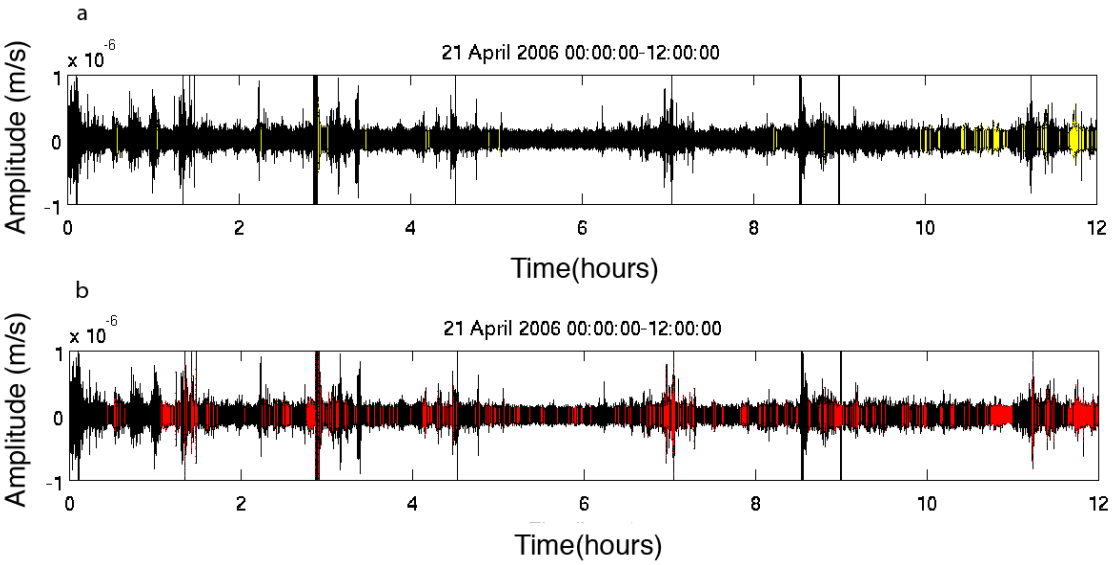

Figure 5.18 same as 5.6

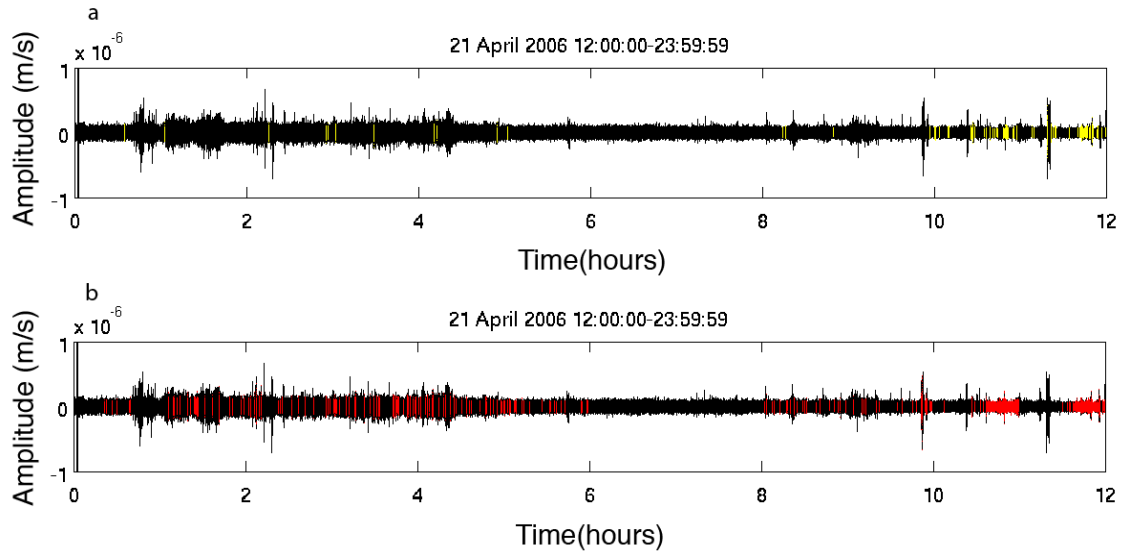

Figure 5.19 same as 5.6

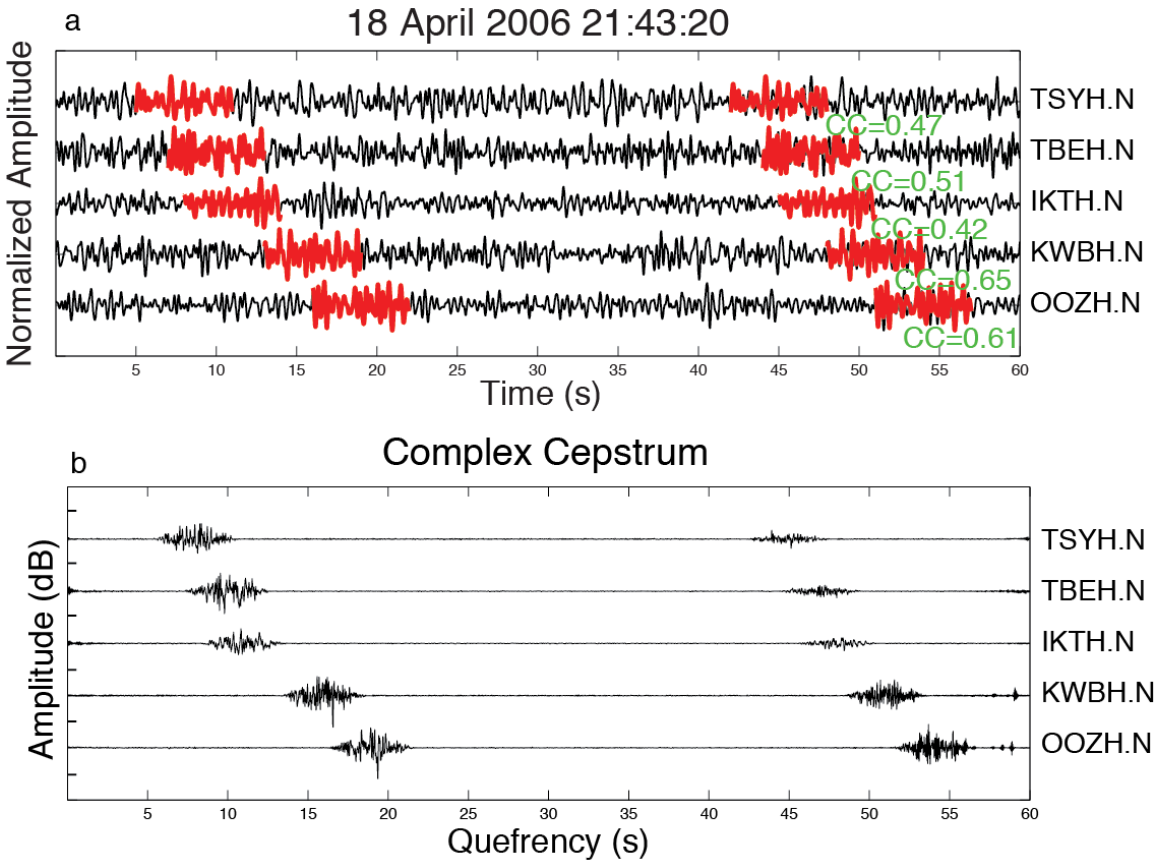

Figure 5.20 LFE detection from complex cepstrum analysis. a) Two similar LFEs occurring within 60 seconds with moveout are shown. Red traces are 6-seconds in duration and plotted on top of the continuous data shown in black. The first event yields strong correlation with an event approximately 30 seconds later with a slightly different

moveout as determined from waveform cross-correlation-derived differential times (correlation coefficients are shown to the right). b) Complex cepstral peaks demonstrating the corresponding arrival time for both events.

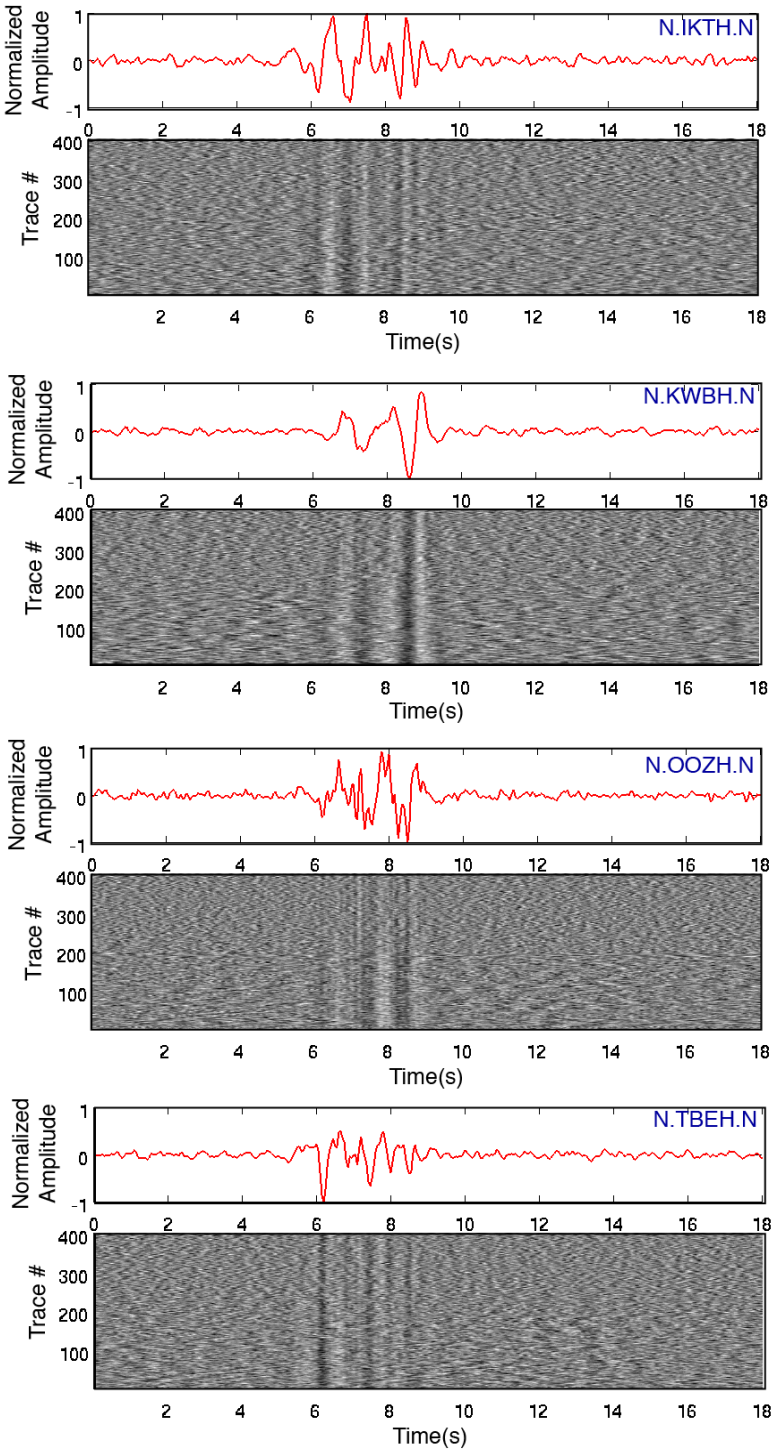

Figure 5.21. Waveform alignment and stack of 404 LFE detections from tremor at 5 Hi-Net stations. The events are coherent across 2.5 seconds.

CONCLUSIONS

LFEs within tremor can be detected using cepstral analysis. Sharp peaks in the quefrency domain correspond to time offsets of multiple phases in the tremor time series. We also get a false alarm rate from a synthetic test. We also get a noise level threshold. The method is fast. We applied this method on twelve hours of tremor recorded on eight 3-component Hi-Net stations in western Shikoku and successfully recover previously identified LFEs in addition to an order of magnitude more. Waveform cross-correlation at sample precision of the LFE detections reveal a high degree of similarity for groups of LFEs. Double difference locations reveal LFE locations in western Shikoku between 25 and 35 km depth on the plate interface consistent with previous studies in southwest Japan (Shelly et al., 2006) and LFE locations in other subduction zones (Brown et al., 2009). This technique could be promising for understanding the complex nature of tectonic tremor in other tectonic settings.

REFERENCES

Bogert, B. P., M. J. R Healy, and J. W. Tukey (1963), The quefrency analysis of time series for echoes: Cepstrum, pseudo-autocovariance, cross-cepstrum, and saphe cracking, in Time Series Analysis, M. Rosenblatt, Ed., Ch. 15: 209–243.

Brown, J. R., G. C. Beroza, and D. R. Shelly (2008), An autocorrelationmethod to detect low frequency earthquakes within tremor, Geophys. Res.Lett., 35, L16305, doi:10.1029/2008GL034560.

Brown, J. R., G. C. Beroza, S. Ide, K. Ohta, D. R. Shelly, S. Y. Schwartz, W. Rabbel, M. Thorwart, and H. Kao (2009), Deep low-frequency earthquakes in tremor localize to the plate interface in multiple subduction zones, *Geophys. Res. Lett.,* 36, L19306, doi:10.1029/2009GL04002.

Davies, J. B. and S. W.Smith (1969), Source parameters of earthquakes and discrimination between earthquakes and nuclear explosions, *Bull. Seis. Soc. Amer.,* 58, 5, 1515-1517.

Gibbons, S. J., and F. Ringdal (2006), The detection of low magnitude seismic events using array-based waveform correlation, *Geophys. J. Int.*, 165, 149 – 166.

Hedlin, M. A. H., J. B. Minster and J. A. Orcutt (1990), An automatic means to discriminate between earthquakes and quarry blasts, *Bull. Seis. Soc. Amer.*, vol. 90, 68, pp 2143-2160.

Obara, K., (2002), Nonvolcanic deep tremor association with subduction in southwest Japan, *Science,* 296, pp. 1679-1681.

Reymond, D., O. Hyvernaud, J. Talandier and E. A. Okal (2003), *T*-wave detection of two underwater explosions off Hawaii on 13 April 2000, *Bull. Seis. Soc. Amer.*, vol. 93, 2, pp 804-816.

Rogers, G. and H. Dragert (2003), Episodic tremor and slip in Cascadia subduction zone: The chatter of silent slip, *Science,* 300, pp. 1942-1943.

Shelly, D. R., G. C. Beroza, and S. Ide (2007a), Non-Volcanic Tremor and Low Frequency Earthquake Swarms, *Nature* 446, 305-307, doi:10.1038/nature05666

Shelly, D. R., G. C. Beroza, and S. Ide (2007b), Complex evolution oftransient slip derived from precise tremor locations in western Shikoku,Japan, *Geochem. Geophys. Geosyst.*, 8, Q1 00 14, doi:10.1029/2007GC001640.

Shelly, D. R., G. C. Beroza, S. Ide, and S. Nakamula (2006), Low frequency earthquakes in Shikoku, Japan, and their relationship to episodic tremor and slip, Nature, 442, 188 – 191, doi:10.1038/nature04931.

Tribolet, J.M., (1978), Applications of short-time homomorphic signal analysis to seismic wavelet estimation. In: C.H. Chen (Editor), Computer-Aided Seismic Analysis and Discrimination. Geoexploration, 16: 75-96.

Wei, F. and M. Li (2003), Cepstrum analysis of seismic source characteristcs, *Acta Seis. Sinica,* DOI: 10.1007/s11589-003-0006-9

Zhang, H. and C. H. Thurber (2003), Double-difference tomography: The method and its application to the Hayward fault, Northern California, *Bull. Seis. Soc. Amer.*, vol. 3, 5, pp. 1875-1889.